Universidad de Alcalá

ACTA DE EVALUACIÓN DE LA TESIS DOCTORAL

Año académico 2018/19

DOCTORANDO: **GARCIA POBLACION, OSCAR**
D.N.I./PASAPORTE: ******4453H**

PROGRAMA DE DOCTORADO: **D443-INVESTIGACIÓN ESPACIAL Y ASTROBIOLOGÍA**
DPTO. COORDINADOR DEL PROGRAMA: **AUTOMÁTICA**
TITULACIÓN DE DOCTOR EN: **DOCTOR/A POR LA UNIVERSIDAD DE ALCALÁ**

En el día de hoy 08/07/19, reunido el tribunal de evaluación nombrado por la Comisión de Estudios Oficiales de Posgrado y Doctorado de la Universidad y constituido por los miembros que suscriben la presente Acta, el aspirante defendió su Tesis Doctoral, elaborada bajo la dirección de **JUAN JOSE BLANCO AVALOS // SEBASTIAN SANCHEZ PRIETO**.

Sobre el siguiente tema: *THE CALMA STATION AND A NEW DATA ACQUISITION SYSTEM FOR NEUTRON MONITORS*

Finalizada la defensa y discusión de la tesis, el tribunal acordó otorgar la CALIFICACIÓN GLOBAL[1] de (**no apto, aprobado, notable** y **sobresaliente**): _SOBRESALIENTE_

Alcalá de Henares, 8 de Julio de 2019

EL PRESIDENTE   EL SECRETARIO   EL VOCAL

Fdo.: DANIEL MEZIAT LUNA   Fdo.:ANTONIO DA SILVA FARIÑA   Fdo.: CHRISTIAN STEIGIES

Con fecha 24 de Julio de 2019 la Comisión
Delegada de la Comisión de Estudios Oficiales de Posgrado,
a la vista de los votos emitidos de manera anónima por el
tribunal que ha juzgado la tesis, resuelve:

☒ Conceder la Mención de ''Cum Laude''
☐ No conceder la Mención de ''Cum Laude''

La Secretaria de la Comisión Delegada

FIRMA DEL ALUMNO,

Fdo.: GARCIA POBLACION, OSCAR

---

[1] La calificación podrá ser "no apto" "aprobado" "notable" y "sobresaliente". El tribunal podrá otorgar la mención de "cum laude" si la calificación global es de sobresaliente y se emite en tal sentido el voto secreto positivo por unanimidad.

INCIDENCIAS / OBSERVACIONES:

En aplicación del art. 14.7 del RD. 99/2011 y el art. 14 del Reglamento de Elaboración, Autorización y Defensa de la Tesis Doctoral, la Comisión Delegada de la Comisión de Estudios Oficiales de Posgrado y Doctorado, en sesión pública de fecha 24 de julio, procedió al escrutinio de los votos emitidos por los miembros del tribunal de la tesis defendida por *GARCIA POBLACION, OSCAR*, el día 08 de julio de 2019, titulada, *THE CALMA STATION AND A NEW DATA ACQUISITION SYSTEM FOR NEUTRON MONITORS* para determinar, si a la misma, se le concede la mención "cum laude", arrojando como resultado el voto favorable de todos los miembros del tribunal.

Por lo tanto, la Comisión de Estudios Oficiales de Posgrado y Doctorado **resuelve otorgar** a dicha tesis la

MENCIÓN "CUM LAUDE"

EL VICERRECTOR DE INVESTIGACIÓN Y TRANSFERENCIA
F. Javier de la Mata de la Mata
Documento fechado y firmado digitalmente

Copia por e-mail a:
Doctorando: GARCIA POBLACION, OSCAR
Secretario del Tribunal: ANTONIO DA SILVA FARIÑA
Director/a de Tesis: JUAN JOSE BLANCO AVALOS // SEBASTIAN SANCHEZ PRIETO

DILIGENCIA DE DEPÓSITO DE TESIS.

Comprobado que el expediente académico de D./Dª _____

reúne los requisitos exigidos para la presentación de la Tesis, de acuerdo a la normativa vigente, y habiendo

presentado la misma en formato: ☐ soporte electrónico ☐ impreso en papel, para el depósito de la

misma, en el Servicio de Estudios Oficiales de Posgrado, con el nº de páginas: _____ se procede, con

fecha de hoy a registrar el depósito de la tesis.

<div align="center">Alcalá de Henares a _____ de _____ de 20_____</div>

Fdo. El Funcionario

D/Dª _Javier Rodríguez-Pacheco Martín_____, Coordinador de la Comisión Académica del Programa de Doctorado en __Investigación Espacial y Astrobiología_____

HAGO CONSTAR que la Tesis Doctoral titulada **The CaLMa Station and a new data adquisition system for neutron monitors** __, presentada por D/Dª__Óscar García Población_____, bajo la dirección del / de la Dr/a. __Juan José Blanco Ávalos_y Sebastián Sánchez Prieto___, ha sido realizada por compendio de artículos, reuniendo los requisitos exigidos a este tipo de tesis, así como los requisitos científicos de originalidad y rigor metodológicos para ser defendida ante un tribunal. Esta Comisión ha tenido también en cuenta la evaluación positiva anual del doctorando, habiendo obtenido las correspondientes competencias establecidas en el Programa.

Para que así conste a los efectos del depósito de la tesis, se firma en Alcalá de Henares a 6 ____ de ___Noviembre____ de ____2018_____

Fdo.:

Universidad de Alcalá

SEBASTIÁN SÁNCHEZ PRIETO, Catedrático de Universidad del área de Arquitectura y Tecnología de Computadores de la Universidad de Alcalá,

HACE CONSTAR

Que el trabajo "**The CaLMa Station and a new data adquisition system for neutrón monitors**", presentado por D. Óscar García Población, ha sido realizado en el Grupo de Investigación del Espacio (SRG-UAH) bajo mi codirección, reuniendo los méritos suficientes para optar al grado de doctor, por lo que puede proceder a su depósito y lectura.

Alcalá de Henares, 6 de marzo de 2019

Fdo.: Dr. Sebastián Sánchez Prieto

Universidad de Alcalá

JUAN JOSÉ BLANCO ÁVALOS, Profesor Titular del área de Física Aplicada de la Universidad de Alcalá,

HACE CONSTAR

Que el trabajo **"The CaLMa Station and a new data adquisition system for neutrón monitors"**, presentado por D. Óscar García Población, ha sido realizado en el Grupo de Investigación del Espacio (SRG-UAH) bajo mi codirección, reuniendo los méritos suficientes para optar al grado de doctor, por lo que puede proceder a su depósito y lectura.

Alcalá de Henares, 11 de marzo de 2019

Fdo.: Dr. Juan José Blanco Ávalos

Universidad de Alcalá

Programa de Doctorado en Investigación Espacial y Astrobiología

The CaLMa station and a new data acquisition system for neutron monitors

Tesis Doctoral presentada por

Óscar García Población

Directores:
D. Juan José Blanco Avalos
D. Sebastián Sánchez Prieto

Alcalá de Henares, 2019

The CaLMa station and a new data acquisition system for neutron monitors

by
Óscar García Población

Abstract

Neutron monitors are state-of-the-art ground-based detectors designed to measure high-energy particles that arrive to the Earth's atmosphere mainly from the outside of the Solar System. Since its initial conception by Professor A. Simpson, in the University of Chicago in 1948, it has undergone different upgrades, not in its basic conception but in the new technologies available for its construction, distribution and analysis of its data.

The combination of new databases technologies and the Internet network have made possible to unify and centralize the data provided by many stations around the planet in the so called Neutron Monitor Database (NMDB). This project has open a new path in the research of Solar Physics, Energetic Particles and Earth-Sun interaction and Cosmic Rays. This thesis work stars by using the data provided by the NMDB to study the observable effects of Interplanetary Coronal Mass Ejections on ground level neutron monitor counting rates. The data from the NMDB helped us to provide a framework of requirements for a new data acquisition design, and the results are also included in this document.

Next in this work, the design and construction of the new Castilla-La Mancha Neutron Monitor, CaLMa is presented. This is a NM64-type neutron monitor located in Guadalajara (Spain), $40°38'32.2"N$, $3°9'44.4"W$ at 708 m above sea level, and it has a calculated vertical cut-off rigidity of 6.95 GV. This station is integrated in the Neutron Monitor Database and provides high-resolution 1-minute real time data, that is publicly available through the NMDB distribution channels.

Along with the CaLMa Neutron Monitor, a new data acquisition system has also been designed from scratch to address obsolescense problems and to provide new features by means of applying FPGA-based technologies. This new system has been already running in other stations, so a comparative data analysis has also been provided from old and new acquisitions systems. This will allow us to performs validation analysis for the new system.

Acknowledgments

CaLMa would not have seen the light of day without the financial support of the ACTEPARQ 2009 program, but such power couldn't have been summoned without the magic of José Medina Doctor, Juan José Blanco Avalos and the people in the Science and Technology Park in Guadalajara, especially of Edurne Fernández Segarra.

Another major force that contributed to my endeavor was the FP7 program that made the Neutron Monitor Database (NMDB) possible. I am very grateful to all the members of this consortium, especially to his technical and spiritual leader Christian Steigies, from the Christian Albrechts Universität zu Kiel, Germany.

Another very important ignition spark to this project came from Karl-Ludwig Klein from l'Observatoire de Paris, LESIA, and the people from the Laboratoire Astrophysique de Toulouse in Tarbes, France. Thank you very much for donating the firsts counter tubes of the CaLMa Station (and that are now happily counting in the Spanish Antarctic Base Juan Carlos I).

And finally, last but by no means least, I would like to express my gratitude to all my teammates in the Space Research Group in the Alcalá University, starting from his father founder Daniel Meziat Luna, Sebastián Sánchez Prieto, Manuel Prieto Mateo, Raúl Gómez Herrero, Sindulfo Ayuso de Gregorio, and especially to my beloved CaLMa-Team, with whom I have worked so many times hand by hand, been through so many incredible experiences and had so much fun, Juan Ignacio García Tejedor and Juan José Blanco Avalos.

A las tres mujeres de mi vida,
mi madre Julia,
mi hermana Sonia,
y mi hija Amélie

A mi abuelo Román y mi padre Luis

THIS PAGE INTENTIONALLY LEFT BLANK

Contents

Appendices 94

List of Figures

THIS PAGE INTENTIONALLY LEFT BLANK

List of Tables

THIS PAGE INTENTIONALLY LEFT BLANK

Chapter 1

Introduction and document structure

A neutron monitor is a scientific instrument designed to measure the number of high-energy particles, called cosmic rays, that arrive to the atmosphere from the space. These incoming particles are mostly protons and alpha particles, with at least two different populations, galactic cosmic ray (GCR), i.e. particles accelerated in our own galaxy, and solar cosmic rays, also known as solar energetic particles (SEP) originated by the Sun and that are part of the low energy component of the CR. Although the SEP origin is clear, the Sun, the origin of GCR is still controversial. While some authors point out the supernovae explosions as the source[1], others suggest that magnetically active starts[2], quasars, gamma-ray bursts and active galactic nuclei might be the source. CR are interesting because of their effect on microelectronics and life forms, but also because they are heavily influenced by the Sun activity, and therefore they are key to understand Sun to Earth relationship.

Cosmic rays arrive to the Earth with a wide range of energies. The figure 1-1 shows the CR flux[8] versus its energy[1], but not all the cosmic rays will make it through the Earth's magnetosphere. Since CR are charged particles their trajectories are strongly affected by magnetic and electric fields in a very complex way. Galactic magnetic field changes CR trajectories according to a random path. In particular, once the CR arrive Earth, the Earth's magnetosphere acts as an efficient shield that deflects CR depending on its energy and incidence angle. If the CR energy is very high, then it will travel thought the magnetosphere and into the atmosphere with little or no trajectory deviation. As the energy of the arriving particle decreases, the effect of the magnetic field on the particle's path increases, bending it more and more, until a point in which the particle is reflected back to the space. This energy threshold is known as the geomagnetic cut-off rigidity and it measures the shielding for CR provided by the magnetosphere for a given location and CR trajectory. In the Earth's poles the magnetic field lines are almost radial. If a CR reaches this region it would be able to reach the atmosphere without any interference with energies as low as some hundreds

---

[1]By Sven Lafebre (own work, after Swordy.[1]) [GFDL (http://www.gnu.org/copyleft/fdl.html), CC-BY-SA-3.0 (http://creativecommons.org/licenses/by-sa/3.0/) or CC BY-SA 2.5-2.0-1.0 (http://creativecommons.org/licenses/by-sa/2.5-2.0-1.0)], via Wikimedia Commons
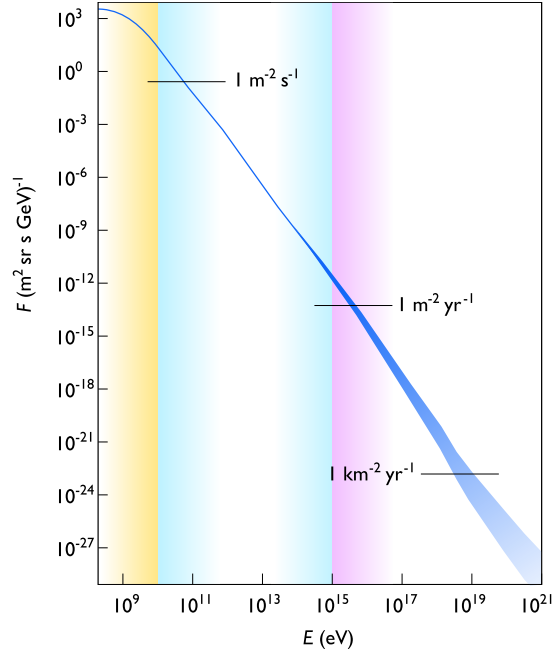
Figure 1-1: Cosmic ray flux versus particle energy.

of MeV. If instead the incoming particle arrives in the equatorial plane, then it will find the magnetic field lines perpendicular to its trajectory and then it will need energies higher than 15 GeV to break through it to reach the Earth's atmosphere. As a conclusion, this means that a neutron monitor located in equator will read a different range of cosmic rays that one located in the poles. The combination of the measurements of neutron monitors located in places with different cut-off rigidity is therefore very interesting to conduct complex studies about the cosmic rays nature.

When a CR reaches the upper part of the atmosphere it interacts with the increasing number of atoms and molecules, mostly oxygen and nitrogen, by ionizing or colliding with them. Ionization is a common effect because of electromagnetic force's long range, but the energy lost by relativistic protons is very low to cause any important effect because they behave as minimum-ionizing particles or MIPS. On the other hand, collision with atomic nuclei creates multiple and complex effects. If the energy is high enough it can kick nucleons out of the target or even produce pions, kaons or more exotic particles causing a mini cascade in the same direction of the original particle due to conservation of momentum. If the original particle remains in the target nucleus, it is left in an excited state known as compound-nucleus. Because of this, the nucleus emits gamma rays and further evaporation nucleons in the MeV energy range. All these particles resulting of the CR interaction with the atmosphere all called secondary cosmic rays, and they lose energy as they penetrate the atmosphere causing the so called cosmic rays cascade. The atmospheric cascade is made up of many products that can be grouped in three categories: the muonic component and neutrinos, the hadronic component and the electromagnetic component. The muons are the least likely to interact with the atmosphere, and therefore they are the most

common secondary CR that can be detected at sea level. From the hadronic components, neutrons and protons reach also the ground but they lose energy because of collision with other atoms, especially protons that also lose energy by ionization.

Even though the first Neutron Monitor design dates from the fifties of the last century, they are still the state-of-the-art instrumentation for CR ground level measurement. There are two types of standardized neutron monitors: IGY and NM64. The first type was use to record the variation of cosmic rays during the International Geophysical Year in 1957/1958, from where it takes its name. It was created by J.A. Simpson in 1957[18]. Later, in 1968, Carmichael developed an improved version called "super" neutron monitor NM64, which became the most popular design up to now.

The origin of the research activity that motivated this work was in the European Geosciences Union congress 2008, where José Medina and Juan José Blanco, from the Alcalá University, and Marisa Storini from the Rome University hold a conversation about the possibility of locating a Neutron Monitor in the center of Spain, as this would cover a energy range not yet covered by the neutron monitors in the existing neutron monitor database. Only a few months before, Christian Steigies from the Christian Albrechts University of Kiel, Germany and I talked about collaborating in the design of a data acquisition system for neutron monitors in the context of the FP7 project of the Real-Time database for high resolution Neutron Monitor measurements, NMDB. As a result of both conversations, the Space Research Group of the Alcalá University joined the NMDB work package 3, Guidelines for Data Acquisition in January 2009. In this same year, funds were requested to build the Castilla-La Mancha Neutron Monitor, CaLMa, in the Science and Technology Park of Guadalajara (Guadalab). This was done in the Arteparq 2009 call PEP-470000-2009-001 "Adquisición de Equipamiento para un Monitor de Neutrones". Meanwhile, in November 2010, thanks to the initiative of Ludwig Klein from L'Observatorie de Paris, nine NM64 counter tubes were donated for the CaLMa station.

These tubes were characterized and three were chosen to be the first components of the CaLMa station. In October 2010 these counter tubes started registering counts with the new data acquisition system. It will not be until July 2011 that CaLMa will reach its definitive configuration. In this same year, in November 2011, the data acquisition system is installed in the KIEL neutron monitor station and starts registering data in the NMDB under the KIEL2 call sign. Later, in August 2012 the CaLMa station starts publishing data in the NMDB. Having two data acquisition systems running in two different stations allowed us to compare the results between them, but also in KIEL to compare also with the old system that was kept running in parallel.

As a result of the work during all these years, the three main articles that support this thesis work were published. The first, Observable Effects of Interplanetary Coronal Mass Ejections on Ground Level Neutron Monitor Count Rates, in May 2013, was related to the use of the data in the NMDB. The second, Castilla-La Mancha neutron monitor, in 2013, covers the design and construction of the CaLMa Neutron Monitor, and finally the third, Embedded data acquisition system for neutron monitors, in 2014 describe the data acquisition system designed as a result of the WP3 of the NMDB project.

Figure 1-2: Decommissioned NM64 counter tubes from the Pic-du-Midi observatorie in the future placement of CaLMa in Guadalajara.

The research work of this Thesis is divided five chapters. The introductory chapter presents the scientific background, the original research goal and the path followed to achieve this goal. The second chapter shows the first approach to the Neutron Monitor Database and its data usage. From this data we will determine the worst operating conditions of the future data acquisition system, and also we will obtain valuable information that resulted in the paper "Observable effects of Interplanetary Coronal Mass Ejections on ground level neutron monitor counting rates"[3], published by Solar Physics in 2013. The third chapter is about the design and construction of the CaLMa Neutron Monitor Station. This work was also published in Nuclear Instruments and Methods en Physics Research in 2013, with the title "Castilla-La Mancha Neutron Monitor"[15]. The fourth chapter studies the Data Acquisition System designed for neutron monitors, as a result of our participation in the Real-time database for high-resolution neutron monitor measurements (NMDB) project, funded by the Seventh Framework Programme FP7 of the European Commission. This work was also published in the Journal of Instrumentation in 2014 with the title "Embedded data acquisition system for neutron monitors"[16]. Finally the fifth and last chapter is about the conclusions of this research.

Chapter 2

The Neutron Monitor Database

The Neutron Monitor Database is a join effort to build, populate and maintain a centralized database of high resolution data from neutron monitor stations of all over the world.

This initiative was funded by the Seventh Framework Programme (FP7) of the European Commission, as a e-Infrastructure project of the Capacities Programme. The main goals of the project were to upgrade existing stations so they could provide real-time, high-resolution data, to build a centralized database with distributed database mirrors, to populate the database with the historical data available, to develop application and access tools so the data could be accessed using different techniques and to create a public outreach to inform about the project and its results.

At the time this document was written the NMDB includes 68 stations all over the world. Out of them, CaLMa and another 27 provide one-minute real-time measurements. The real-time data is used mainly to feed early alarm systems, while historical data is used for research purpose, radiation dosimetry and other space weather applications.

In this work the use of the NMDB was twofold: firstly to retrieve data to study the Observable Effects of Interplanetary Coronal Mass Ejections on Ground Level Neutron Monitor Count Rates[3], and secondly to obtain an estimation of the maximum count rate that a neutron monitor data acquisition system should be able to handle. This estimation will be very useful when determining the requisites of the *embedded data acquisition system for neutron monitors*[16] that will be presented later in this document.

In this chapter we will introduce the usage of the NMDB, showing how the data is accessed and describing in detail its structure. Then we will use the data to determine the maximum count rate registered and finally there will be a brief introduction to Fordbush Decreases, and their role in the article The Observable Effects of Interplanetary Coronal Mass Ejections on Ground Level Neutron Monitor Count Rates, presented in this work.

2.1   Accessing the data in the NMDB

The web page of the project with full information can be found in `http://www.nmdb.eu`. In this page there are information about the project itself, some introductory material about cosmic rays and neutron monitors, etc. Among this information there is also the recommended procedure to access NMDB data, that is by using the NEST tool in `http://nest.nmdb.eu`. This tool is an interactive web application designed to explore the data available from all the stations, and it can also be used to download raw ASCII data automatically for further processing. Upon a special request, a read-only account to the database was provided, and this was the way we accessed the data for our work. This method allows to execute complex SQL queries with arbitrary filters.

To help to understand the data available from the NMDB, in the next section the different tables of the database will be described.

2.2   The NMDB database format

The NMDB contains a set of five tables per station. Each table is described as follows:

`<STATION>_ori` it contains the timestamp of the sample, the length of the measurement period in seconds (typically 60), the uncorrected counts, the counts corrected for efficiency and for pressure, and the atmospheric pressure in hectopascals. This is a write-only table. Once the data has been written, it won't be deleted or updated.

`<STATION>_rev` it has the same structure as `<STATION>_ori` but this is meant for data correction. When a new data is inserted the field `last_changed` is automatically generated and a `version` field can be filled with a number.

`<STATION>_1h` it holds average data for 1h.

`<STATION>_env` it contains environmental data for the station.

`<STATION>_meta` it contains arbitrary data for the station. This table is meant to be used as a log for events that might affect the data of that station for a given period of time.

There is also another `<STATION>_revori` table that is a view that conveniently combines the `<STATION>_ori` with `<STATION>_rev`, so for a given timestamp, if shows the corrected data if available, and the original if not.

In the last descriptions, the placeholder `<STATION>` is a four letter station's call sign. For the CaLMa station this call sign is `CALM`, therefore the tables are named `CALM_ori`, `CALM_1h`, etc.

From the data point of view, the most important is the `_ori` table, or its utility view `_orirev`, as they contain the original station raw data. The schema view of this table reveals the following fields.

```
+------------------------+---------------+------+-----+---------+-------+
| Field                  | Type          | Null | Key | Default | Extra |
+------------------------+---------------+------+-----+---------+-------+
| start_date_time        | datetime      | NO   |     | NULL    |       |
| length_time_interval_s | decimal(10,0) | YES  |     | NULL    |       |
| uncorrected            | double        | YES  |     | NULL    |       |
| corr_for_efficiency    | double        | YES  |     | NULL    |       |
| corr_for_pressure      | double        | YES  |     | NULL    |       |
| pressure_mbar          | double        | YES  |     | NULL    |       |
+------------------------+---------------+------+-----+---------+-------+
```

Most of them are self explanatory. The first one `start_date_time` is the time stamp of the measurement, expressed as year, month, day, hour, minute, and second in Universal Coordinated Time. The `length_time_interval_s` is the length of the measurement time interval in seconds. Typically this value is 60, as this is the goal resolution of all the neutron monitors in the network. The next three fields are versions of the counts of the station.

uncorrected this is the raw value resulting from the data editor implemented in each station. In the chapter 4 of this document there is a description about the data editor used in CaLMa and some other stations.

corr_for_pressure this the raw value corrected to account for the atmospheric pressure effect on the counts.

corr_for_efficiency this is the raw value, corrected for pressure and also corrected by some other factor about the station itself. This is used by the station owners to adjust the counts when there are changes in the measurement conditions, i.e. changes in the instrument, changes in the environment, etc.

pressure_mbar this the atmospheric pressure in millibars.

Finally there is a common table for all the stations called `station_information` that has a row for each station for storing general data such as the station full name, the contact information, latitude and longitude, geomagnetic cutoff, etc.

2.3 Worst case scenario for the data acquisition system

In this section we will use the data from NMDB to get an estimation of the required limits of operation of a data acquisition system for a neutron monitor, specially in the higher count limit that the acquisition system must address.

Every time that a neutron is detected the amplifier generates a digital pulse. The old BP28 amplifier and the new ACHNA98 generates a fix width pulse of about $22\mu s$, but there are new interesting design alternatives in which the pulse is variable as a function of the energy of the acquired pulse. This is the case of the New Hampshire's University amplifier that generates a pulse with a variable width ranging from $15\mu s$

to $50\mu s$, depending on the energy of the originating particle[1]. The main goal of the data acquisition system is to count and measure these pulses.

The NMDB Consortium stated that the stations should provide data every minute, and therefore the data acquisition system has to be able to count the number of events that happen at least in one minute per counter tube. To provide a worst case scenario, we will study next what is the highest count ever recorded in the NMDB data.

The galactic cosmic rays (GCR) flux is the main source of the neutrons detected by neutron monitors, this flux can vary in average about a 2% with respect the mean of the count rate, when there are not significant solar events in progress, but this rate can vary in far more than 10% under special solar activity conditions. Also this flux follows a long term variation influenced by the solar activity cycle, with a clear periodic behavior with a period of 11 years, in coincidence with Sun spot number, and with a period of 22 years related to the global solar magnetic field inversion.

The figure 2-1 shows the energy distribution of the neutron flux recorded in the german station of Koldewey, in Spitsbergen, from January to February 2008[20]. This plot shows three peaks, being the first one the Maxwell-Boltzmann peak that is due to thermalized neutrons, then there is a flat region, followed by two peaks of 10 MeV and 100 MeV which originate in secondary products of the interaction of cosmic rays in the higher parts of the atmosphere.
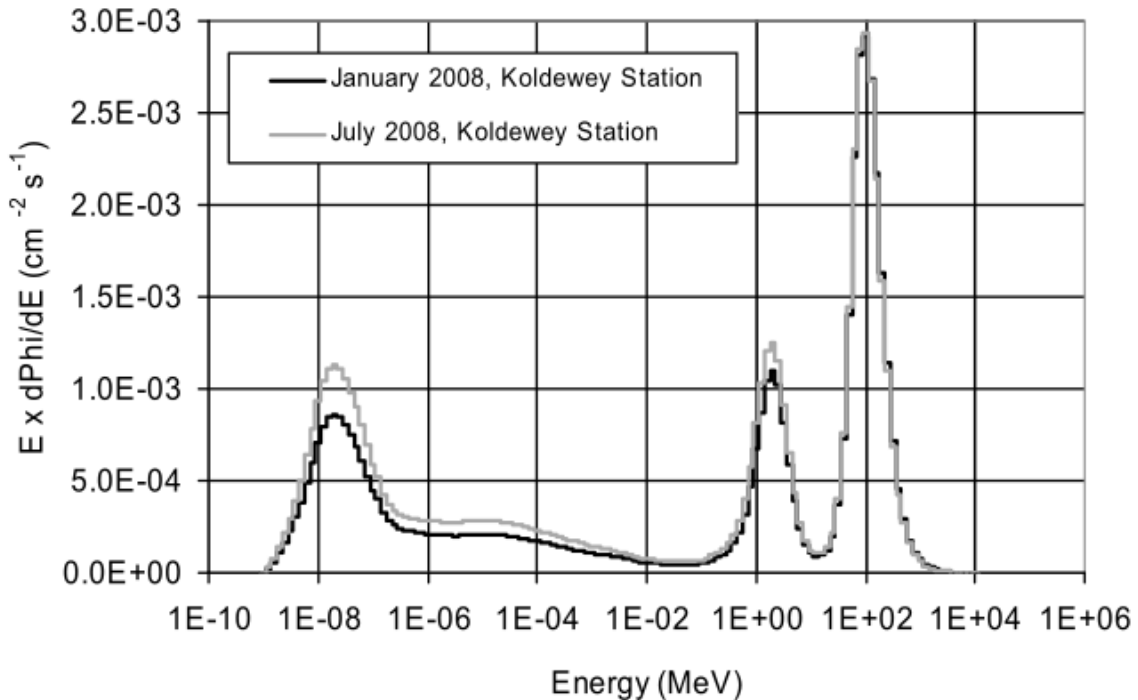

Figure 2-1: Energy flux distribution of the cosmic rays in the Koldewey.

---

[1]This is an unpublished work and this values come from informal personal communications with the author

The moments with the highest count rates are these when a *ground level enhancement* or GLE is in progress. These enhancements are produced by solar particles with energies higher than some hundreds of MeV usually related to the strongest solar flares.

There is not a precise definition of what level of increase it is to be considered a GLE, but several authors have come out with different algorithms and expressions to determine the presence of a GLE for their alarm systems, for example, a 4% increase recorded at three stations in 3 min averaged data[13], or a number of times the standard deviation of the baseline level of a given station[19]. Another commonly accepted by the cosmic rays community since the 1970s is as follows:

> A GLE event is registered when there are near-time coincident and statistically significant enhancements of the count rates of at least two differently located NMs

But after the start of operation of high altitude polar stations such as the South Pole Neutron Monitor and DOMC/DOMB stations, a new definition was needed. These stations have a negligible geomagnetic cutoff rigidity, and since they are in high altitude, they have much less atmospheric attenuation than the sea-level stations. These two things make high altitude polar stations extremely sensible to Solar Energetic Particles, and therefore they together detect events that would be classified as GLE while not being detected by any sea-level station. This new events would distort the historical GLE list and new GLE could not be compared with the previous. This is the reason why the GLE had to be reformulated, and also why the Sub-GLE definition was introduced [17]. According with these authors, the new GLE definition is:

> A GLE event is registered when there are near-time coincident and statistically significant enhancements of the count rates of at least two differently located neutron monitors including at least one neutron monitor near sea level and a corresponding enhancement in the proton flux measured by a space-borne instrument(s).

In their article, they also propose a suitable definition for Sub-GLE:

> A sub-GLE event is registered when there are near-time coincident and statistically significant enhancements of the count rates of at least two differently located high-elevation neutron monitors and a corresponding enhancement in the proton flux measured by a space-borne instrument(s), but no statistically significant enhancement in the count rates of neutron monitors near sea level.

At the time of writing the GLE database is maintained by the University of Oulu in Finland. The first GLE was labeled as `#5 GLE` in 1956-02-23, and the last as `#72 GLE` in 2017-09-10. There are also five Sub-GLE, the first dated on 2012-01-27 and the last on 2015-10-29.

The NMDB keeps a table with information about when was the onset of some registered GLE, starting in February 1942 and ending with the last one registered in September 2017, by the time this document was written.

We have calculated what was the max count registered in all GLE in all stations that have data in these dates. The data obtained are the counts per second in each station. In order to get the count per counter tube per minute, this data has been converted to counts per minute and has been divided by the number of counter tubes of each station, assuming that the counts are equally distributed among the tubes. The number of counter tubes per station is also available in the NMDB. With this procedure we can get only an approximation of the real count rate per counter tube, because the rate in counts/s published in NMDB is the result of applying an algorithm, generally known as data editor, that is particular to each station.

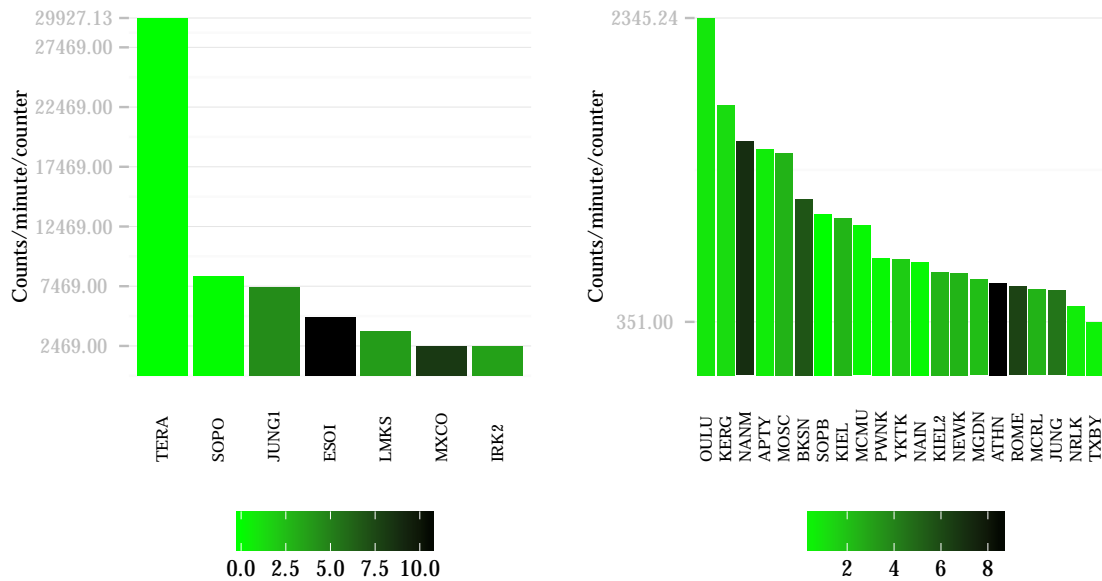The bar chart in fig 2-2 shows the results obtained.

Figure 2-2: Maximum count rate registered in all GLE for all the stations.

In the left chart of the figure 2-2 we can see the maximum registered, observed through all the data available, of all the station which counts were above the 3rd quantile, and in the right the rest of the stations.

The maximum value was registered by TERA which is the Terre-Adélie French neutron monitor in Antarctica, $66°39'S$, $140°"E$ at 32 m ASL, that has an effective vertical cutoff rigidity of 0.0 GV. The maximum peak for this station happened on GLE69, (2005/20/01 6:51 UTC). It was increase of about 4400% above of its normal base line of 111.6 counts/s. At 06:54 hours it reached a maximum of 4489.07 counts/s, given that it has 9 counter tubes, then $4489.07 * 60/9 = 29926$ counts/min. The figure 2-3 and the table 2.1 shows this result and a comparison with other stations for the
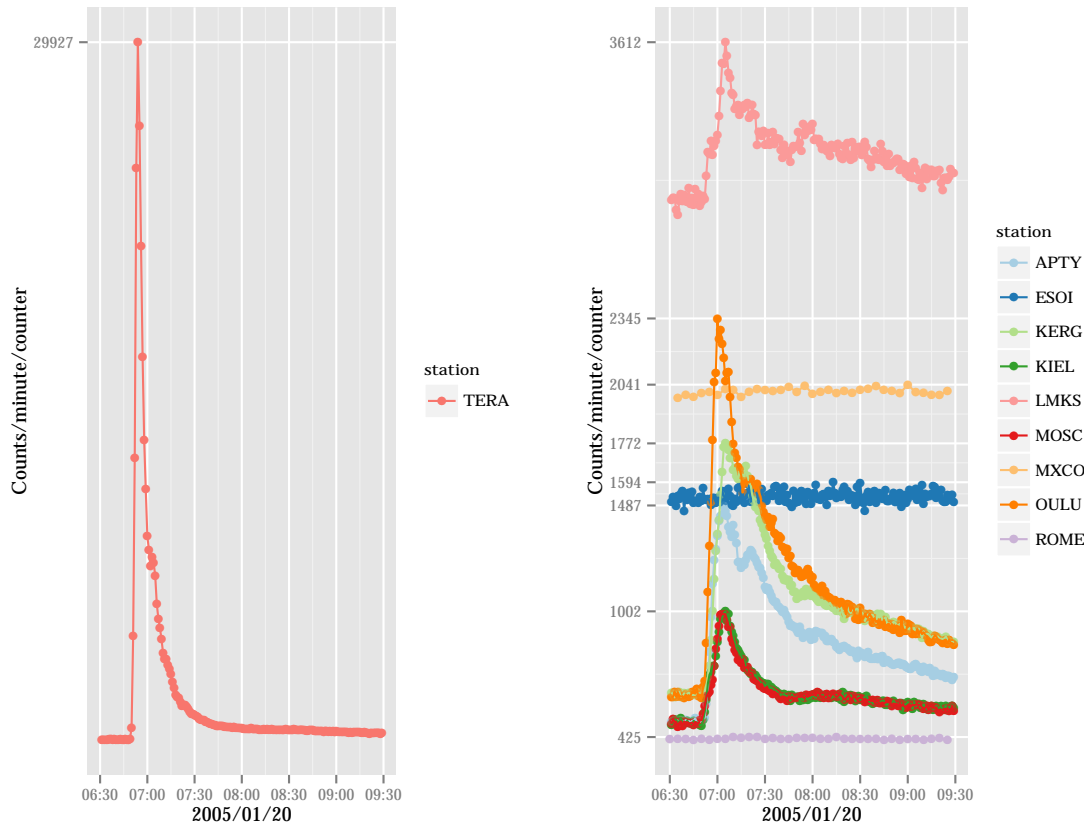
same event.

Figure 2-3: GLE in TERA and in other stations.

The right box plot in figure 2-4 shows the values without the large increment of TERA, so they can be rescaled. Putting away this value, the median for the maximum count is much lower, close to 1000 counts per minute per counter, and the 50% of the stations maximum values lie between 1534 and 629. Despite all this, GLE are intrinsically exceptional, happening one per year in approximately, and so are the values reached during them. These values can be considered as the worst case scenario that the data acquisition system would cope with.

2.4   Forbush decreases

Forbush decrease[9] (FD) is a very common phenomenon in the readings from a neutron monitor. It is a significant drop in the counts of a neutron monitor during some hours, and a slow recovery during some days. The reduction, that can be between of 10% and 30% of the baseline, is related with the strength and the size of the magnetic field, and the speed and deceleration of a Interplanetary Coronal Mass Ejection (ICME). This is also shown in the paper presented in this chapter, Observable

	station	base	max	incr
1	APTY	498.93	1487.67	198.17
2	ESOI	1521.71	1594.20	4.76
3	KERG	622.16	1772.37	184.87
4	KIEL	495.56	1002.11	102.22
5	LMKS	2886.94	3612.13	25.12
6	MOSC	491.14	989.18	101.40
7	MXCO	1989.00	2041.67	2.65
8	OULU	616.14	2345.24	280.64
9	ROME	416.55	425.71	2.20
10	TERA	653.23	29927.13	4481.44

Table 2.1: Counts increase during GLE69

Effects of Interplanetary Coronal Mass Ejections on Ground Level Neutron Monitor Count Rates[3],

To study the relationship between ICME and the FD that they unchain, 59 ICME events were selected, out of a list by Gopalswamy et al. (2010) proposed during the Living With a Star Coordinate Data Analysis Workshop hosted in San Diego (2010) and Alcalá (2011). To analyze the characteristics of these FDs, the measurement of some neutron monitor stations have been retrieved from the Neutron Monitor Database. The figure 2-5 shows the representation of one FD recorded in the OULU station in september 2005. It represents the number of counts per minute registered during the days before and after the FD. Over the cloud of points, an smoothed curve has been adjusted to help to visualize the overall tendency of the counts during this phenomenon. The solid horizontal line show the baseline of the station during the previous days of the event, and the dashed one is set 10% below of this base line. This lines are a visual aid to identify the drop in the counts in this FD.

The following article, *Observable Effects of Interplanetary Coronal Mass Ejections on Ground Level Neutron Monitor Count Rates*, by Juan José Blanco, Edwing Catalán, Miguel Ángel Hidalgo, José Medina, Javier Rodríguez-Pacheco and myself, was published in Solar Physics in 2013. In this year, the Journal Citation Reports assigned an index impact factor of 3.014 to this journal, and the Astronomy and Astrophysics category was placed in the second quartile (Q2). By the time this work was written, Google Scholar showed 17 cites for this article, and Scimago classified the journal in the first quartile (Q1) in two categories: Space and Planetary Science and Astronomy and Astrophysics.
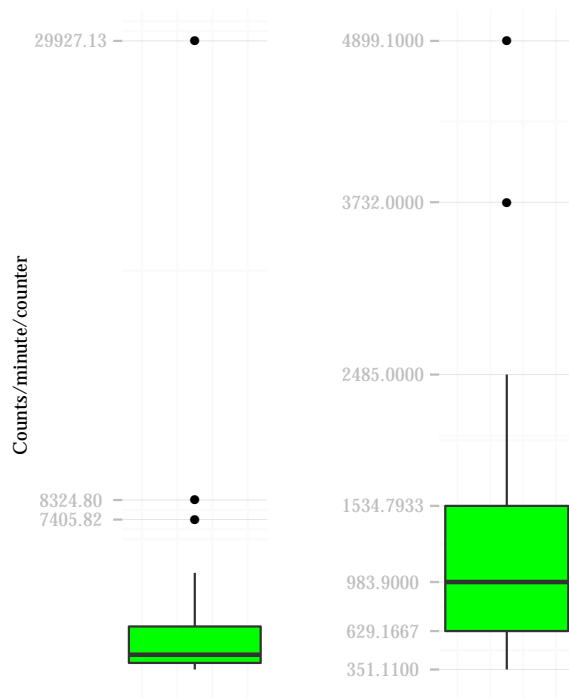
Figure 2-4: Boxplot statistics for the maximum count per minute per counter tube in all the available data.
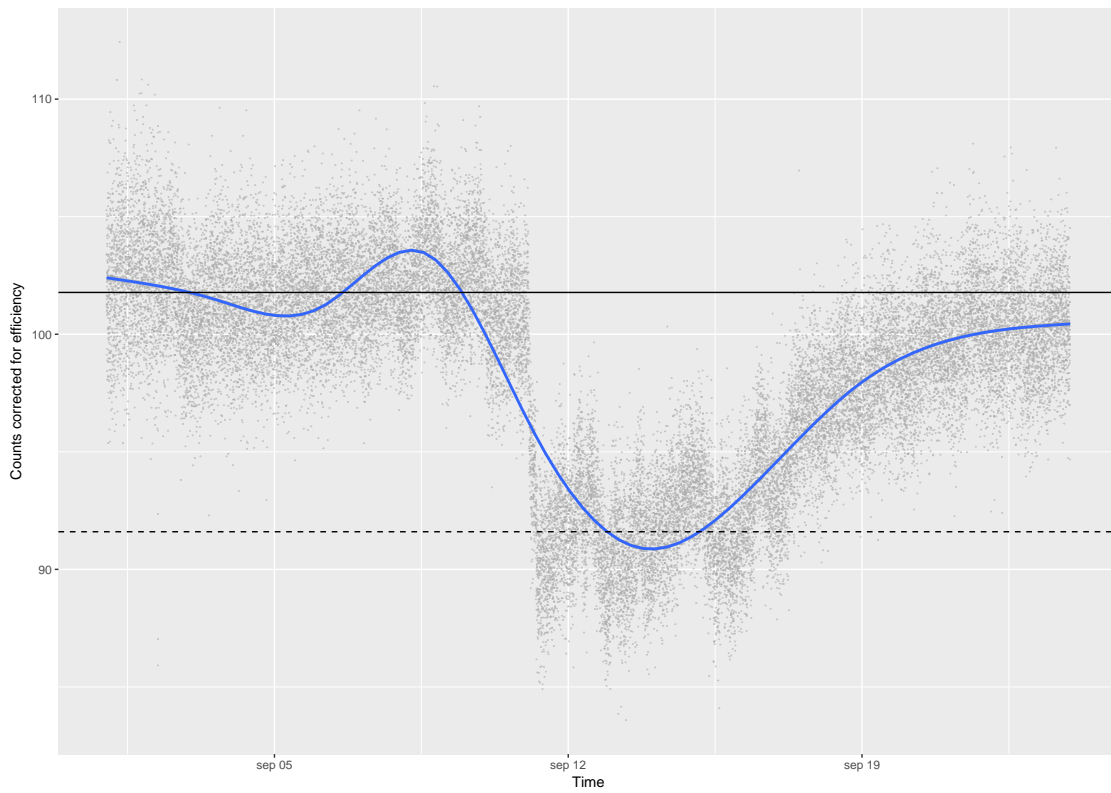
Figure 2-5: A Forbush decrease as seen by OULU in september 2005

Observable Effects of Interplanetary Coronal Mass Ejections on Ground Level Neutron Monitor Count Rates

J. J. Blanco, E. Catalán, M. A. Hidalgo, J. Medina, O. García & J. Rodríguez-Pacheco

ONLINE FIRST

Solar Physics

283/1

Image Processing in the Petabyte Era
Guest Editors: J. Ireland and C.A. Young

Springer

ISSN 0038-0938

Springer

FLUX-ROPE STRUCTURE OF CORONAL MASS EJECTIONS

Observable Effects of Interplanetary Coronal Mass Ejections on Ground Level Neutron Monitor Count Rates

**J.J. Blanco · E. Catalán · M.A. Hidalgo · J. Medina ·
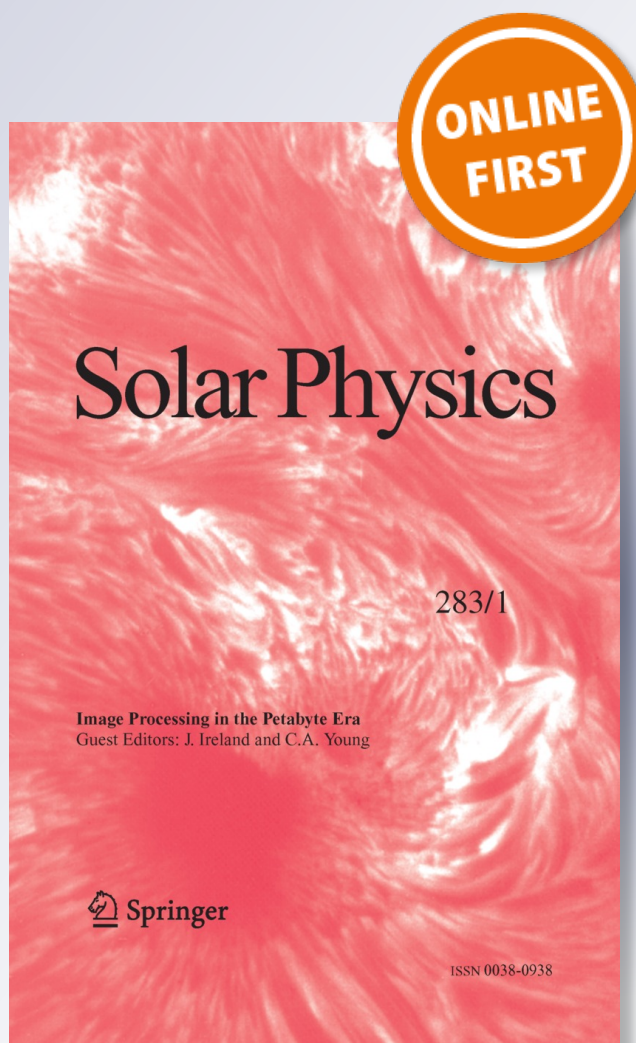O. García · J. Rodríguez-Pacheco**

Abstract In this work, non-recurrent Forbush decreases (FDs) triggered by the passage of shock-driving interplanetary coronal mass ejections (ICMEs) have been analyzed. Fifty-nine ICMEs have been studied, but only 25 % of them were associated to a FD. We find that shock-driving magnetic clouds (MCs) produce deeper FDs than shock-driving ejecta. This fact can be explained regarding the observed growing trends between decreases in neutron monitor (NM) count rate and MC/ejecta speed and its associated rigidity. MCs are faster and have higher associated rigidities than ejecta. Also the deceleration of ICMEs seems to be a cause for producing FDs, as can be inferred from the decreasing trend between NM count rate and deceleration. This probably implies that the interaction between the ICME traveling from the corona to the Earth and the solar wind can play an important role in producing deeper FDs. Finally, we conclude that ejecta without flux rope topology are the ones less effective in unchaining FDs.

1. Introduction

Ground level neutron monitors (NMs) are able to monitor the galactic cosmic ray (GCR) fluxes arriving to the Earth surface with energies between 0.5 to 20 GeV (Simpson, 2000). The geographical location of a NM determines the minimum energy of GCRs that reach each

J.J. Blanco (✉) · E. Catalán · M.A. Hidalgo · J. Medina · J. Rodríguez-Pacheco
Space Research Group, Physics Department, Alcalá University, Ctra. Madrid-Barcelona km 33.600,
28871, Alcalá de Henares (Madrid), Spain
e-mail: juanjo.blanco@uah.es

O. García
Space Research Group, Computing Engineering Department, Alcalá University, Ctra.
Madrid-Barcelona km 33.600, 28871, Alcalá de Henares (Madrid), Spain

Springer

station. This is traditionally quantified by the geomagnetic cutoff expressed in GV. Particles with less magnetic rigidity than the NM geomagnetic cutoff cannot reach the monitor. The NM count rate can be strongly affected by solar flares (Firoz *et al.*, 2011), coronal mass ejections (CMEs) (Gopalswamy *et al.*, 2012) and solar wind structures such as interplanetary coronal mass ejections (ICMEs) (Jordan *et al.*, 2011), interplanetary shocks (Cane, Richardson, and von Rosenvinge, 1994), and interaction regions (Richardson, Wibberenz, and Cane, 1996). While the first two can produce a significant increase in the NM count rate, known as ground level enhancement (GLE) (Shea and Smart, 2012), the other three may induce decreases in NM count rate called Fosbush decrease (FD). These FDs can be divided into recurrent or non-recurrent, depending on if they are observed along several solar rotations and are associated with corotating stream interaction regions (Richardson, Wibberenz, and Cane, 1996) or if they last for several days and are caused by transient events as interplanetary shocks or ICME passages (Cane, 2000 and Belov, 2008). In this work we focus on non-recurrent decreases and we will refer to them as FDs. A Forbush decrease (FD) is observed as a decrease in the cosmic ray intensity and it was first reported by Forbush (1937). It is characterized by a fast decrease, as much as 20 % in the order of hours, and a slow recovery phase that can last several days. As a first approach, it can be assumed that the decreases in the cosmic ray counts are due to changes in the propagation conditions at the surrounding region where the FD is observed. It can be said that FD is a local phenomenon restricted to a small region when compared with the whole heliosphere. These changes can be related to enhancements in solar wind speed, variation in the magnetic field topology, enhancements in the interplanetary magnetic field magnitude, and the presence of magnetic turbulence. ICMEs are large structures (around 0.1 AU) that propagate at high speeds (up to 2000 km s^{-1}) and produce shocks and magnetic turbulence in the background solar wind. Moreover, about one third of ICMEs show a closed magnetic topology defined by a relatively strong magnetic field and a smooth field rotation which is usually known as magnetic cloud (MC) (Burlaga *et al.*, 1981; Lepping, Jones, and Burlaga, 1990). It is generally accepted that an ICME passage can produce decreases in the count rate of NMs (Cane, 2000; Ifedili, 2004; Papaioannou *et al.*, 2010). These decreases are short-term events with the decreasing phase lasting for about one to two days and the recovery phase over one week of duration.

During a shock-driving ICME passage, the shock may initiate a decrease in NM counts maintained along the sheath region, *i.e.*, the highly turbulent region between the shock and the ICME. This decrement can be steeper at leading edge of the ICME. This scenario is path dependent. This means that depending on the trajectory of the spacecraft or the Earth through the shock/ICME structure one of these two effects might not be observed (Richardson and Cane, 2011).

The FD shape may vary from one event to another, especially if complex structures converge on the observation point. Jordan *et al.* (2011) point out that each FD has to be studied separately and that small-scale structures, between shock and ICME, can greatly affect the FD shape and question the two-step FD picture.

To answer the question "do all the CMEs have a flux rope structure?" we proposed to analyze a list of 59 shock-driving ICMEs extracted from Gopalswamy *et al.* (2010) during Solar Cycle 23 during the Living With a Star Coordinate Data Analysis Workshop hosted in San Diego (2010) and Alcalá (2011). This subset (these 59 events) was selected using a CME source region criterion (E15° $\leq$ source longitude $\leq$ W15°). This roughly implies that only CMEs from the central solar disk region were considered. Although the main goal in this workshop was the study of the magnetic structures observed into ICMEs, we investigated the role of these structures in the propagation of cosmic rays, especially during their arrival at Earth.

In this work we analyze the effect of the ICME passage on Oulu NM station count rates with the goal to study which part of an ICME, *i.e.*, shock, MC or flux rope, magnetic field magnitude and induced turbulence plays the most important role in producing observable FDs.

2. Data Analysis

The 59 shock-driving ICMEs selected from the list in Gopalswamy *et al.* (2010) has been studied from January 1997 to September 2006. In 24 of them, clear signatures of MC were found. We considered that an MC has been detected when the solar wind follows the Burlaga criteria (Burlaga *et al.*, 1981; Lepping, Jones, and Burlaga, 1990), *i.e.* low temperature, smooth magnetic field rotation combined with intense magnetic field, and the magnetic field can be fitted with Hidalgo's model (Hidalgo and Nieves-Chinchilla, 2012). The other 35 events did not show clear evidence of an MC, but a depression in solar wind proton temperature is observed with low plasma beta. Generally speaking, we named them ejecta (Ej). If the magnetic field within the Ej is organized as a flux rope that can be fitted by Hidalgo's model, then this Ej is cataloged as ejecta plus (Ej+), and ejecta minus (Ej−) in the opposite case. The ICME pool was separated into MC (24), Ej+ (23) and Ej− (12). The details of this classification can be found in Hidalgo, Nieves-Chinchilla, and Blanco (2013).

Key parameters with a time resolution of 92 s from the *Solar Wind Experiment* (SWE) (Ogilvie *et al.*, 1995), 1 min time resolution data from the *Magnetic Field Instrument* (FMI) (Lepping *et al.*, 1995) on board the *Wind* spacecraft, 64 s time resolution data from the *Solar Wind Electron, Proton, and Alpha Monitor* (SWEPAM) (McComas *et al.*, 1998), and 4-min resolution data from the magnetic field experiment (MAG) (Smith *et al.*, 1998) on board ACE spacecraft have been used. Data have been retrieved from the CDAWeb web page. In this work, it is assumed that an FD is observed when the NM count rate decreases more than 3 % below the GCR background measured before the shock arrival. Because of its relative low geomagnetic cutoff (0.81 GV), cosmic rays arriving with energies higher than some hundreds of MeV are detected by the Oulu (Finland) NM. Counts of 5 min of time resolution from Oulu have been used (Kananen *et al.*, 1991). This station is located at 65.05°N, 25.47°E and at 15 m above sea level. The monitor is made up by 9 NM-64 tubes. The data from this station have been collected from the Neutron Monitor Database (NMDB) (Mavromichalaki *et al.*, 2011) that integrates the readings of many different NM stations located mainly in Europe and Asia. The high-count cadence lets us perform comparable observations with measurements acquired by space-borne instruments with similar temporal resolution to the one used in our analysis of MC magnetic structure. Although using 5-min NM data is not the standard approach to study FDs, where hourly averaged measurements are commonly used (*e.g.* Cane, 2000; Usoskin *et al.*, 2008; Papaioannou *et al.*, 2010; Richardson and Cane, 2011), this high-count cadence is required to make a direct comparison between the results given by Hidalgo's model, *i.e.* MC and/or Ej+ existence and limits, and the role of MCs, Ej+ and Ej− on the depth of FDs.

Only 15 ICMEs from the selected sample of 59 triggered the detection of an FD in the Oulu NM. Eight of them were MC and other six Ej+. Only one Ej− was able to induce an observable FD at Oulu. The latter Ej was preceded by a strong interplanetary shock. It is clear that flux ropes (MC or Ej+) within ICMEs play a crucial role in producing FD (94 % of FD associated with flux ropes). The decrease percentage of the resulting FD ranged between 5.2 % and 26.1 %, those related to MCs being deeper (Table 1). The transit time, *i.e.* the time that it takes a CME to arrive at Earth, has been calculated using the onset times from the

Table 1 ICME associated with FD. The columns give the year, time interval between the MC nose and its rear as estimated by Hidalgo's model, CME transit time, magnetic rigidity cut off associated with the flux rope, FD percentage, and FD location within the ICME. The asterisk in MC* means a complex event where two consecutive MCs were observed but the FD is not resolved into two separate events.

Year	ICME interval (doy)	Type	Travel time (day)	Rigidity (GV)	FD (%)	FD location
1998	124.442 → 125.234	Ej−	1.95	167	7.5	Ejecta
1999	178.942 → 179.108	Ej+	3.38	27	6.24	Sheath
2000	197.911 → 198.298	MC	1.46	419	16.00	Ejecta
2000	261.221 → 262.599	MC	1.77	283	8.86	Ejecta
2000	311.964 → 312.74	MC	3.2	215	6.96	Ejecta
2000	332.458 → 333.131	Ej+	3.23	80	9.01	behind Ej+
2001	102.367 → 103.279	MC*	2.14	139	12.63	Ejecta
2001	118.892 → 119.662	MC	2.37	106	8.17	Sheath
2001	285.205 → 285.360	Ej+	2.73	24	7.67	Sheath
2003	302.554 → 303.151	MC*	1.07	162	26.13	Ejecta
2004	22.558 → 23.282	Ej+	2.55	142	10.09	Sheath
2004	315.195 → 315.705	MC*	4.11	188	12.42	Sheath
2005	135.464 → 136.004	MC	1.75	354	11.89	Sheath
2005	149.495 → 149.638	Ej+	2.6	27	6.10	Ejecta
2006	232.630 → 233.625	Ej+	3.94	80	5.24	Ejecta

LASCO CME list (http://cdaw.gsfc.nasa.gov/CME_list/) and the ICME *in-situ* times using measurements from instruments on board the *Wind* and ACE spacecraft. From Table 1, it seems that the shorter the travel time, the deeper the FD. This will be discussed in the next section. In our list of 15 ICMEs connected to CMEs from the central region of solar disk, the deepest GCR decrease rate was measured in eight events during the ejecta's passage, in six events during the ICME sheath's and one behind the ejecta's passage. Only in three events, 12 April 2001, 29 October 2003 and 10 November 2004, the FDs could have been affected by other structures. The former two during their recovery phases, because of the presence of a subsequent interaction region and a later ICME, respectively, and the third during its main phase due to a previous ICME which reduced the GCR level before the 10 November MC's arrival. Five events produced decreases higher than 10 %. All of them were ICMEs with MC and in three of them some interaction with previous or subsequent structures might have happened, as has been explained above.

For every event, the shock strength, the Ej size, its mean speed and mean magnetic field have been computed. As an example, the analysis of two events is shown in detail. On 15 May 2005 a shock arrived at *Wind*'s location ($X_{\mathrm{GSE}} = 200\ R_{\mathrm{E}}$, near L1) followed by a sheath and three hours later by an ICME with an MC structure. The ICME front is marked by a jump higher than 30 nT and a fast field rotation (less than 4 h) characterized by an elevated thermal speed. This region coincides with the deepest point in the FD measured by the Oulu NM. At the MC nose, *i.e.* when the field begins to rotate due to the MC passage, a magnetic field intensity of 55 nT and a speed of 990 km s^{-1} were observed. Under these conditions, the ICME reached the Earth 23 min later. The arrival of the shock at Earth was observed in coincidence with a steep decrease in the counts measured at Oulu, triggering a clear FD (Figure 1, bottom panel, where 5-min Oulu NM data have been smoothed using a

Figure 1 Example of an ICME with an MC. Data from the *Wind* spacecraft and the Oulu neutron monitor have been used.
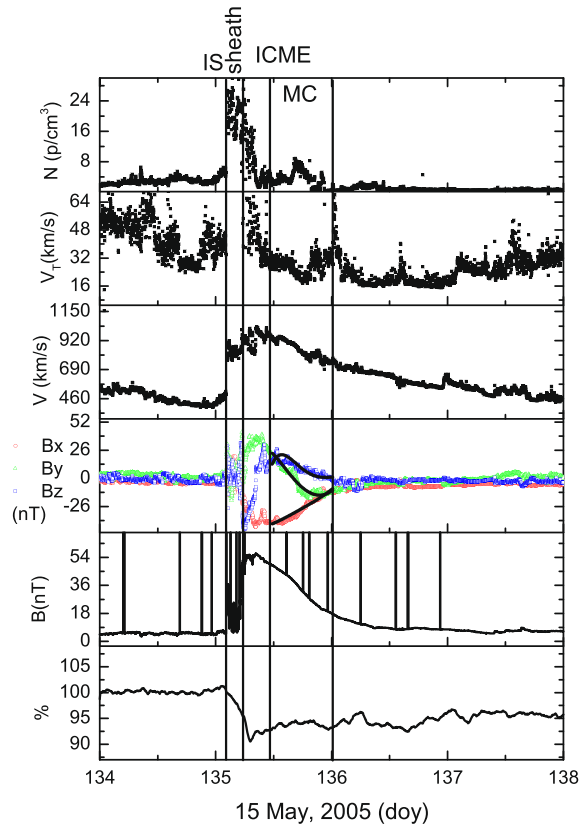

1-h running average). At ICME front arrival, the FD slope changed, clearly being the second step in this particular FD. In the figure, divided into panels, we show from top to bottom:

 i) solar wind density,
 ii) thermal velocity,
 iii) solar wind speed,
 iv) magnetic field components in GSE system (red circles B_x, green triangles B_y and blue squares B_z) over plotted with continuous lines, which are Hidalgo's model results,
 v) the magnetic field strength, and
 vi) the percentage of the normalized NM count rate.

The decrease was even steeper when the ICME leading edge hit the Earth. The FD's deepest point was measured within the fast rotating region before the MC nose arrival, and a soft recovery phase started during the MC passage (marked with vertical lines in Figure 1). The FD lasted more than five days until the previous neutron monitor count rate was recovered (doy 140, not shown in Figure 1). The MC showed a well-organized magnetic flux rope. This is clear when comparing to the over plotted continuous lines which show Hidalgo's model results. During this FD, the count rate dropped to 12 % with respect to the GCR background before the shock arrival, following, in our opinion, a two-step FD shape. This event has been analyzed by Dasso *et al.* (2009) in terms of the magnetospheric response. They argue for the

Figure 2 Example of an ICME with Ej+. Data from the ACE spacecraft and the Oulu neutron monitor have been used.
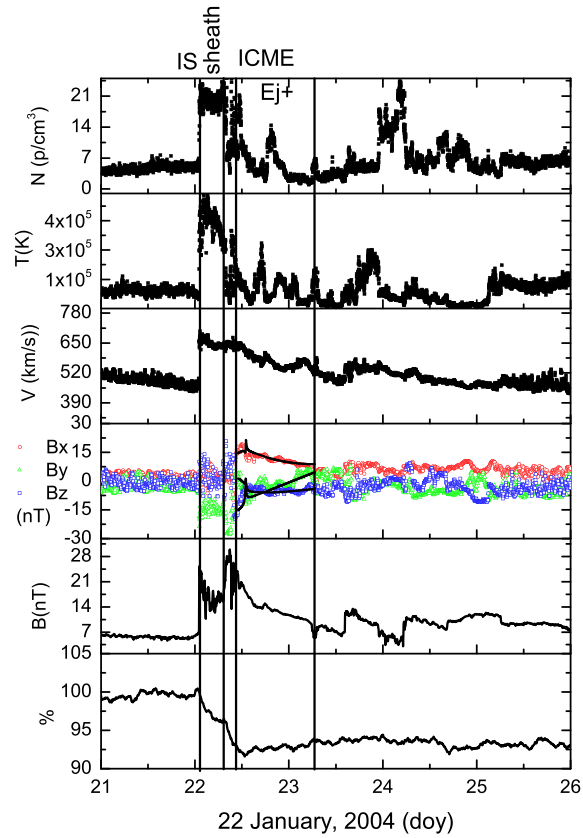
presence of two consecutive MCs. The first one in coincidence with the fast-rotating region mentioned above and the second one with the MC presented in Figure 1. In our opinion, the temperature is too high to be sure that such a rotation may result from a small MC.

On 22 January 2004 a shock arrived at *Wind*'s location in $(-210, 42, -2)$ Earth radii in GSE coordinate system, *i.e.* on the night side of the Earth. To avoid possible interactions with the magnetotail, data from the ACE spacecraft have been used to analyze this event. ACE was located at L1. This event is shown in Figure 2. Plots are organized as in Figure 1. There is one difference though. In the second panel from the top the proton temperature appears instead of the thermal speed. As in Figure 1, the Oulu count rate has been smoothed using a running average of 1 h to get a clearer structure of the FD. The FD started with the interplanetary shock arrival. During the sheath between the shock and the ICME front the NM counts were reduced by 4 %. Six hours later, when the ICME arrived, a change in the FD slope was detected. Two hours later the flux rope nose, confirmed by Hidalgo's model (continuous lines in Figure 2), was observed. The FD minimum and the beginning of the recovery phase occurred within the flux rope. The Ej were characterized by a mean magnetic field of about 10 nT with a smooth field rotation that lasted almost one day and a solar wind speed of 600 km s^{-1} in the low solar wind temperature region. As for the FD shape, it showed a two-step behavior with a harder slope in coincidence with the ICME leading edge passage. The recovery phase was slower than that seen in Figure 1, lasting up

to 10 days. The neutron monitor registered a decrease of 10 % of its counts compared to the GCR background on 21 January.

3. Results

The FD depth can be influenced by various ICME properties. One of the possible causes of an FD can be the size of the magnetic structure and the intensity of its magnetic field. Cane (1993) found a clear correlation between the percentage decrease of GCRs and the magnetic field strength in the ICME. The effect of these two elements can be evaluated by the expression $R = Brc$, which gives the magnetic rigidity in GV, B being the magnetic field intensity, r the particle gyroradii and c the light speed. We assume the value of B to be the mean value inside the ICME and r the size of the ICME section because the particle gyroradius has to be in the order of this size to be affected in its normal movement. In a recent paper, Kubo and Shimazu (2010) analyzed the effect of a finite Larmor radius on GCR penetration into flux ropes, concluding that it can be relevant at 1 AU. The mean B and the structure size have been computed using Hidalgo's model both for MCs and Ej+. As for the only Ej−, its size was assumed to be equal to the size of the ICME. The resulting plot of the FD minimum *versus* the estimated rigidity is presented in Figure 3a. Red circles represent MCs, blue triangles Ej+, and the green square Ej−. The growing trend of GCR count rate percentage with rigidity is clear, ICMEs with MC being more effective than Ej+ and Ej− in producing FDs. This can be understood, as larger MC sizes and more intense magnetic fields imply higher associated rigidity. One of the MCs (the 29 October 2003 event) showed a percentage decrease higher than 25 %. Nevertheless, its rigidity was relatively low. This event had a sheath with a magnetic field as high as 50 nT and an MC mean field of only 12 nT. In this event, the role of the sheath seems to be more important than that of the MC in terms of reducing the Oulu NM count rate.

It can be argued that the shocks observed ahead of some ICMEs play an important role in the FD depth themselves, but what we observed in Figure 3b is that those shocks associated with MCs are related to deeper FD. The shock strength is defined here as the ratio of the difference between the downward and the upward magnetic field at shock passage. It is important to point out that the shock driven by the Ej− (green square) was the third more intense, but it only caused a modest FD of 7 %. The conclusion that can be extracted from Figure 3 is that an MC strengthens the shock effect on the neutron monitor count rate. A red continuous line and a blue dashed line are the linear fits to MCs and Ej+ with slopes of 13.6 and 4.7 and Pearson's coefficients (Pc) of 0.76 and 0.66, respectively. The shock triggers the FD but the MC makes it deeper. This result is in agreement with Richardson and Cane (2011) concerning the role that MCs may play in producing FD. Also the observed relationship between Ej rigidity and FDs could support the argument of MCs being closed magnetic structures.

Another important parameter that deserves to be studied focusing on the causes of FDs is the speed of the ICME. There are three different speeds that can be associated with the ICME propagation. We have the CME emergence speed that is calculated from coronagraph images, the ICME transit speed that can be estimated from the CME onset time and the ICME arrival time at the spacecraft location and the solar wind speed measured within the ICME. A common conclusion inferred from the three speeds is that the faster CME or ICME, the deeper the FD (Figure 4). This result agrees with those by Richardson and Cane (2011) who used a pool of more than 300 ICMEs. As they affirm in their paper, the dependence of the decrease on the CME/ICME/MC speed can be explained arguing that in faster-propagating
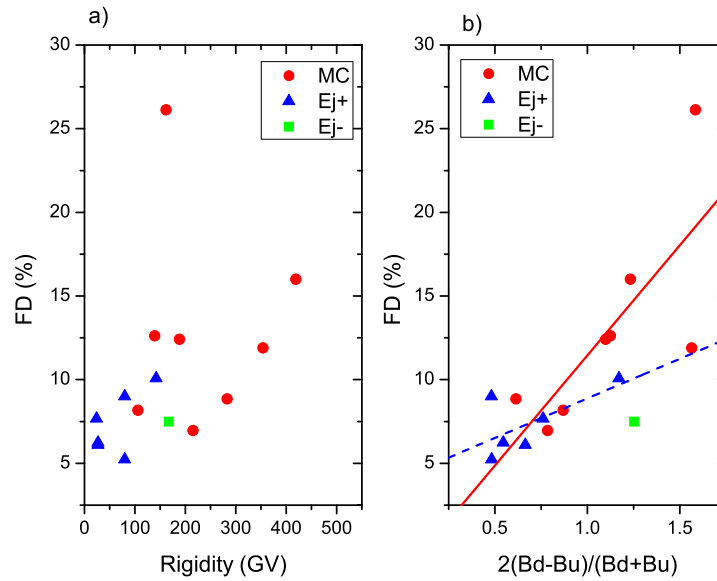
Figure 3 FD dependence on rigidity (a) and shock strength (b).

events GCRs have less time to fill up the closed magnetic structure of an MC. On the other hand, the range of values of the three speeds is different. The CME speed ranges between 300 and 3000 $km\,s^{-1}$ (Figure 4a), the transit speed between 500 and 2000 $km\,s^{-1}$ (Figure 4b), and the solar wind speed between 300 and 1300 $km\,s^{-1}$ (Figure 4c). Again, MCs are, generally speaking, faster than Ej events. On the other hand, taking a closer look at Figure 4c, it is clear that Ej velocities are in a narrow range of 500 $km\,s^{-1}$ (250 to 750 $km\,s^{-1}$) without a clear linear relationship (blue dashed line) with the associated FD ($Pc = 0.33$). Nevertheless, the FDs produced by MCs show a good linear correlation (red continuous line) and a clear growing trend with the MC speed at 1 AU ($Pc = 0.71$).

Non-recurrent FDs are observed by NMs at ground level as local phenomena related to solar wind conditions around Earth, given that most of them can be directly related to the passage of an ICME. No relationship of CME speed, transit speed and FD should be expected other than the dependence between these two velocities on the solar wind speed. Nevertheless, important variations in the speed from the CME onset to the ICME arrival at the Earth are depicted in Figure 4. This can be explained by assuming that an effective interaction between ICMEs and solar wind occurs during the ICME's travel in the interplanetary space (Vršnak, 2001). In almost all the events a deceleration is observed. This deceleration can be due to an effective kinetic energy exchange between the ICME and the solar wind. This exchange can produce intense shock waves and turbulence ahead (sheath) the ICME and therefore make the ICME able to change the propagation conditions of GCRs with energies from hundreds to thousands of MeV. This is expected for propagating diffusive barriers (Wibberenz *et al.*, 1998). The ICME acceleration can be estimated from the difference between the solar wind speed and the CME speed divided by the travel time. In Figure 5, this acceleration is plotted against the percentage decrease of GCRs displaying a clear negative slope. Those ICMEs that are more intensively decelerated produce deeper FDs. Only two of 15 ICMEs show a positive acceleration. Although acceleration could produce an effective
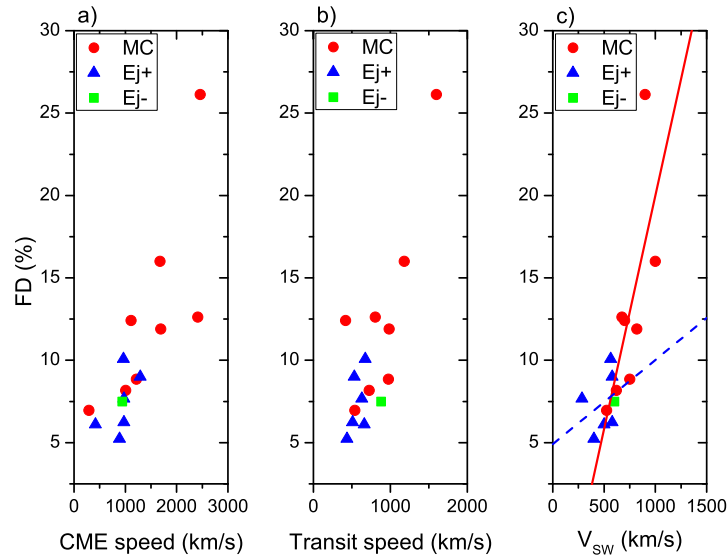
Figure 4 FD dependence on CME speed (a), transit speed (b) and solar wind speed measured during an ICME passage (c).
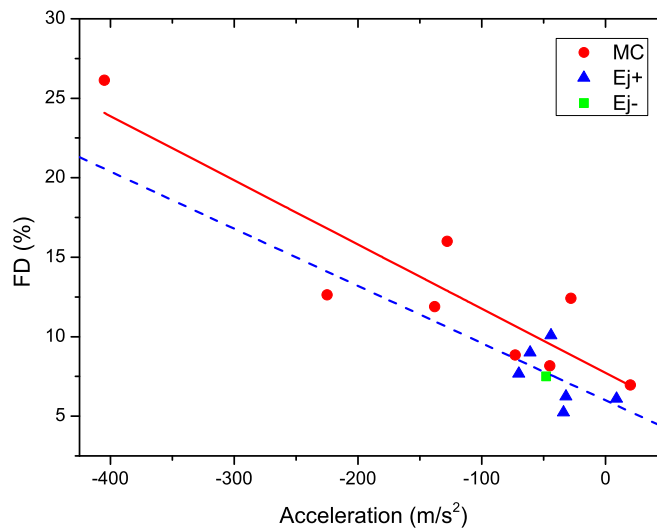

Figure 5 FD dependence on ICME acceleration. This acceleration has been estimated by means of the expression $(V_{SW} - V_{CME}) \times$ ICME travel time.

interaction with the solar wind, two events provide little statistical evidence to affirm that a change in the acceleration slope appears. Moreover, this cannot be considered as a conclusive result because of the uncertainty in CMEs speed estimations. MCs and Ej+ events have

similar slopes (red continuous and blue dashed lines, respectively) of 0.04 and 0.035 but different *Pc*s, -0.89 for MCs and -0.53 for Ej+. MCs are more efficiently decelerated. This may be due to their larger size, more intense magnetic field and higher speed. Moreover, the FD depth is better correlated with MC acceleration than with any other physical quantities considered in this work (rigidity, shock strength, and speed). The deceleration/acceleration of ICMEs plays a very important role in the development of FDs. Intense accelerations imply strong interaction between ICME and solar wind. This interaction drives stronger shocks and makes the solar wind more turbulent. These two features greatly affect the propagation of cosmic rays in the range of the detectable energies by the neutron monitors.

4. Conclusions

The role of CMEs originating from near the center of the solar disk and their associated ICME on FDs detected by the Oulu NM have been analyzed. Cosmic rays with energies higher than a few hundreds of MeV are the main component of the energetic particle population detected by this NM. A pool of 59 shock-driving ICMEs has been classified into three groups, MC (24), ejecta with flux rope (23) and ejecta without apparent flux rope structure (12). Only around 25 % of them were able to produce decreases in the NM count rate higher than 3 %, eight MC, six Ej+ and one Ej−. This result seems to show that an isolated shock is rarely able to produce FD. Moreover, similar shocks may induce stronger FDs if they are driven by an MC or an Ej+. Therefore a closed magnetic structure such as MC or flux rope strengthens the effect of shocks on FDs. Richardson and Cane (2011) reached the same conclusion.

The rigidity associated with MCs and Ej events affects the CGR propagation into ICMEs. This rigidity has been compared with the GCR decreases concluding that higher rigidities are related to deeper FDs. The higher rigidities correspond to MCs because they are larger and their magnetic fields are more intense than those of the Ej events.

The shock strength and its relationship with FD have also been analyzed. Stronger shocks produce higher decreases in the GCR count rate, but when considering similar shocks, those driven by MC are more effective (almost three times more effective) in shielding the Earth from the arriving GCRs. This can be explained assuming that MCs interact more strongly with the underlying solar wind than Ej events driving turbulence into the sheath region and therefore, affecting in a more efficient way the propagation of the GCRs into the ICME.

Another analyzed aspect is the effect of ICME speed on GCR count rates. The observations show that faster structures (MC or Ej) are more efficient to produce FDs, and at least in the sample analyzed, MCs are faster than Ej events. Moreover, FDs associated with ejecta show an increasing trend with CME speed and transit speed but the relation is not so clear with their measured speed at 1 AU ($Pc = 0.33$). As for MCs these three velocities show similar increasing trends with the FD depth and a good correlation between MC speed and FD depth ($Pc = 0.71$). This result is also in agreement with the conclusion by Richardson and Cane (2011).

Finally, we have observed that the deceleration/acceleration of ICME between the Sun and the Earth can play an important role in the development of FDs. Higher decelerations induce deeper FDs. This can be explained in terms of effective energy exchange between the ICME and solar wind. This interaction can lead to the formation of a stronger shock ahead of the ICME. MCs decelerate stronger. Closed magnetic structures as MCs with stronger magnetic field and larger size than those observed in Ej events seem to be more effective in interacting with the solar wind. Moreover, we find the best correlation between deeper

FDs and the MC acceleration. The linear correlation gives a *Pc* equal to -0.89. This value implies that the interaction between MC and solar wind is very important in the shielding effect that an ICME has over GCRs.

Richardson and Cane (2011) propose that MCs are effective in excluding GCRs because they are closed magnetic structures. Our results support this conclusion but also the importance of MC/solar wind interaction on GCR decreases as can be inferred from the clear relationship between MC acceleration and GCR count rates.

Hidalgo, Nieves-Chinchilla, and Blanco (2013) have found that most of the ejecta from the initial list of 59 shock-driving ICMEs showed axes close to the Sun–Earth line. This implies that the passage of the spacecraft through the corresponding ejecta event was probably by its flank and this may be seen as support for the idea of MCs and Ej events being observed at different parts of a flux rope. According to this picture and the results showed in this work we conclude that the effect of shock-driving ICMEs on GCR count rates may also depend on which region of the flux rope hits the Earth.

In conclusion, shock-driving MCs produce deeper FDs than Ej+ and Ej− events, because the MCs have higher rigidity, higher speed, and higher deceleration, and they interact more effectively with the solar wind.

References

Belov, A.V.: 2008, In: Gopalswamy, N., Webb, D. (eds.) *Universal Heliophysical Processes. Proc. IAU Symp. 257*, Cambridge Univ. Press, Cambridge, 439. doi:10.1017/S1743921309029676

Burlaga, L.F., Sittler, E., Mariani, F., Schwenn, R.: 1981, *J. Geophys. Res.* **86**, 6.

Cane, H.V.: 1993, *J. Geophys. Res.* **98**, 3509.

Cane, H.V.: 2000, *Space Sci. Rev.* **93**, 55.

Cane, H.V., Richardson, I.G., von Rosenvinge, T.T.: 1994, *J. Geophys. Res.* **99**, 21429.

Dasso, S., Mandrini, C.H., Schmieder, B., Cremades, H., Cid, C., Cerrato, Y., Saiz, E., Démoulin, P., Zhukov, A.N., Rodríguez, L., Aran, A., Menvielle, M., Poedts, S.: 2009, *J. Geophys. Res.* **114**, A02109.

Firoz, K.A., Moon, Y.-J., Cho, K.-S., Hwang, J., Park, Y.D., Kudela, K., Dorman, L.I.: 2011, *J. Geophys. Res.* **116**, A04101.

Forbush, S.E.: 1937, *Phys. Rev.* **51**, 1108.

Gopalswamy, N., Xie, H., Makela, P., Akiyama, S., Yashiro, S., Kaiser, M.L., Howard, R.A., Bougeret, J.-L.: 2010, *Astrophys. J.* **710**, 1111.

Gopalswamy, N., Xie, H., Yashiro, S., Akiyama, S., Makela, P., Usoskin, I.G.: 2012, *Space Sci. Rev.* **171**, 23.

Hidalgo, M.A., Nieves-Chinchilla, T.: 2012, *Astrophys. J.* **748**, 109.

Hidalgo, M.A., Nieves-Chinchilla, T., Blanco, J.J.: 2013, *Solar Phys.*, in this issue. doi:10.1007/s11207-012-0191-6.

Ifedili, S.O.: 2004, *J. Geophys. Res.* **109**, A02117.

Jordan, A.P., Spence, H.E., Blake, J.B., Shaul, D.N.A.: 2011, *J. Geophys. Res.* **116**, A11103.

Kananen, H., Tanskanen, P.J., Gentile, L.C., Shea, M.A., Smart, D.F.: 1991, In: *Proc. 22nd ICRC* **3**, 145.

Kubo, Y., Shimazu, H.: 2010, *Astrophys. J.* **720**, 853.

Lepping, R.-P., Jones, J.A., Burlaga, L.F.: 1990, *J. Geophys. Res.* **95**, 11957.

Lepping, R.P., Acuna, M., Burlaga, L., Farrell, W., Slavin, J., Schatten, K., Mariani, F., Ness, N., Neubauer, F., Whang, Y.C., Byrnes, J., Kennon, R., Panetta, P., Scheifele, J., Worley, E.: 1995, *Space Sci. Rev.* **71**, 207.

Mavromichalaki, H., Papaioannou, A., Plainaki, C., Sarlanis, C., Souvatzoglou, G., Gerontidou, M., Papailiou, M., Eroshenko, E., Belov, A.A., Yanke, V., Fluckiger, E.O., Butikofer, R., Parisi, M., Storini, M., Klein, K.-L., Fuller, N., Steigies, C.T., Rother, O.M., Heber, B., Wimmer-Schweingruber, R.F., Kudela, K., Strharsky, I., Langer, R., Usoskin, I., Ibragimov, A., Chilingaryan, A., Hovsepyan, G.A., Reymers, A., Yeghikyan, A., Kryakunova, O., Dryn, E., Nikolayevskiy, M., Dorman, L., Pustilnik, L.: 2011, *Adv. Space Res.* **47**, 2210.

McComas, D.J., Bame, S.J., Barker, P., Feldman, W.C., Phillips, J.L., Riley, P., Griffee, J.W.: 1998, *Space Sci. Rev.* **86**, 563.

Ogilvie, K.W., Chorney, D.J., Fitzenreiter, R.J., Hunsaker, F., Keller, J., Lobell, J., Miller, G., Scudder, J.D., Sittler, E.C. Jr., Torbert, R.B., Bodet, D., Needell, G., Lazarus, A.J., Steinberg, J.T., Tappan, J.H., Mavretic, A., Gergin, E.: 1995, *Space Sci. Rev.* **71**, 55.

Papaioannou, A., Malandraki, O., Belov, A., Skoug, R., Mavromichalaki, H., Eroshenko, E., Abunin, A.S., Lepri, S.: 2010, *Solar Phys.* **266**, 181.

Richardson, I.G., Cane, H.: 2011, *Solar Phys.* **270**, 609.

Richardson, I.G., Wibberenz, G., Cane, H.V.: 1996, *J. Geophys. Res.* **101**, 13483.

Shea, M.A., Smart, D.F.: 2012, *Space Sci. Rev.* **171**, 161.

Simpson, J.A.: 2000, *Space Sci. Rev.* **93**, 11.

Smith, C.W., L'Heureux, J., Ness, N.F., Acuña, M.H., Burlaga, L.F., Scheifele, J.: 1998, *Space Sci. Rev.* **86**, 613.

Usoskin, I.G., Braun, I., Gladysheva, O.G., Horandel, J.R., Jamsen, T., Kovaltsov, G.A., Starodubtsev, S.A.: 2008, *J. Geophys. Res.* **113**, A07102.

Vršnak, B.: 2001, *Solar Phys.* **202**, 173.

Wibberenz, G., Le Roux, J.A., Potgieter, M.S., Bieber, J.W.: 1998, *Space Sci. Rev.* **83**, 309.

Chapter 3

The CaLMa design and construction

This chapter is about the design and the construction of the CaLMa Neutron Monitor. CaLMa is located in Guadalajara, Spain, and is made up of four main parts: the counter tubes, the moderator, the producer and the deflector. The counter tubes need a biasing high voltage power supply to operate, so one will be provided to this end, along with a splitter box, so all the tubes will share this same power supply. This same approach will be followed to power the amplification electronics up, one single low voltage power supply shared by all the amplifiers.

In the following sections each of these elements will be described in depth. Also there will be a mechanical description of the overall assembly and the wiring of the station.

3.1 Placement description

CaLMa is located in Guadalajara, Spain (see figure 3-1), $40°38'32.2"N$, $3°9'44.4"W$ at 708 m above sea level), in the basement of the Edificio de Nuevas Empresas. This place is part of the facilities of the Science and Technology Park of Guadalajara (GUADALAB),

Guadalajara is at the East of Castilla-La Manchna region, in the plateau in the center of Spain. It is between the parallels $40°7'N$ and $41°18'N$, and the meridians $1°32'W$ and $3°29'W$, and its weather is mostly continental, with the lowest monthly average temperature of 4.9° in January, and the highest 23.7° in July. The snow days in winter are roughly one on February, and therefore show accumulation is not relevant to the station operation.

The space in where CaLMa is located was initially built to be an office, so the floor has been reinforced in the surface where the Neutron Monitor lies on. The monitor location is isolated with crystal walls from the rest of the laboratory. This isolation allows better control of the room temperature with its own independent HVAC equipment.

Figure 3-1: Geographical location of CaLMa in Spain.

3.2 Neutron monitor design

As it is commented above, a neutron monitor has the goal of measuring neutrons from the interaction between cosmic rays and atmospheric molecules. A neutron monitor is made by concentric layers with different functionalities. From the inner layer to the outermost one, the layers are: the counter tubes, the moderator, the producer and the deflector.

In the next sections each of these elements will be described in more detail.

3.2.1 The counter tubes

Neutrons are non-charged particles that are difficult to detect. Some nuclei are able to capture them in an unstable compound, that turns in two new electrically charged nuclei. These charges can then be detected using electric fields. The detectors in the CaLMa station are based on the fact that some chemical compounds interacts with neutrons, being the products of this interactions easier to detect and measure than the neutrons themselves.

The `cross section` is defined as the area in which two particles must meet in order to interact with each other, and it is measured in barn (1 barn $= 10 \times 10^{-28}$ m^2). When talking about interacting with neutrons, the likelihood of this interaction is therefore proportional to the cross section. There are two elements with high neutron cross section that are commonly use in neutron detection: ^3He with 5530 barn, and ^{10}B with 3840 barn [6]. Despite the ^3He higher cross section, ^{10}B compounds are often selected because of economical reasons. Boron cross section is higher at thermal energies, about 0.025 eV, that means that neutrons arriving to a neutron monitor has to be slowed down in some orders of magnitude.

The detectors in CaLMa are filled with BF_3. This is an inorganic compound,

colourless, enriched up to 96% of the ^{10}B isotope and with a boiling point of $-100.3\,^{\circ}\mathrm{C}$ at atmospheric pressure. The pressure inside the detectors, or counting tubes, is 0.27 bar, therefore it is in gas phase.

The counters are operated in the proportional range and, when a neutron interacts with a BF_3 molecule, the following nuclear reaction takes place:

$$^{10}B + n \rightarrow ^{7}Li^* + ^{4}\alpha + 2.310 MeV$$
$$^{10}B + n \rightarrow ^{7}Li + ^{4}\alpha + 2.792 MeV$$
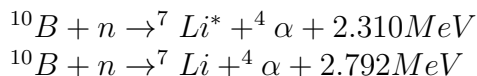
The kinetic energy of the particles resulting from the (n, α) reaction with ^{10}B is 2.31 MeV in the 93% of the reactions, and 2.792 MeV in the remaining 7%. Depending on the product's trajectories, this energy will be dissipated either in the gas or in the detector's walls. If we assume that all the energy is dissipated in ionizing the gas, then it is possible to estimate the total electrical charge generated in one event. Given that the ionization energy W_i of the BF_3 is 33 eV, the dissipated energy, on the most probable of the nuclear reactions written above, W_p is 2.310 MeV and the modulus of the electron charge e is 1.6×10^{-19} C, then the generated charge q will be given by:

$$q = \frac{W_p}{W_i}e = 0.0112\,\mathrm{pC} \tag{3.1}$$

If the charge is left uncollected, the electrons will recombine and no measurement could be made. To solve this, an electrical field is applied by means of a high voltage power supply applied between the detector case, that acts as the cathode, and a very thin filament across the tube that acts as the anode. The electric field under this conditions is given by

$$\vec{E} = \frac{1}{r}\frac{V_0}{ln(b/a)} \tag{3.2}$$

Where r is the distance to the central wire, V_0 is the electric potential between the anode and the cathode, b is the cylinder inner radius and a is the wire radius. As a result of this field, electrons are accelerated towards the anode, leading to further ionization events, depending on the electric field strength. The way that detectors behave, depending on the biasing voltage, is described with more detail in the section 3.4 of this document. Neutron monitors generally operate in the so called proportional zone. In this zone the biasing voltage is high enough to accelerate the charges towards the electrode, creating in their way new ionizations. The ratio between the primary ionization and the total amount of charges collected is a constant known as gas amplification factor (M).

In most of the neutron monitors applications, this multiplication factor M is around 40. Introducing this factor in the previous equation, we get 0.45 pC, that is the charge per event the amplifiers will be designed for:

$$q = \frac{W_p}{W_i}eM \tag{3.3}$$

There are two kind of detector tubes in the CaLMa station: BP28 and LND2061.

The table 3.2.1 summarizes the main characteristics of both detectors being used. The final CaLMa configuration includes three BP28 counters, kindly donated by the Midi Pyrénées Observatory in November 2010, and 12 LND2061.

Counter type	BP28	LND2061
Effective diameter (cm)	14.85	14.91
Cathode material	Stainless steel	Stainless steel
Gas filling	BF_3 (96% 10^B)	BF_3 (96% 10^B)
Gas pressure (mm Hg)	200	200
Effective length (cm)	190.8	195.63
Effective volume (liters)	33	34.1
Operating voltage (V)	-1800	1000-2000
Wall thickness of the tube (cm)	0.084	0.211

Table 3.1: Side-by-side comparative between BP28 and LND2061 detectors.

The main difference between both counters is the biasing voltage. While in the classical BP28 it is negative, in the LND2061 it is positive. Also, for the BP28 operating voltage is well known, but not for the new LND. To determine the operating voltage a plateau test has been conducted. This test is described later in this document, in section 3.4. We have to point out that the LND2061 tube replaces the old model BP28. This LND2061 is a custom design built by the manufacturer under our specifications. Nowadays, it is the model used as replacement of BP28 in some of the neutron monitors around the world.

3.2.2 The moderator

The probability of a neutron producing interesting interactions decreases with the neutron speed in a 1/V way, being V the speed of the neutron. In order to enhance the probability of being detected, neutrons must be slowed down to thermal energies of about 0.025 eV. Is in this range of energies where BF_3 reaches its higher neutron cross section. For this slow neutrons the typical interactions are [12] elastic scattering and neutron-induced nuclear reactions, but since kinetic energy is small, little energy can be transferred to the target nucleus by means of elastic collisions to cause any notable effect. On the other hand, neutron-induced nuclear reactions like the one that takes place in BF_3 detectors, are much more interesting because the resulting products are charged particles, with high enough energy so they can be detected by means of electronic devices.

To increase the probability of detection, incident neutrons must be slowed down to thermal energies. This is the goal of the moderator. The moderator is based on elastics collisions to reduce the energy of the neutrons. The most effective way of doing this is by introducing a target nucleus with a mass close to the neutron's mass, i.e. an Hydrogen ^1H nucleus (a proton). When building the moderator, materials rich in Hydrogen are often used, such as paraffin or polyethylene.

In CaLMa the element used is a tube of polyethylene of 2082.80 mm length, 253 mm of diameter and 40 mm thickness. All dimensions can be found in the cor-

responding scheme in the appendix A.1. This is a commercial size and therefore the detector tube doesn't fit exactly. To overcome this problem a wood chuck has been placed as a spacer to center the detector inside the moderator.

3.2.3   The lead producer

The producer is a layer whose goal is to increase neutron detection probability by two means. In first place, high energy neutrons that enter the producer react with the lead emitting low energy evaporation neutrons with a peak energy of $2\,\mathrm{MeV}$ and up to $15\,\mathrm{MeV}$ and in second, there are about 15 evaporation neutrons for each incident high energy neutron, increasing this way the detection probability.

CaLMa is made up of 1440 half-rings of 99.9% lead. The design of these half-ring can be seen in the appendix A.1, in the page 2, and the way they were placed in the page 3. Taking the lead density of $11.34\,\mathrm{g\,cm^{-3}}$ and the volume of the piece of $1887.834\,\mathrm{cm^3}$, the weight of a single piece is $21.408\,\mathrm{kg}$, which can be handle without special equipment.[1]

3.2.4   The deflector

The deflector prevents environmental low energy neutrons from entering the monitor, while at the same time reflects back to the detector evaporation neutrons from the lead producer. The deflector is built in the same material than the moderator, that is, polyethylene, and surrounds all the monitor providing also a convenient casing for the experiment.

In the CaLMa neutron monitor the deflector is made up of several polyethylene slabs, each of $75\,\mathrm{mm}$ thick, under the commercial denomination PE 500. This refers basically to a density of $0.96\,\mathrm{g\,cm^{-3}}$ of the polyethylene. The slabs are resistant enough to support the weight of the lead producer and the counters, so the deflector is also used to provide a convenience housing for the neutron monitor. The schematic in the appendix A.1 page 1, shows the different slab sizes used to build the moderator housing for a six LND counters section. CaLMa is made up of two of these, plus another which is half the size with room for three BP28 counter tubes, reaching a total count of 15 detectors.

3.2.5   The overall assembly

All the neutron monitor is contained in a box made up of polyethylene slabs that also acts as neutron deflector. The main problem with the mechanical assembly is related with the heavy mass of the elements, which makes it difficult to handle. The drawings in the appendix A.1 includes also the mass estimations for some parts. These estimations are derived from the volume and the density of each element. Both the volume and density are also approximations but the outcome is enough to give a

---

[1]The Spanish regulations on work safety RD487/1997 recomends a maximum of $25\,\mathrm{kg}$ of weight when manipulating loads without any special tool or mechanical assistance.

Table 3.2: Mass breakdown for the monitor assembly.

	2	Wook chucks	0.022 kg	0.044 kg	
	1	Detector LND 2061	8.040 kg	8.040 kg	
	2	Wook strips	6.610 kg	13.32 kg	
	80	Lead half-rings	21.408 kg	1712.64 kg	
	1	Moderator tube	29.928 kg	29.928 kg	
6		Detector set		1763.377 kg	10 579.932 kg
2		Bottom polyethylene slabs		246.605 kg	493.31 kg
2		Rear polyethylene slabs		38.828 kg	76.656 kg
2		Lateral polyethylene slabs		55.586 kg	111.172 kg
20		Top polyethylene slabs		23.337 kg	476.64 kg
2.5		6T-Section		11,737.71 kg	29,343.325 kg

rough estimation of the weight and its implications in handling and in the structural overload of the surface that supports the monitor.

Table 3.2 shows the mass breakdown of the components in the neutron monitor. There are some components that have not been included, such as the wiring, connectors, etc. but their mass, compared with the total can be considered negligible for the sake of handling, and for the sake of determining the structural overload.

A single section of the neutron monitor lies over two big polyethylene slabs, each of 2.194 m x 1.575 m, that is a overall surface of 6.913 m^2. Assuming little or no deformation of these slabs under the pressure of the rest of the parts located over them, the weight would be distributed evenly over the surface in contact with the ground. Therefore, if the weight of a single section is 11 737.21 kg, this will result in a surface structural overload of 1697.85 kg m^{-2}. This is an important value to take into account when choosing where to place the monitor, specially if it is to be located in a building floor. If these floor surfaces were built with no special requirement, normally they are designed to support a use overload ranging from 2 kN m^{-2} to 5 kN m^{-2}, that is approximately between 200 kg m^{-2} and 500 kg m^{-2}.

3.3   Wiring

There are three wiring harnesses in CaLMa: low voltage power distribution, high voltage power distribution and amplifier output signals. For the high voltage distribution a splitter box has been designed and built. This box has one input and four outputs, one that is to be use in cascading connection and three to feed the bias input voltage of each counter tube. In the appendix A.2 there is a 3D model of the splitter box, along with its schematics. The connector used is a BNC-HT, which is rated for at least 6.000V and is cheaper than a typical SHV. A wiring schematic is shown in the figure 3-2. This diagram shows how the splitter box distributes the high voltage power supply to each counter tube, and how the next box is connected.

In this diagram it can also be seen that the low voltage power supply for the amplifiers is distributed in a daisy-chain fashion. The amplifiers have one power input and one power output connector aimed to the next cascade amplifier. The ACHNA98 charge amplifier needs symmetrical +12V/-12V power supply as shown in
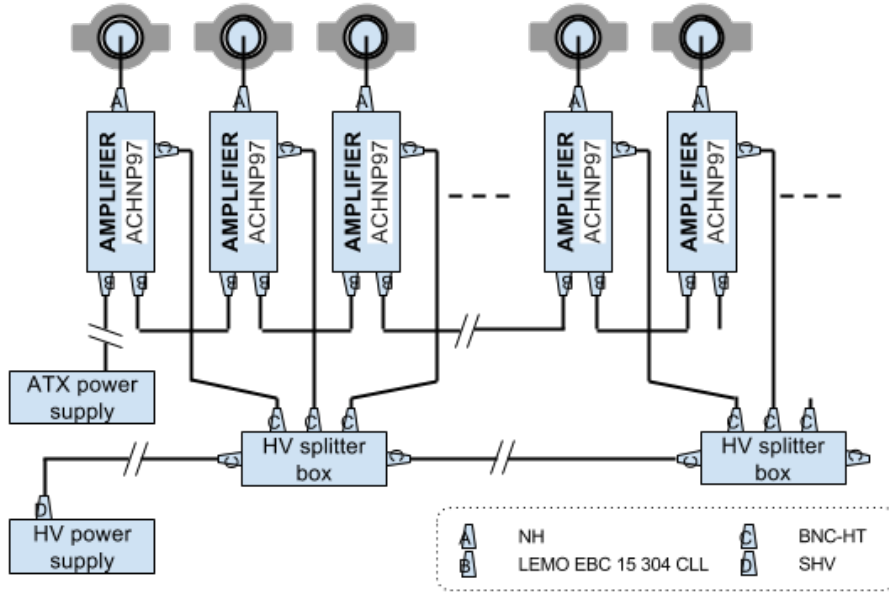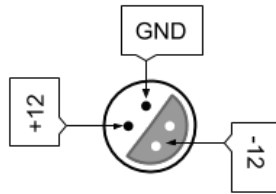
figure 3-3

Figure 3-2: The CaLMa wiring schematics.

Figure 3-3: ACHNA98's low voltage connector.

This schematic does not include signal wiring not to clutter it. It consists of one single coaxial RG174 cable for each detector with a LEMO ERN 00 250 RTL connector that connects the amplifier signal output with the data acquisition system.

3.4 Biasing high voltage supply

As it has been previously said, when a neutron interacts with a BF_3 molecule, the alpha and lithium nuclei produced during the interaction, cause ionization in the gas. When an electric field is applied the electrons will be attracted to the anode and the positive ions to the cathode producing an electrical current that can be measured. A counter can be operated in different regions depending on the biasing voltage. Figure 3-4 shows these regions.

If the voltage applied is too low then the electrons will recombine and no charge will be collected, so this area is not used in practical applications. As the voltage
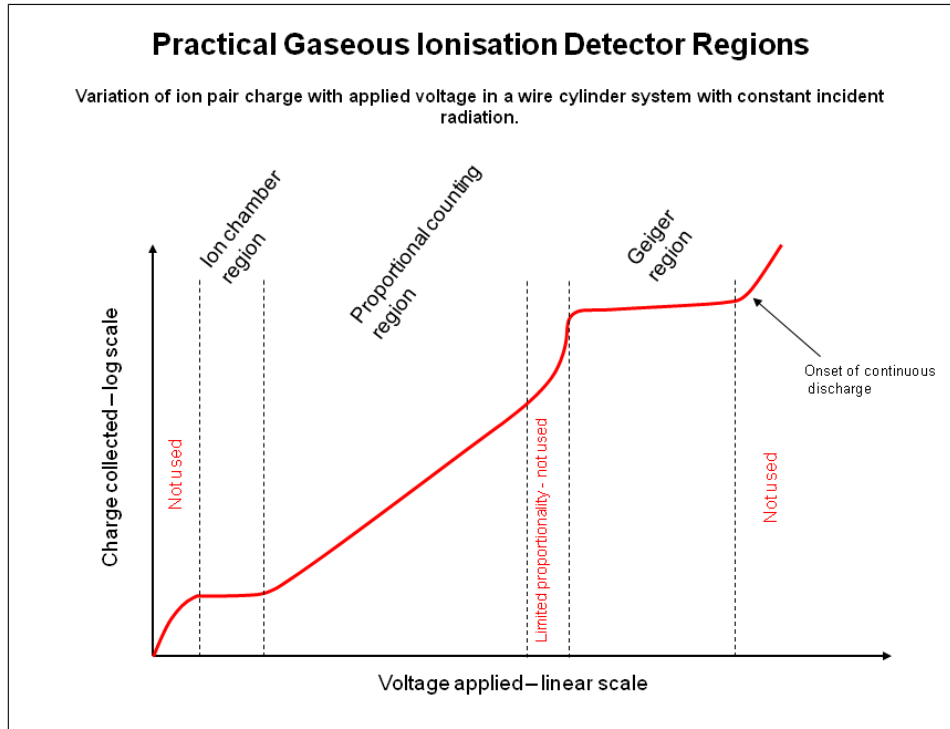
Figure 3-4: Detector tube operation regions [7].

increases the ionization region is reached. Within this region only the original ion pair is collected. If the voltage is further increased the ions gain much more energy causing secondary ionization in their way to the electrodes. This second ionization is referred as gas amplification. The current measured in this region is the number of ionizations caused by the original radiation multiplied by the gas amplification of the counter tube. This region is known as the proportional region. The pulse height of the output is proportional to the energy dissipated inside the detector so particle identification and measurement are possible. At the end of this region the multiplication factor can be as high as 10^4, beyond that point the electrical field is so high that the original electron-ion pair can cause an avalanche of electron-ion pair by itself. This is the Geiger-Müller region. The output signal is very strong and is also independent of the particle energy and type. The CaLMa neutron monitor is designed to operate in the proportional region.

To determine the bias voltage operation point in CaLMa a plateau test was conducted [15]. This test consists of taking samples of the count rate over a wide voltage range. Figure 3-5 shows the results of this test on the new LND2061 counter tube. Initially, when the applied voltage is too low no pulses are generated by the tube. When the voltage reaches the starting potential, the pulses start, and their rate increase rapidly until the voltage gets to another voltage point called the threshold. From this point the counting rate slope decreases to 10% per 100 V, and continues steady until a point from where the counting rate increases rapidly again and enters

in the continuous discharge zone. The counter tube should not be operated in this point to preserve the life of the counter tube.

The plateau slope depends on the design of the counter tube. For the LND2061[14] the manufacturer indicates that the maximum slope shouldn't exceed 3 % per 100 V. For the BP28 [5] the specifications states that its slope shouldn't be higher that 1 % per 100 V over a range of approximately 500 V.
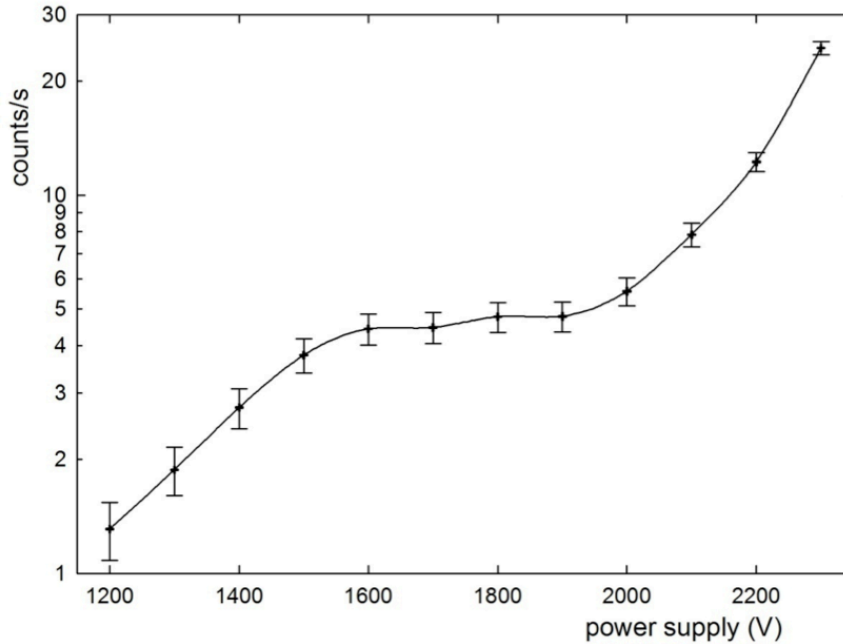
Figure 3-5: Plateau test for a LND2061 counter tube.

3.5   The amplifier/discriminator

The goal of this element is to measure the amount of charge deposited in the anode by the electrons that were originated in the ionization caused by the interaction of a neutron with a BF_3 molecule. This charge is estimated to be 0.45 pC collected in 4 μs. Amplifier input configuration depends on the biasing high voltage polarity. The schematic in figure 3-6 shows a typical configuration for a negative biased counter tube such as the BP28.

The input to the amplifier is also the return path of the anode to ground via R3. Since the cathode is the tube itself it is very important to isolate it properly, otherwise an accidental contact with somebody touching the ground could be dangerous as he would become the return path to ground. The tube output is coupled to the amplifier via C2. This amplifier is a charge-amplifier that acts as a charge-to-voltage converter. The output voltage is inversely proportional to the C1 reference capacitor and directly proportional to the charge per time unit.
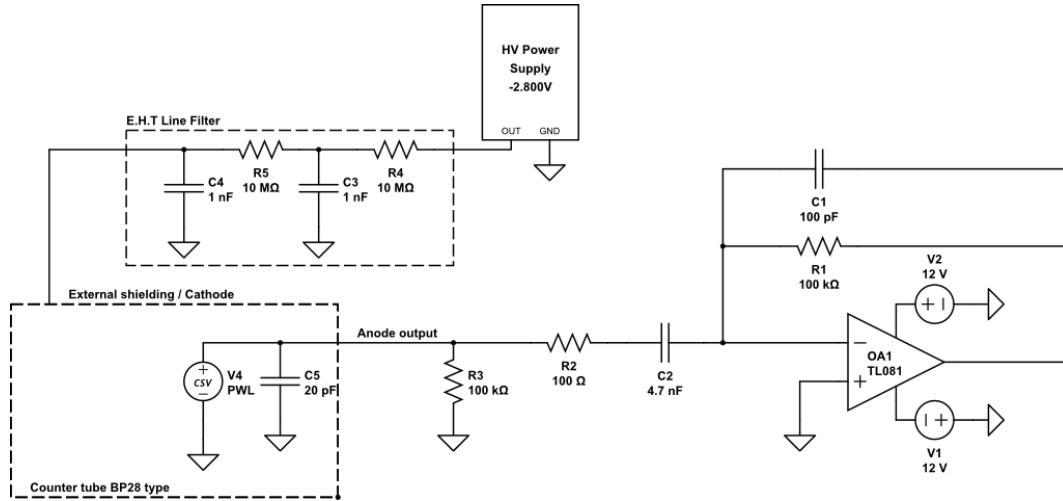
Figure 3-6: Typical charge amplifier in negative bias.

3.6 First measurements

The first official measurement published by the CaLMa Neutron Monitor in the Neutron Monitor Database is of 2012-07-11 11:35:00, and at the time of writing there are 2,970,214 events recorded in the original data table `CALM_ori`. Although there are gaps in the measurement, most of them were caused by network connectivity problems. Since the original data is stored in the data acquisition system, if the network is restored within 48 hours, the system itself retries to upload the data, otherwise it has to be uploaded manually.

The article that follows, *Castilla-La Mancha neutron monitor*, written by the CaLMa Team, José Media, Juan José Blanco, Raúl Gómez-Herrero, Edwin Catalá, Ignacio García, Miguel Hidalgo, Daniel Meziat, Manolo Prieto, Javier Rodríguez-Pacheco, Sebastián Sánchez and myself, was published in Nuclear Instruments and Methods in Physics Research on November 2013.

This journal is indexed by the Journal Citation Report, with an impact index of 1.316. This this year it was in the second quartile (Q2) in the Instruments and Instrumentation and Nuclear Science and Technology categories. Also, in 2013, it was in the first quartile (Q1) according to Scimago for the Instrumentation category.

Castilla-La Mancha neutron monitor

CrossMark

José Medina [a,b,*], Juan J. Blanco [a,b], Oscar García [a,c], Raúl Gómez-Herrero [b],
Edwin J. Catalán [a], Ignacio García [a,c], Miguel A. Hidalgo [b], Daniel Meziat [c],
Manuel Prieto [c], Javier Rodríguez-Pacheco [b], Sebastián Sánchez [c]

[a] Castilla-La Mancha Neutron Monitor, Space Research Group, Parque Científico y Tecnológico de Guadalajara, Avda. de Buendía 11, 19005 Guadalajara, Spain
[b] Physics and Mathematics Department, Space Research Group, Universidad de Alcalá, Ctra. Madrid-Barcelona, km 33,6, 28871 Alcalá de Henares, Spain
[c] Computing Engineering Department, Space Research Group, Universidad de Alcalá. Ctra. Madrid-Barcelona, km 33,6. 28871 Alcalá de Henares, Spain

ARTICLE INFO

ABSTRACT

This work presents the ongoing development of the new Castilla-La Mancha Neutron Monitor located in the Science and Technology Park of Guadalajara (Spain). The instrument is integrated by fifteen proportional counter tubes. Three of them are old tubes of the well-known BP28 standard. The other twelve are the new tubes (model 2061) manufactured by LND Inc. (USA), which intend to provide a valid replacement for the old BP28 model. Testing results of the new detector cross calibration between BP28 and LND2061 counters and comparison with other stations in the Neutron Monitor Data Base are presented.

© 2013 Elsevier B.V. All rights reserved.

1. Introduction

A neutron monitor (NM) is a ground level instrument designed to measure the galactic cosmic radiation by means of the detection of secondary particles, mostly neutrons, generated by the interaction of primary galactic cosmic rays (GCR) with atoms of the upper atmosphere [1].

NMs are designed to detect the low energy part of the GCR spectrum, as well as solar energetic particles (SEP) with sufficient energy to reach the ground. They provide a detection system very well suited for registering temporal variations of the cosmic ray fluxes. This includes short-term variations related to transient solar activity phenomena and long-term GCR variations related to the solar cycle. Different periodicities can be observed in NM measurements. These periodicities are related to the solar activity cycle [2], the Earth rotation, and the transit of Corotating Interaction Regions (CIRs) formed in the solar wind when the fast solar wind interacts with the preceding slow wind, which reappear following the solar rotation rate [3–6]. Non-recurrent transient variations related to solar activity are also observed. These variations normally last less than a few days and can be enhancements (ground level enhancement (GLE) [7]) due to solar energetic particles accelerated up to some GeV by flares and/or shock waves driven by coronal mass ejections (CMEs) or decreases in the NM count rates (Forbush decreases (FD) produced by shocks, interplanetary mass ejections with or without magnetic clouds or a combination of both when arriving at the Earth location [8–11]).

There are different types of NM, some are based on proportional counters filled with a gas that interacts with thermalized incident neutrons, while others combine scintillators and proportional counters in order to achieve a direct detection of solar neutrons [12]. Most of the NMs with proportional counters are based on standard designs named IGY and NM64 [13]. A NM following one of these standards essentially consists of a proportional counter surrounded by several concentric layers with different purposes. The four main layers, from outermost to innermost are:

- The reflector which prevents the entrance of environmental neutrons and reflects back toward the inner counter those neutrons produced inside the detection system.
- The producer or target which produces neutrons via inelastic interactions between the incoming particles and the nuclei of the target material (usually lead).
- The moderator which slows down the evaporating neutrons produced in the target to thermal energies.
- The counter, filled with a gas, which can interact with thermal neutrons and yields a measurable signal. BF_3 has been intensively used as detector gas for many years. However, since BF_3 is dangerous for humans, safer ^{3}He-based counter tubes became a common alternative standard. Nevertheless, the high price of this gas during the last years has induced a progressive return to the traditional designs based on BF_3.

Secondary cosmic ray particles produce neutrons in the lead target, which are thermalized when crossing the moderator. These thermal neutrons reaching the counter tube undergo nuclear

---

* Corresponding author. Tel.: +34 949 881611.
E-mail address: jose.medina@calmanm.es (J. Medina).

interaction with the gas nuclei (^{10}B or ^{3}He). The energy of the incident particles is lost in the detection process, i.e. during their interaction with the NM layers, thus the system operates only as a counter. However, the magnetosphere–atmosphere system works as an enormous calorimeter that provides some information about the energy of the primary incident particle. The minimum energy required for a cosmic ray to produce secondary particles that reach the ground is determined by its local vertical cutoff rigidity. The vertical cutoff rigidity depends on the neutron monitor geomagnetic location and ranges between 20 GV at Earth equator and 0 GV at the poles. Moreover, the atmosphere can stop cosmic rays with energies about some hundreds of MeV. This implies that a global network of neutron monitors can measure cosmic rays with rigidities between 1 and 20 GV, providing also rough spectral information.

The numbers of studies that can be carried out using data provided by the NMs increases when single NMs are integrated into a global network, covering different longitudes and magnetic rigidities. This detection network provides a way to estimate the energy of the incoming cosmic rays or solar energetic particles, minimizing the effect of the Earth rotation. Nowadays, there exists a global database infrastructure to collect the measurements of many NM stations that minutely uploads their count rates. This is called the Neutron Monitor Data Base (NMDB) (http://www.nmdb.eu) [14].

In this work we present the implementation, response tests, first light, comparison with other stations into NMDB and first working year of the Castilla-La Mancha Neutron Monitor (CaLMa) (http://www.calmanm.es/start).

2. Experimental setup

CaLMa is located in Guadalajara, Spain (40°38'N, 3°9'W at 708 m above sea level). The initial design of CaLMa dates back to 2009. It was originally planned to integrate 18 ^{3}He proportional counters, following the NM64 standard design [15]. The budget was awarded in 2010, but from January of that year the price of ^{3}He-based counters increased by 625%, while the lead price rose by 50%. These increases in the cost greatly exceeded the available budget and resulted in a re-design of the CaLMa experimental setup, using Boron Trifluoride (BF$_3$) neutron counters instead. Since industrial production of BF$_3$ counters stopped a long time ago, we requested from LND Inc. the design of a new model of BF$_3$ counter analogous to the Chalk River BP28 counter. In spite of the delay required to develop and manufacture the new LND 2061 (finally delivered in March 2012), the cost of this model allowed for the purchase of 13 counters within our budgetary constraints, leaving one of them as spare. The LND 2061 tubes were designed to have an effective counting volume similar to the BP28 model and to be compatible with a Canberra ACHNA98 amplifier discriminator. To fulfill this requirement, a HN connector and a positive bias high voltage is needed, contrary to the BP28 model, which needs a high voltage negative bias.

The final experimental setup of CaLMa neutron monitor was arranged in mid-2012 and comprises 12 LND 2061 and three BP28 counters (transferred from the Midi Pyrénées Observatory in November 2010). This results in 15 counters following the NM64 standard. Table 1 shows a side-to-side comparison of the characteristics of both, the BP28 and LND 2061 models. More detailed information and the response of the new LND 2061 counters are described later in section 3.

Although we followed the typical NM64 mechanical design, we were forced to introduce small changes in the shape of the pieces of the lead target. In the original design these pieces were single elements of about 80 kg of weight each. This weight and size were difficult to manufacture by the industry located near us

Table 1
Main characteristic of two counters.

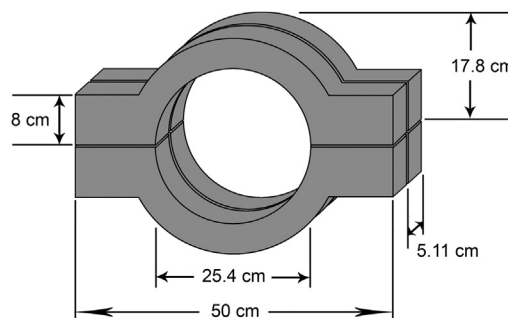| Counter type	BP28	LND2061
Effective diameter (cm)	14.85	14.91
Cathode material	Stainless steel	Stainless steel
Gas filling	BF$_3$ (96% ^{10}B)	BF$_3$ (96% ^{10}B)
Gas pressure (mm Hg)	200	200
Effective length (cm)	190.80	195.63
Effective volume (liters)	33	34.1
Operating voltage (V)	−2800	1000–2000
External shape	Wavy	Smooth
Wall thickness of the tube (cm)	0.084	0.211
Outer tube	Aluminum	No

Fig. 1. Design of the lead pieces of 99.9% purity. These four pieces are equivalent to one of the NM64 original design.

in Guadalajara. For this reason we decided to divide the original design in four identical pieces (Fig. 1) of 22 kg each, which are much easier to manufacture and handle than the original, this implies that we need 80 pieces to cover the entire length of the counter. The rest of the mechanical design follows the NM64 standard [13].

The BP28 counters have an amplifier incorporated in the counter assembly, but this is not the case for the LND 2061 counters. For these counters, we have used an external Canberra ACHNA98 amplifier. This model was originally designed for ^{3}He proportional counters and basically consists of a charge amplifier, a shaping and gain amplifier chain, and a discriminator with adjustable threshold. The ACHNA98 model is a compact design ($17 \times 6 \times 3$ cm^3 including connectors), and works with positive bias voltages between 0 and 3000 V. It also provides an analog output obtained just before the discriminator stage, and the digital output provided by the discriminator itself. It permits the chain connection of low voltage and digital signal, allowing the sum of these signals. The analog signal varies between 0 and 6 V and the digital is TTL compliant. The first was used for counter testing and the second is used by the acquisition system.

CaLMa uses the same acquisition system that operates in the neutron monitor at the University of Kiel, specifically the one named Kiel2 in NMDB. In CaLMa this acquisition system collects data from 15 counters and atmospheric pressure from a Meteolabor BM35 barometer. Data are stored in counts/minute for further treatment and, starting from February 2013, are sent to the NMDB [16] server, where they become available online for the scientific community. Fig. 2 shows a global sketch of the neutron monitor and the test system.

3. The new counter LND2061

The new LND2061 counter has quite similar characteristics to the previous BP28, however there are some differences (Table 1).
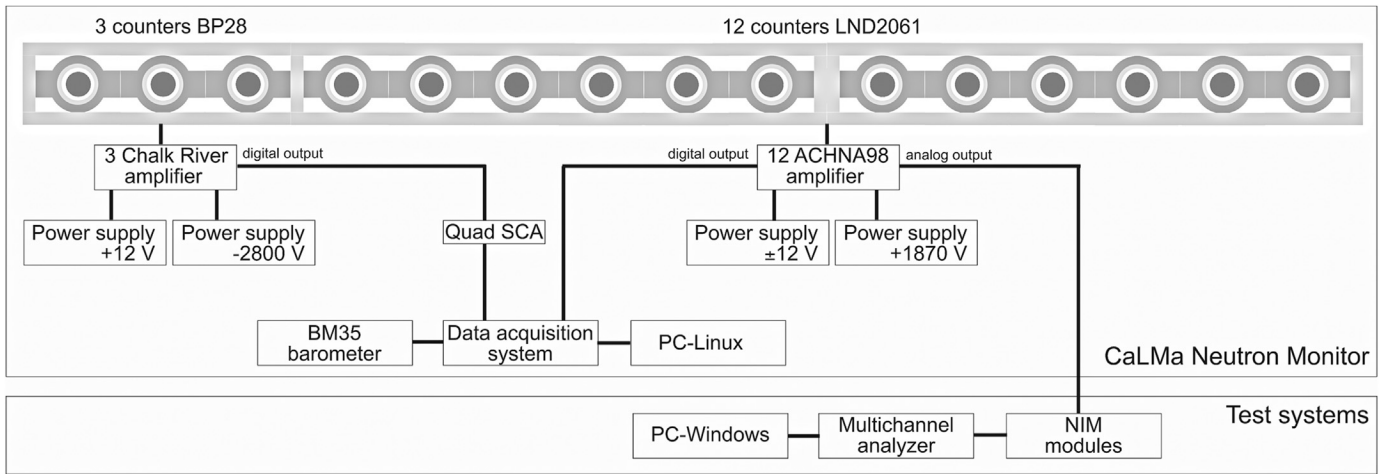
Fig. 2. CaLMa scheme.

The most relevant is the wall thickness, which is narrower for the BP28. Due to their narrower walls, the BP28 external surface is wavy in order to improve its rigidity. Moreover, the Chalk River BP28 is an integrated system, which includes the counter, amplifier, polyethylene moderator and an aluminum tube between the counter and the moderator. In contrast, the LND2061 model integrates only the counter tube, which needs a separate amplifier and moderator. Due to all these differences, the response of the LND2061 model must be characterized to prove its suitability as a replacement for the BP28 tubes in a NM64 neutron monitor. In this section we will describe the different experiments that we have performed to characterize and optimize the working configuration of the LND2061 counters.

The first requirement for the installation of the new model is the determination of the optimal bias voltage. According to the manufacturer specifications, it should be between 1000 and 2000 V (with positive bias). The manufacturer provided individual tests for each of the 13 counters, with optimal operation voltages between 1230 and 1245 V. These values were determined using a PuBe neutron source, an Ortec 142PC preamplifier and an Ortec 570 amplifier.

We have studied the variation of the counter response with the bias voltage. The result is represented in Fig. 3, which shows the counting rate as a function of the bias voltage for one of the LND2061 tubes. We have found a clear plateau for voltages between 1600 and 1900 V, with a slope of 0.1%/V. We have chosen 1870 V as optimal value for all tubes. This value keeps an optimal counting rate compared with the BP28 counters and at the same time provides an acceptable saturation level in the amplifier (as we will describe below). The location of the plateau and the optimal value differs significantly from the manufacturer's specifications mentioned above. This difference is probably due to the electronics used in our setup compared with the one used by LND.

The Canberra model ACHNA98 charge amplifier was chosen because it is the only model currently available featuring preamplifier, amplifier and digital output, all in one single module with suitable dimensions. This model was specifically designed and optimized for ^{3}He counters (which have an energy peak of 764 keV, significantly lower than the 2.30 MeV main peak characteristic of the BF$_3$ counters). For this reason we have studied how the expected over-amplification of the higher pulses of a BF$_3$ counter affects the spectra and counting rate.

The test has been performed injecting pulses of increasing amplitude from a pulse generator (Canberra 814FP) in the test input of the ACHNA98. We obtained a good linear behavior for input pulses with amplitude under 0.25 V. Test pulses with
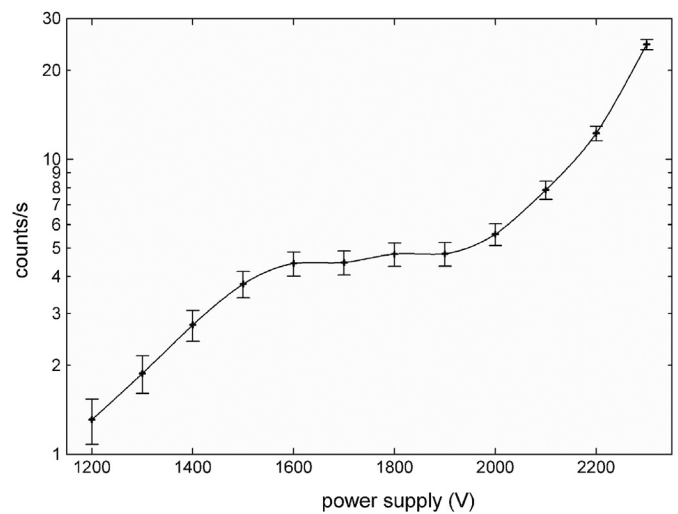
Fig. 3. Counting rate versus voltage for one of the LND2061 counters. Note the clear plateau between 1600 and 1900 V.
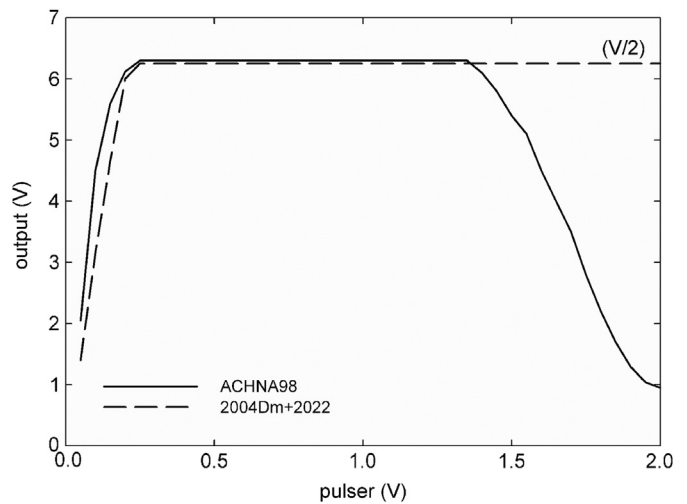

Fig. 4. ACHNA98 response to variation of the input pulse amplitude compared with a standard combination.

amplitude between 0.25 V and 1.4 V lead to a constant output analog signal of 6 V. (meaning that ACHNA98 analog response saturates). Above this 1.4 V the amplifier starts to depart from the

ideal linear behavior and we obtain progressively decreasing output analog signals (Fig. 4), while a standard combination of preamplifier and amplifier (Canberra 2004Dm and 2022) gives a continuous saturation line (dashed line in Fig. 4). Since the expected output of a BF_3 counter is three times higher than that of a ^{3}He counter, the ACHNA98 will be mainly working in this saturated range (or even above it) it, which produces a deformation in the expected spectrum. This is illustrated in Fig. 5, which shows a comparison of the spectrum of a BP28 counter (bottom panel) and a LND2061 with an ACHNA98 amplifier (top panel). These measurements are made at the operating voltage of +1870 V for the LND2061 counter and -2800 V for the BP28 one. The LND2061 is partially deformed when compared with the BP28 spectrum, this effect is mainly caused by the saturation and non-linearity of the ACHNA98 for high input signals, resulting in a narrowing of the main peak (channel 600), the disappearance of
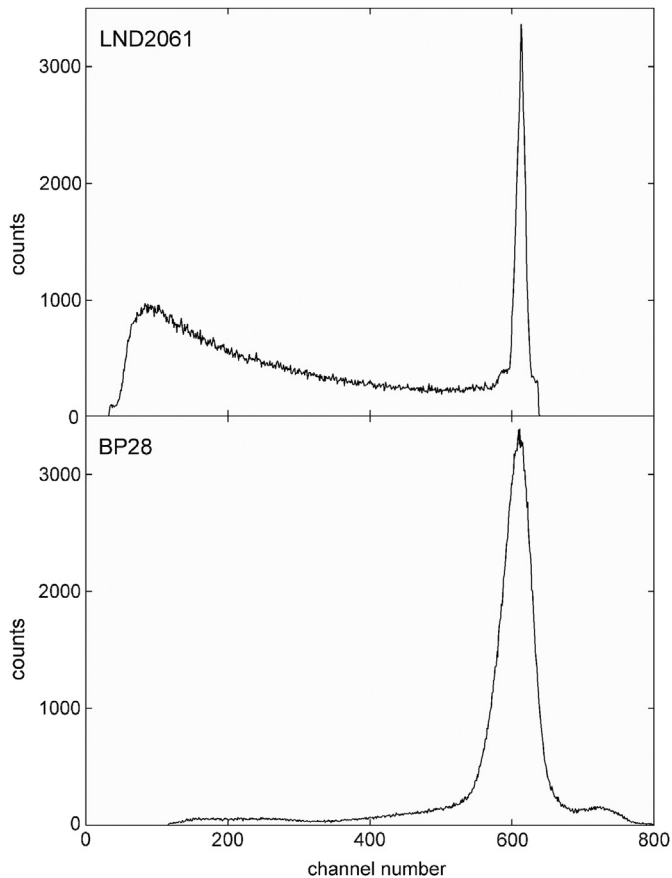
the secondary peak (channel 750) and the appearance of a broad peak (channel 100). This broad peak is obtained as a consequence of the fall of the output signals in ACHNA98 (Fig. 4), and accumulated counts, which should be registered in the right part of the spectrum (main and secondary peaks). We should remark that while the spectral shape is affected, the total number of counts above threshold (i.e. right from the gamma noise peak) remains constant. This fact ensures the suitability of the combination of the ACHNA98 and the LND2061 as a valid counting system, which effectively replaces the BP28 with very similar counting efficiency. This is also clear when comparing the BP28 with ACHNA98 and LND2061 count rates (Fig. 6).

Our station has gone through different stages, with a progressive increase in the number of counters installed. CaLMa has operated with 3, 6, 9 and 15 tubes, which allows us to compare the historical data records with other stations with the same number of tubes. Such comparison is shown in Table 2, which includes the average rates and the standard deviations. Our station is characterized for wider range of variation (larger values of sigma) compared with other stations, mainly due to the fact that our station is temporarily located in the cellar of a 3-stage building. This location reduces the statistics, and we currently get typical rates of only ~5 counts/s/counter, significantly below the 9 counts/s/counter of Apatity or 122 counts/s/counter of Jungfraujoch1. Nevertheless, it can be clearly appreciated how as the number of counters increases, the statistical quality of the data improves. Table 2 shows how the dispersion of our measurements is reduced from 0.4 to 0.1. All these data were obtained during a period of 24 h without solar events.

4. Results

Final data from CaLMa measurements are reduced according to the median filter algorithm procedure described by Belov et al., [17]. The median rates are subsequently corrected from atmospheric pressure effects [18] applying a factor $\exp[-\beta(P-P_0)]$, where $P_0 = 935 \pm 6$ hPa is the station standard pressure and $\beta = -0.0067 \pm 0.0002$ hPa^{-1} is the barometric correction factor. Count rates from BP28 tubes are slightly higher than the corresponding

Fig. 5. Pulse-height spectra obtained for the two types of counters used.

Table 2
Historical evolution of CaLMa compared with other stations.

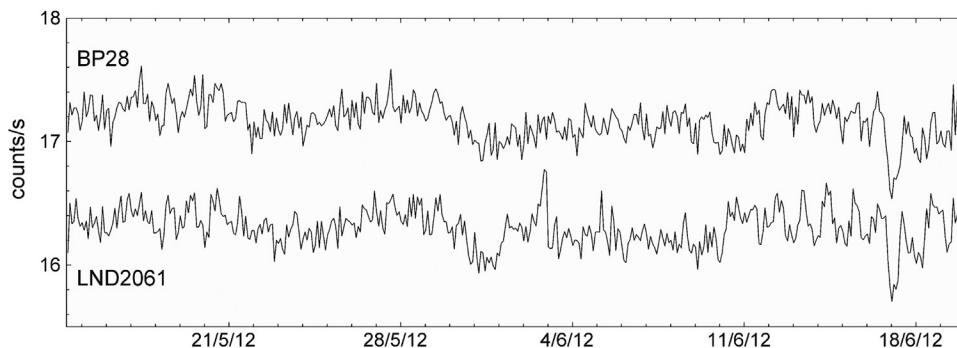| Number of counters	Station	Counts/s/ counter	CaLMa counts/s/ counter
3	Jungfraujoch1	121.7 ± 1.7	5.7 ± 0.4
6	Athens	9.5 ± 0.4	5.7 ± 0.2
9	Oulu	11.8 ± 0.2	5.6 ± 0.2
18/15	Apatity	9.4 ± 0.1	5.3 ± 0.1

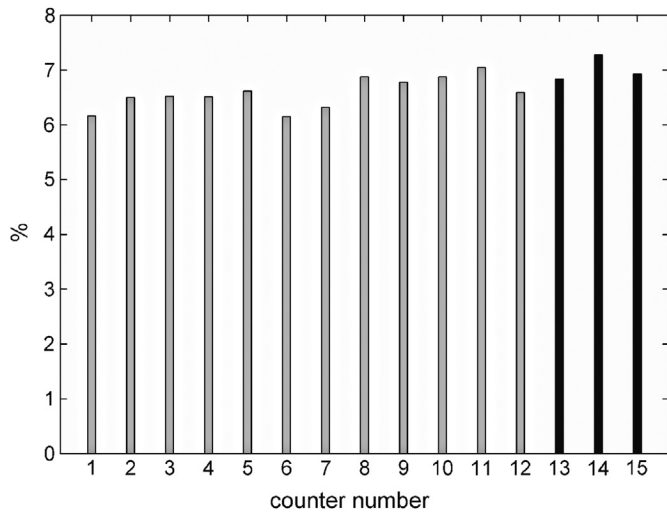**Fig. 6.** Data collected by the three BP28 counters and three 2061 counters.

Fig. 7. Contribution to the median of each of the counters for 50 days, in black the BP28.

LND2061 counters (Fig. 6) and there are also small differences in the efficiency of each tube depending on its location in the monitor. Nevertheless, the possible bias due to different tube efficiencies does not affect the median filter algorithm, which basically consists in taking the median of the counting rates normalized to reference values for each counter. The median relative counting rate is normalized afterwards to the sum of the reference values from each counter. This algorithm ensures the rejection of transient anomalous values from one or more tubes departing from the general trend. Fig. 7 shows the percentage of occurrence of each counter in the median value during a 50-day period. The obtained values range between 6.2% for counter number 6 and 7.3% for counter number 14, meaning that all of them have comparable rates of occurrence when the median filter is applied. This confirms the equivalence between the two counter models and supports the suitability of the LND2061 counter as reliable replacement for the BP28 tubes.

Fig. 8 shows the measurements acquired along its four building phases of CaLMa. Count rates are given in counts per second and counter to get comparable measurements during these four phases
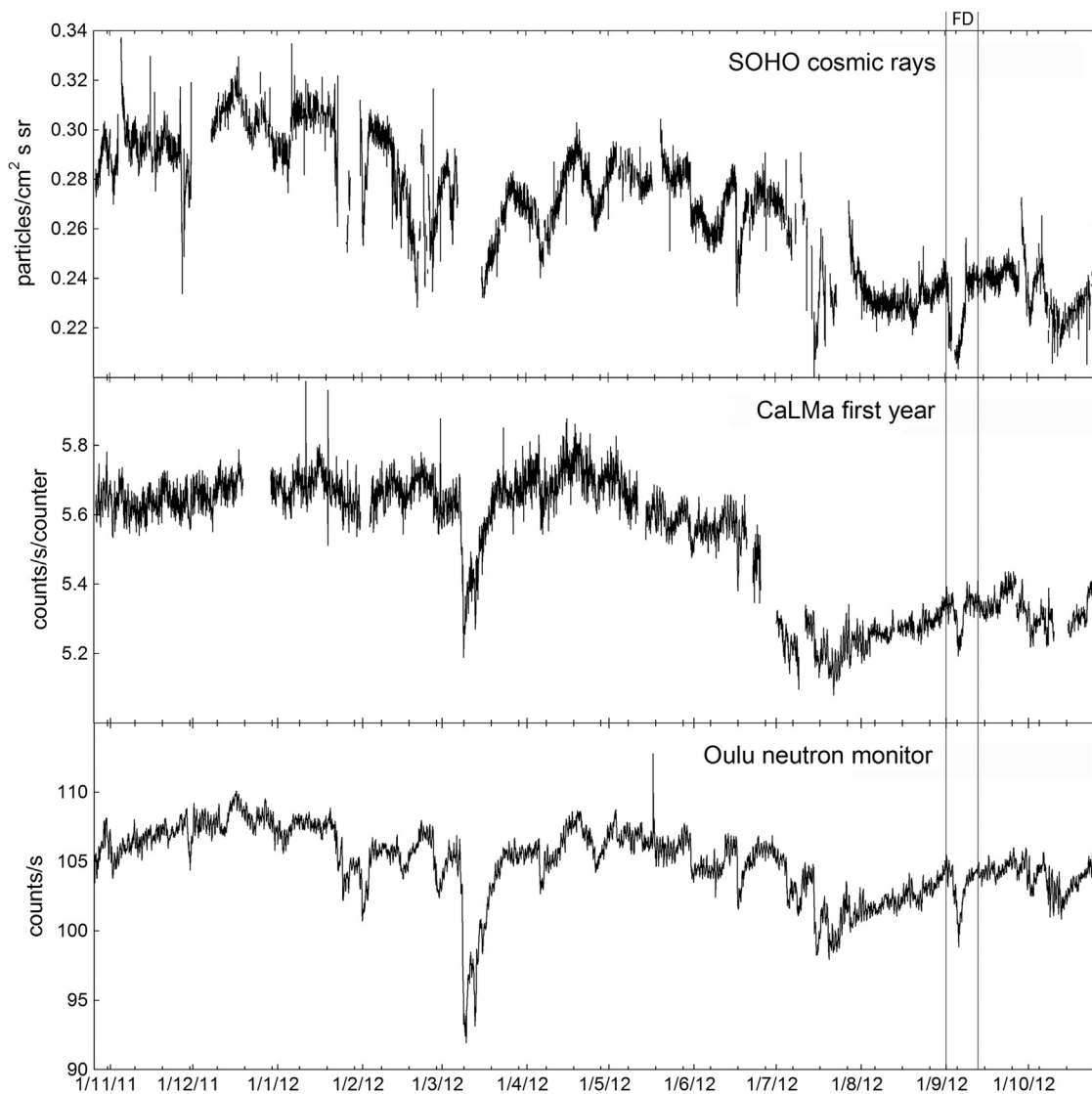
Fig. 8. Data from the first year of CaLMa. FD is the Forbush decrease discussed later.

with 3, 6, 9 and 15 counters. CaLMa is compared with Oulu NM (bottom panel) measurements and the integral channel of the Electron Proton and Helium Instrument (EPHIN) [19] on board the Solar and Heliospheric Observatory SOHO (upper panel). EPHIN integral channel is sensitive to protons above 53 MeV. CaLMa (6.95 GV) obtained count rate variations comparable with both, Oulu (0.81 GV) and EPHIN (located at L1 out of the magnetosphere). As can be seen in Fig. 8, CaLMa, Oulu and EPHIN recorded some decreases in count rates during the CaLMa first year simultaneously. One of them was clearly observed on September 2012 as it is highlighted by the vertical lines in Fig. 8. This FD will be analyzed in detail in next paragraphs. Although one year is a too short period to evaluate the CaLMa's response to GCR variations due to solar cycle modulation, it can be directly observed that CaLMa response is similar to Oulu response. Moreover, the long-term decrease detected about end of June 2012, seems to confirm the CaLMa's response to solar modulation.

CaLMa station is also able to follow the short-term solar activity. Because of its geographic location, with a rigidity cut-off of 6.95 GV, it can measure enhancements at ground level on the cosmic ray background with energies higher than 6.07 GeV/amu. Nevertheless, no ground level enhancement (GLE) has been detected by CaLMa during its first year in operation. Other stations reported the detection of the 71 GLE on 17 May 2012 [20]. Only stations with rigidities lower than 2.36 GV informed about positive detections. CaLMa is clearly out of the detections range in terms of
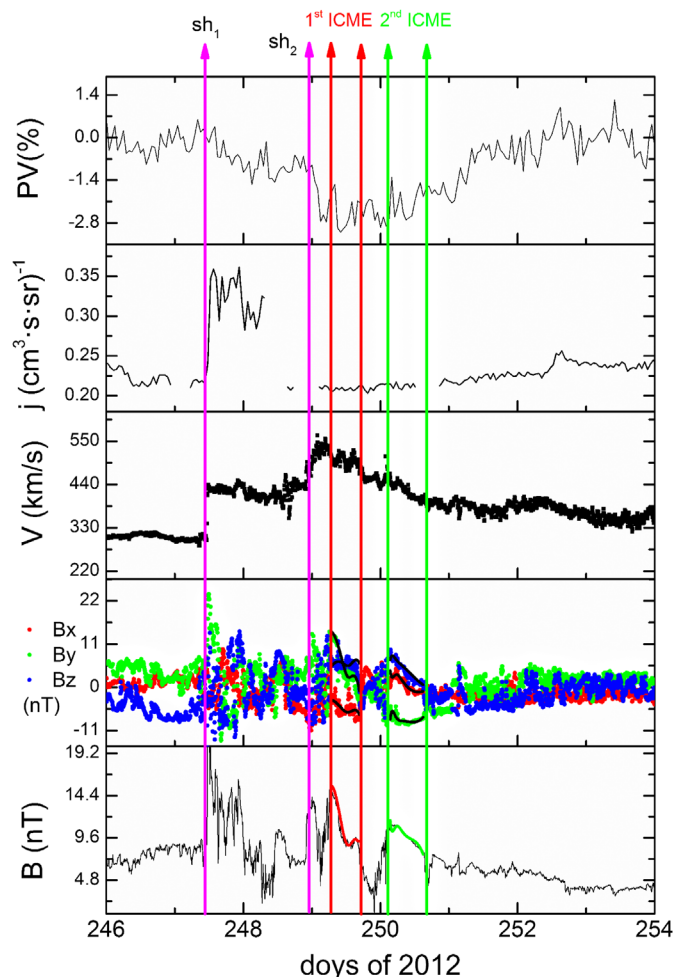
rigidity. Regarding to this event, Gopalswamy et al. [21] point out, as possible solar source, a moderate flare (M5.1) and a fast CME with a well developed shock, concluding that the driven shock plays the main role in GLE particle production, especially if they are well connected with the shock nose. The response to rigidities lower than 2.36 GV could be explained if the shock is the main source of GLE particles in this event.

A Forbush decrease (FD) is a short-term decrease in the neutron monitor count rate. It normally lasts several days and it is related to solar wind phenomena at 1 AU such as interplanetary shocks, magnetic clouds (MC), ejecta and stream interaction regions. CaLMa has detected six FD since November 2011. As an example we show the FD measured on 4 September 2012. The vertical lines in Fig. 8 mark this FD. The solar wind context and CaLMa count rate can be seen in Fig. 9. On 3 September 2012, 10:40 UTC a strong interplanetary shock arrived at the Advanced Composition Explorer (ACE) spacecraft location at L1. This shock is identified by a simultaneous jump in solar wind density, temperature, speed and magnetic field. Nevertheless, this shock did not have any observable variation on CaLMa count rate (upper panel Fig. 9). At the end of 4 September (21:55), a second shock arrived at ACE location. Although this shock was weaker than the previous one, CaLMa count rate started to decrease with the shock arrival to Earth. Eight hours later a MC characterized by a smooth magnetic field rotation, low temperature and mean speed of 520 km/s, arrived to Earth causing the deepest FD level observed in CaLMa so far. Continuous lines on experimental points are the expected MD topology following Hidalgo et al. [22]. Half day after (6 September, 01:55) a second MC arrived with a mean speed of 430 km/s. With this MC passage at Earth orbit the low count rate was maintained and the FD recovery phase begun just after the MC passage. The normal CaLMa count rate was achieved on 7 September, i.e. 3 days after the 2nd shock detection. This FD illustrates how CaLMa measurements are sensitive to interplanetary disturbances reaching the Earth environment and affecting Cosmic Ray intensities.

It has been shown in Fig. 6 that BP28 and LND2061 obtain similar count rates when operating together into CaLMa NM. It can be also appreciated similar response to GCR variations, this can be inferred from the curve shapes. Both counters contribute to the final measurement with almost the same statistical weigh (Fig. 7). These two results prove that the new LND2061 counter is an appropriate replacement for the old BP28 model. Moreover, CaLMa has a comparable response to Oulu NM against environmental conditions as it is observed in Fig. 8. This confirms that the combination of BP28 and LND2061 counters works well when it is compared with other NMs equipped with only BP28 counters. Finally, the CaLMa behavior during the FD on 4 September validates this NM to study GCR variations due to solar wind structures (Fig. 9).

5. Conclusions

We have demonstrated that the new BF_3 LND2061 counter is a valid replacement for the old BP28 counters currently operating in many NM64 neutron monitor stations. We have also proven that the compact integrated amplifier ACHNA98, although designed for ^{3}He counters and showing some saturation effects in the pulse-height spectrum when connected to BF_3 tubes, is valid for counting purposes when connected to a LND2061 counter. We have shown how the first scientific measurements obtained with CaLMa are consistent with simultaneous observations by other neutron monitors and space-based observatories, showing clearly the long-term GCR modulation effect, as well as transient Forbush decreases. We have also checked the correlation with space-based observations during a Forbush

Fig. 9. Forbush decrease observed in CaLMa count rate on 4 September 2012. From top to bottom are presented the CaLMa percentage variation with respect to the count rate background just before the first shock arrival, the EPHIN integral channel flux, the solar wind speed, magnetic field components and magnetic field intensity at 1 AU respectively.

decrease in September 2012. All these measurements as well as our laboratory tests confirm the validity of the combination of LND2061 and ACHNA98 as neutron counting system following the NM64 standard. CaLMa scientific data have been recently integrated in the NMDB network and our station is providing real-time data to the scientific community on a regular basis.

Acknowledgments

References

[1] J.A. Simpson, Space Sci. Rev. 93 (2000) 11.
[2] T. Thambyahpillai, H. Elliot, Nature 171 (1953) 918.
[3] I.G. Richardson, G. Wibberenz, H.V. Cane, J. Geophys. Res. 101 (1996) 13483.
[4] V. Pizzo, J. Geophys. Res. 83 (1978) 5563.
[5] R. Gómez-Herrero, et al., J. Geophys. Res. 114 (2009) A05101.
[6] R. Gómez-Herrero, et al., J. Atmos. Sol. Terr. Phys. 73 (2011) 551.
[7] S.E. Forbush, Phys. Rev. 51 (1937) 1108.
[8] A.P. Jordan, H.E. Spence, J.B. Blake, D.N.A. Shaul, J. Geophys. Res. 116 (2011) A11103.
[9] K.A. Firoz, et al., J. Geophys. Res. 116 (2011) A04101.
[10] J.J. Blanco, et al., J. Phys.: Conf. Ser. 409 (2013) 1 012187.
[11] J.J. Blanco, E.J. Catalán, M.A. Hidalgo, J. Medina, O. García, J. Rodríguez-Pacheco, Solar Phys. 284 (2013) 167.
[12] S. Hibata, et al., 22nd Int. Cosmic Ray Conf. 3 (1991) 788.
[13] P.H. Stoker, L.I. Dorman, J.L. Clem, Space Sci. Rev. 93 (2000) 361.
[14] H. Mavromichalaki, et al., Adv. Space Res. 47 (2011) 2210.
[15] H. Carmichael, IQSY Instruction Manual, vol. 7, Deep River, Canada, 1964.
[16] J.M. Clem, L.I. Dorman, Space Sci. Rev. 93 (2000) 335.
[17] A.V. Belov, Y.a.L. Blokh, E.G. Klepach, V.G. Yanke, Kosm. Luchi 25 (1988) 113.
[18] J.A. Lockwood, A.R. Calawa, J. Atmos. Sol. Terr. Phys. 11 (1957) 23.
[19] R. Müler-Mellin, et al., Solar Phys. 162 (1995) 483.
[20] K.G. McCracken, H. Moraal, M.A. Shea, Astrophys. J. 761 (2012) 101.
[21] N. Gopalswamy, et al., Astrophys. J. Lett. 765 (2013) L30.
[22] M.A. Hidalgo, T. Nieves-Chinchilla, Astrophys. J. 748 (2012) 109.

THIS PAGE INTENTIONALLY LEFT BLANK

Chapter 4

OAS: A data acquisition system for Neutron Monitors

In the very beginning of the history of the Neutron Monitors, counting was performed using electromechanical devices, one for each counter tube. A typical setup is 18 counter tubes, but it can vary from station to station. It the early IGY neutron monitors, a camera was placed in front of the panel and a mechanism was set up to take a picture every 15 minutes. Figure 4-1, extracted from the IGY Instruction Manual 1957, shows this camera. Also, the picture in figure 4-2, shows how the mechanical counters looked like.
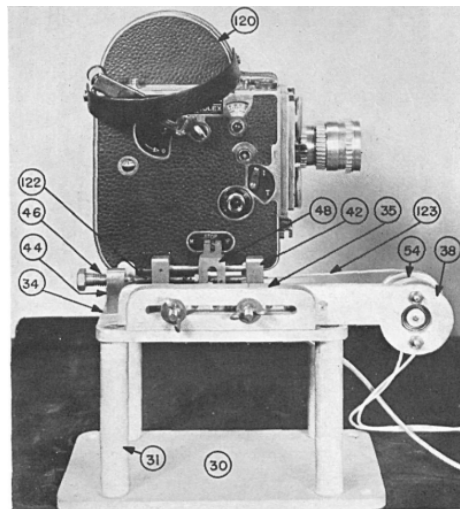
Figure 4-1: 16 mm photo camera used as registration device.

From any of these devices, a human operator would take the reading by hand and would record it in a tabulated paper, probably along with a timestamp with an arbitrary precision. After collecting this data, the operator had to compute the necessary atmospheric corrections and after that calculate the station response by applying some kind of algorithm.
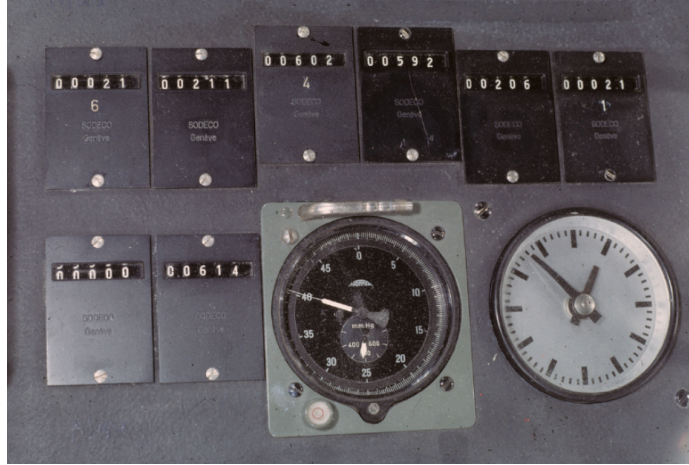
Figure 4-2: Electromechanical counters

The electromechanical counters were then substituted by electronic-based data acquisition systems that recorded the number of events detected, and a general purpose computer so that all the calculations could be automated. The resulting station response could be stored in a magnetic storage device so it could be transferred to another computer for further analysis.

The next step in the evolution was to provide network connectivity, generally through the Internet, so the data could be made available right after it has been calculated. Since the calculations are really fast this could mean that the data could be ready in the near real-time.

Finally, leveraging this connectivity, a third could then collect the data, combine it and make it available for the community. This is the main idea behind the Neutron Monitor Database (NMDB). But for the data to be comparable between different stations, the following set of requisites must be met: the output data representation has to be standardized, it has to be time-stamped with an universal and common time reference and it has to be recorded every minute.

Summarizing the lasts paragraphs we can get a list of the primary requirements of the data acquisition system:

- Count acquisition for multiple channels, typically 18.

- Atmospheric pressure acquisition.

- Network connectivity to the NMDB.

- Universal time source synchronization.

- Computing capability for the following tasks:

  - Run the acquisition loop.
  - Store raw readings in a local storage.

62

- Perform housekeeping task (i.e. time source synchronization).
- Calculate correction for pressure.
- Run the median editor algorithm (or equivalent).
- Upload the results to the NMDB or to an intermediate database.

4.1 The OAS general architecture

The OAS is divided in two main blocks. The first one is dedicated to the events counting, along with some other minor tasks, and the second is mainly for data processing and for interfacing with the outside world.

Since the goal of the first block is to record events with timing constraints, specific FPGA-based hardware has been designed. On the other hand, for data processing, a general computing system has been chosen. The software written for this system will coordinate the operations of the data acquisition system.

The article *Embedded data acquisition system for neutron monitors*, included in this work, proposes a solution to the problems of event counting and data processing. As an introduction to this article, the next sections will describe the problems and goals.

4.1.1 Event counting features

The main goal of the data acquisition system is to count the number of successes per unit of time, typically a minute. This value ranges from a few hundreds counts per minute in equatorial stations, to $30\,000\,\mathrm{count\,min^{-1}}$ in polar stations under severe particle events. This value, specifically $29\,926\,\mathrm{count\,min^{-1}}$ is the highest count recorded by the NMDB till the date. It happened in the Terre-Adélie French neutron monitor in Antarctica (TERA), on January 2005 (see figure 2-3 on chapter 2).

The high resolution Neutron Monitor Database recommends a data collecting interval of one minute. This minute is also globally synchronized with the Universal Time so data from all the station can be later compared. Clock synchronization can be a very challenging task, mostly due to clock reference drift and software-induced latencies. To simplify this task, two assumptions have been taken in this work: since the embedded Linux system is a dedicated hardware with low CPU load, the software latencies can be considered negligible. Also, the time for transmitting the data over the serial line will be considered negligible as well, and this is because transmitting 18 counters of 32 bits at 9600 bps take roughly 75ms, that is very low compared with the 60s of the integration time. Even though we are taking these assumptions, the software will be designed not to accumulate these drifts and will compensate the waiting time for the next activation accordingly.

4.1.2 Event capture

To capture the pulses from the amplifier discriminators, a Field Programmable Gate Array (FPGA) device has been use. It includes a dedicated counter for each tube, so

each pulse is used to directly increment the corresponding counter. When it is time to transfer the counts to the communication serial line, all the counters are copied to a latch register and the counters are set to zero to start a new counting cycle. Now the communication stage has more than enough time to transfer the copied values through the serial line without interfere with the next counting interval.

The FPGA assists the system with an auxiliary task. Since there are many devices with serial ports that could provide data to the system, such as the barometer, high voltage, power supplies, GPS, etc., and a very limited number of serial ports available on the embedded system, a serial port multiplexer has been synthesized in the FPGA. This device allows to connect several communication ports to the FPGA, and to choose which one will be the active one.

The communication system, included also in the FPGA, is based on a Universal Serial Asynchronous Receiver and Transmitter (USART). It is used of course to send the data of the counters, but it is used to receive control commands as well. The most important one is use to instruct the FPGA to latch the counters and send their values back, but there are commands also to reset the entire system and to switch the serial port multiplexer to the desired port.

4.1.3 Data acquisition

All the capturing cycle is performed by the data processing device. This is an AVR32 embedded system running the Linux operating system. The system itself provides the needed network connectivity, NTP time synchronization and the environment to execute the software that has been written ad-hoc to implement the data acquisition cycle.

The data acquisition cycle runs as follow:

1. Get the current time of day and calculate the next activation (next minute).

2. Sleep until the next activation.

3. Send to the FPGA the command to retrieve the counts.

4. Send to the FPGA the command to switch to the barometer channel.

5. Send the command to the barometer to read the current pressure.

6. Store the current timestamp, the counter readings and the barometric pressure in an internal SQLite database.

7. Repeat again.

The data acquisition system stores raw counts minutely in a table in a SQLite database. This table is called `binTable` and has the following schema:

```
CREATE TABLE binTable (
    start_date_time DATE PRIMARY KEY,    -- timestamp in YYYY-MM-DD HH:SS
    ch01            INTEGER,             -- Tube 01, Section 1
```

```
ch02            INTEGER,          -- Tube 02, Section 1
ch03            INTEGER,          -- Tube 03, Section 01
ch04            INTEGER,          -- Tube 04, Section 01
ch05            INTEGER,          -- Tube 05, Section 01
ch06            INTEGER,          -- Tube 06, Section 01
ch07            INTEGER,          -- Tube 01, Section 02
ch08            INTEGER,          -- Tube 02, Section 02
ch09            INTEGER,          -- Tube 03, Section 02
ch10            INTEGER,          -- Tube 04, Section 2
ch11            INTEGER,          -- Tube 05, Section 2
ch12            INTEGER,          -- Tube 06, Section 2
ch13            INTEGER,          -- Tube 01, Section 3
ch14            INTEGER,          -- Tube 02, Section 3
ch15            INTEGER,          -- Tube 03, Section 3
ch16            INTEGER,          -- Tube 04, Section 3
ch17            INTEGER,          -- Tube 05, Section 3
ch18            INTEGER,          -- Tube 06, Section 3
hv1             INTEGER,          -- High voltage output 1
hv2             INTEGER,          -- High voltage output 2
hv3             INTEGER,          -- High voltage output 3
temp_1          INTEGER,          -- Temperature 1
temp_2          INTEGER,          -- Temperature 2
atmPressure     INTEGER           -- Pressure in hPa
);
```

This table structure comes from the legacy one of the old MS-DOS based system. The time stamp applied to all the samples is also a primary key. This helps to combine samples from different stations given that they are time-synchronized.

Also, in parallel with this activities, the system performs the usual house keeping tasks, such as synchronize the local clock with the time from NTP, synchronize the last entries of the internal database with an external MySQL database, and provide the typical operating system services.

4.2   Data processing and editing

Data processing is done in a general purpose computer, that has a network connection with the embedded system and the FPGA, and a connection with Internet to publish the results in the NMDB.

In this section we will introduce the processing techniques applied to the data obtained from the data acquisition system. The goal is to provide a single measurement for the whole station that can be published in the NMDB. We will combine the explanation of the technique with some statistical exploratory data that would help to understand the nature of the data.

4.2.1   Descriptive statistics

At the time of writing there are two databases available, KIEL2 and CALM, from the Kiel Station and from the CaLMa station respectively.
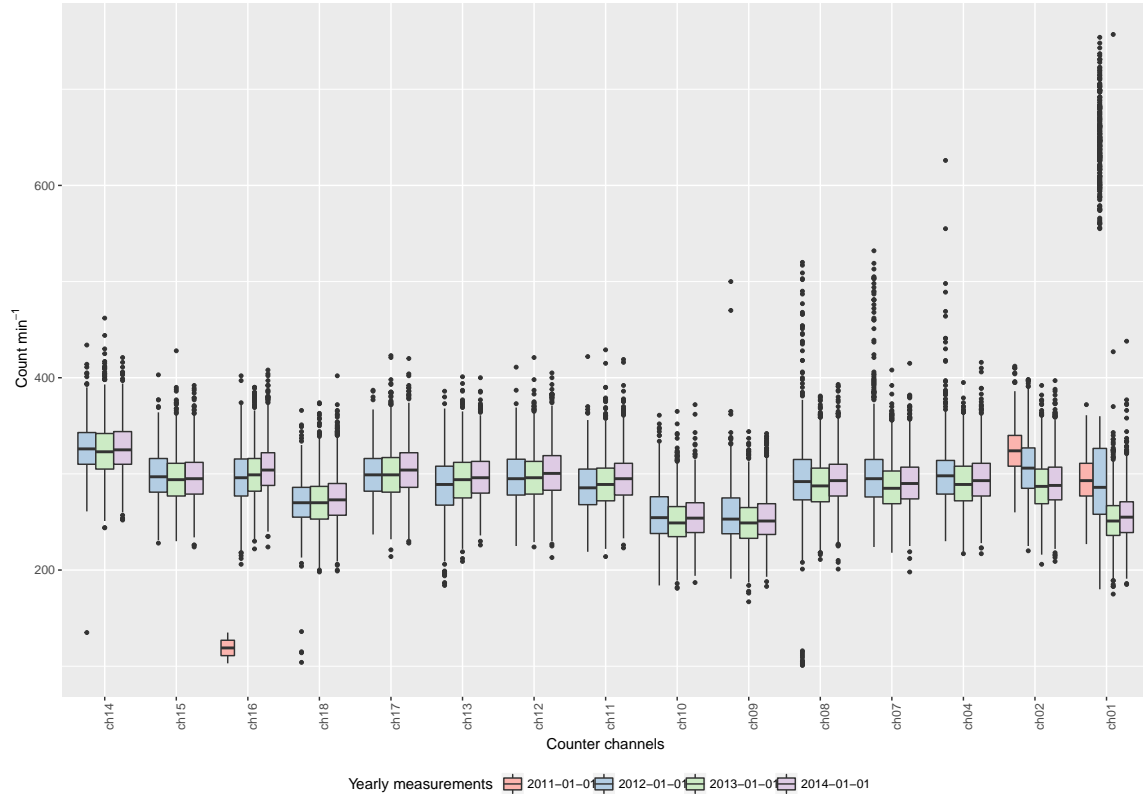
Figure 4-3: Boxplot for CaLMa raw data.

To proceed with the statistical descriptive analysis, The CALM database has been selected. In its `binTable` there are 1 561 904 samples, recorded from 2011-10-26 15:30:00 to 2014-12-16 10:16:00.

A first boxplot representation shown in figure 4-3, taken from the CALM's station official operation start date and summarized by year reveals that even if the counts are centered around the median, there are many (potential) outlier values. The statistical program used to analyze the data considers that the upper whisker reaches from the hinge to the highest value within 1.5 times the inter-quartile range, that is, from the first to the third quartile. All the values above or bellow the whiskers are considered outliers.

The boxplot in figure 4-4 has been replotted without outliers following the previous criteria.

The global tendencies for each year is reproduced in almost all the channels, giving the idea of consensus among them. Also the sizes of the quartiles look similar, which means that the data dispersion around the mean is at first sight comparable.

The presence of this outliers values is something that needs to be further investigated, but they seem to be artifacts from the electronics that are not related with the physics of the experiment. In practice, these spikes are detected visually and manually removed using special tools. It is important to highlight that the original data that contained the outlier value is never removed from the original table in the

66
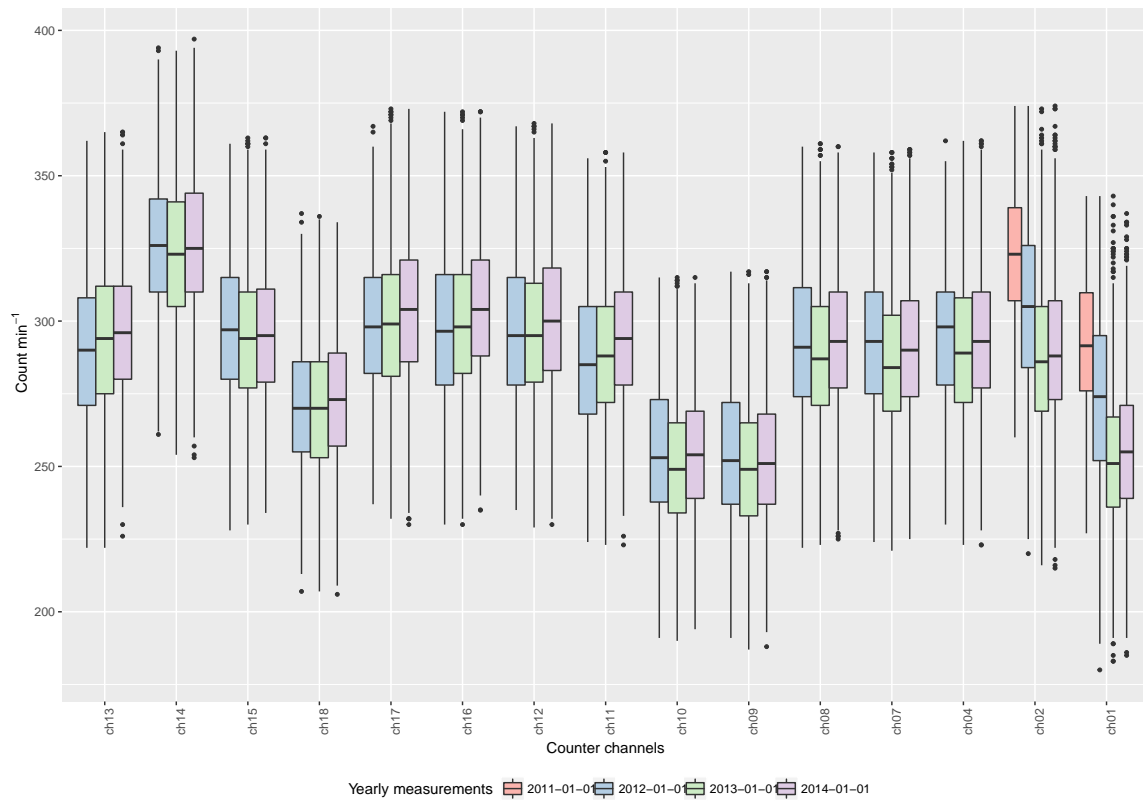
Figure 4-4: Filtered for outliers Boxplot for CaLMa raw data.
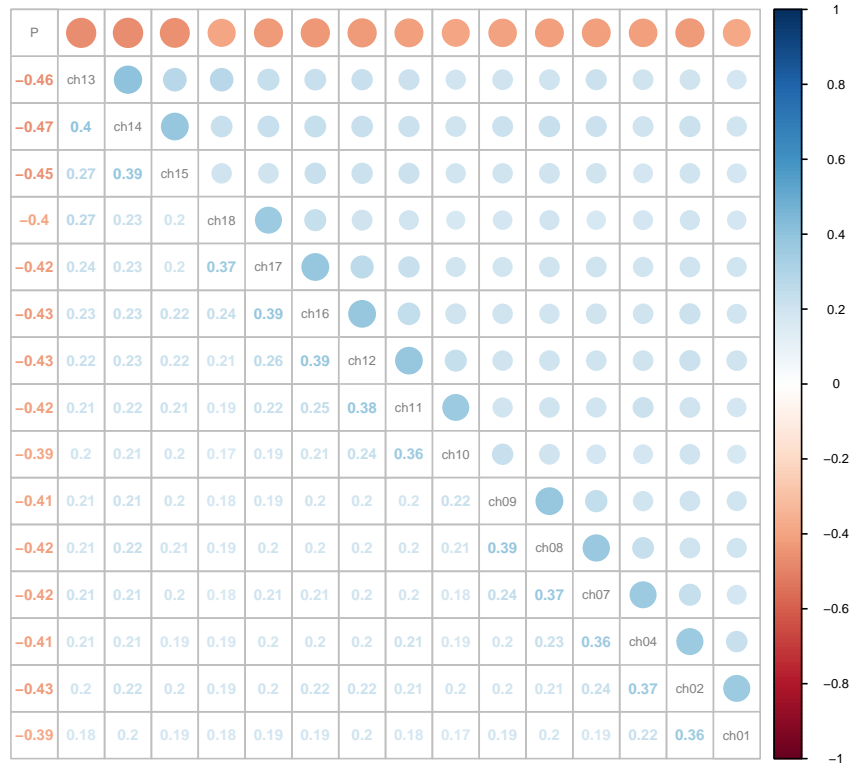
Figure 4-5: Counts and atmospheric pressure correlation matrix.

NMDB. Instead, the corrected value, that is usually NULL to void the measurement, is placed in the `CALM_rev` table. When reading the data from the NMDB, if for the same timestamp there are values in the ORI and in the REV table, the value from the later should be use. There is a convenient database view called `CALM_revori` that do that for us automatically.

4.2.2 The atmospheric pressure effect

The effects on the neutron monitor counts of the atmospheric pressure is a well known phenomenon [4][6]. These effects have to be corrected to further study the variations of the incoming cosmic rays. In this section we will study the effect on the CaLMa station data and will provide a way to correct the data.

Figure 4-5 shows a first check on correlation between measurements and atmospheric pressure. This representation reveals two facts, both expected. The first one is a positive correlation between the counter channels that is stronger between adjacent tubes (see figure 4-6 for the counter tubes physical disposition). Also, the polyethylene separations between the tubes 15 and 16, and 9 and 10 affects also this correlation. The second fact is a strong anticorrelation between counter tubes and atmospheric pressure. This is also known fact, that the air mass above the neutron monitor affects the number of particles that reach the ground level.

To inspect the evolution of the count rate in a monthly scale, data needs to be
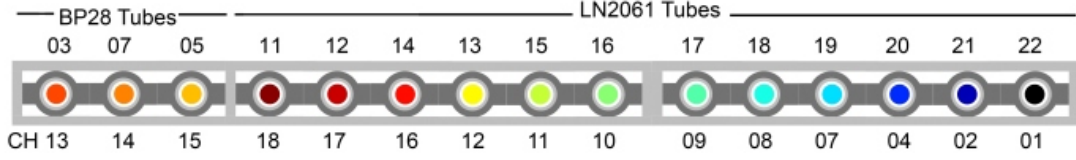
Figure 4-6: Counter tube disposition at the CaLMa station.

aggregated to hourly data. Figure 4-7 shows the results of these aggregation in a range of three months. To normalize counts rates we have to use the t-Student statistic since we don't know the population mean or standard deviation. Instead we will use the sample mean and the sample standard deviation:

$$g(x, X) = \frac{x - \overline{X}}{s} \tag{4.1}$$

Figure 4-7 shows the uncorrected counts per minute of all the channels, stacked together each in a different color, for a selected time span of three months. Overplotted in black is it the evolution of the atmosferic pressure over time. It is easy to appreciate the anticorrelation between the counting rate and the air mass over the station. The bigger the air column the lower number of neutrons being detected. Given this relationship between pressure and counts, we have fit a lineal model using the count rate as a regressor and the pressure as the outcome. The result can be seen in the figure 4-8. Again, the effect of this correlation is obvious, by looking at the slope of the regression line for all the channels. There is roughly one count per 10 hPa of atmospheric pressure. To study the count rate it is therefore necessary to apply a correction that would remove this effect.

4.2.3 Correction for pressure

The most widely used model to account for pressure effect is modeled by the following expression:

$$N = N_0 e^{-\beta(P - P_0)} \tag{4.2}$$

Where:

N is the number of counts per unit of time corrected for pressure.

N_0 is the current number of counts per unit of time recorded.

β is a correction coefficient that is particular for each station in hPa^{-1}.

P_0 is the base line pressure historically recorded for the station in hPa.

P is the current atmosferic pressure readout in hPa.

To calculate the β parameter for the CaLMa station we have proceed as follows:
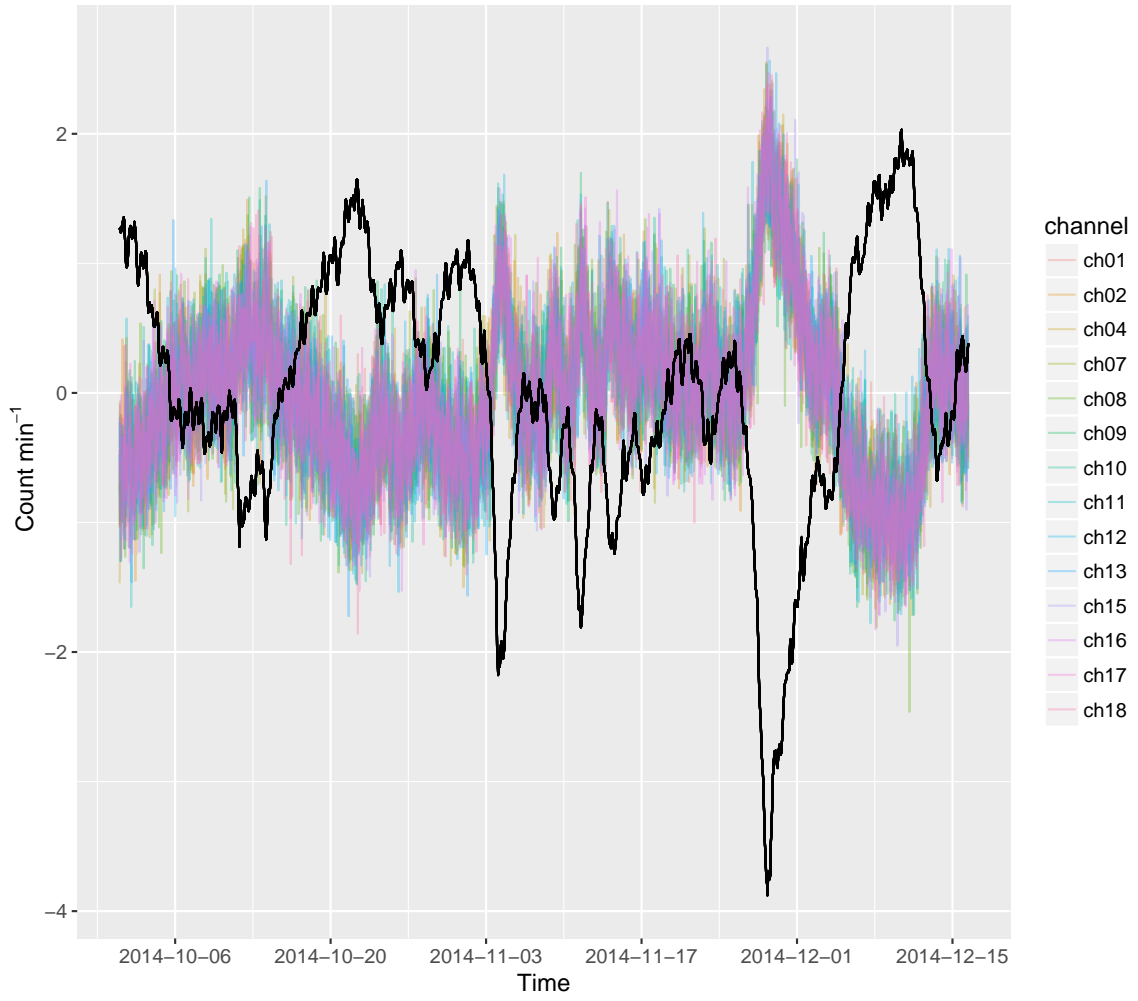
Figure 4-7: Hourly aggregated data and atmospheric pressure influence
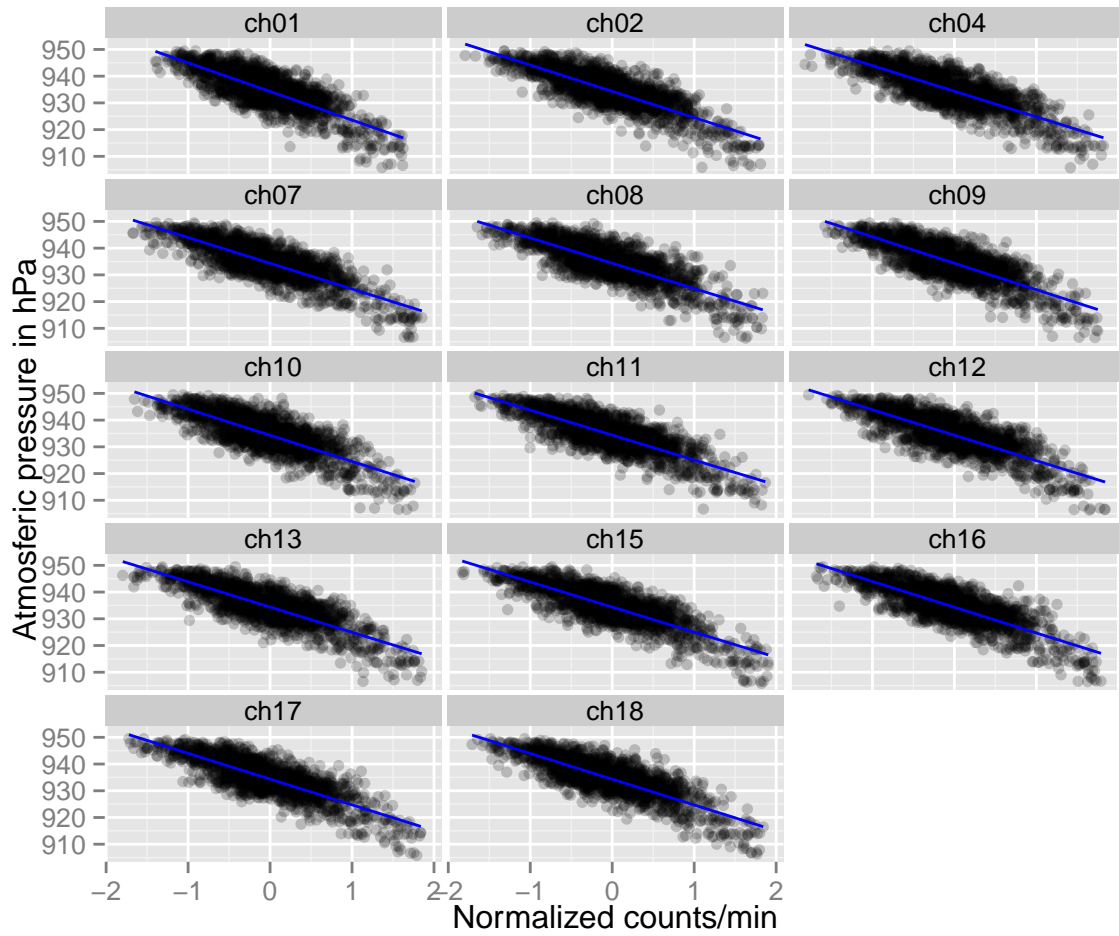
Figure 4-8: Atmosferic influence on the neutron count
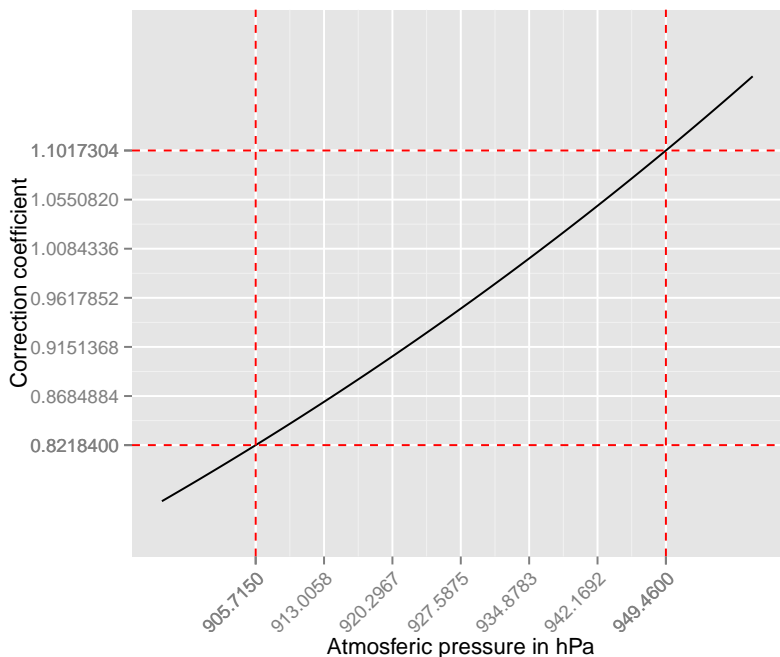
Figure 4-9: Pressure correction function.

1. We obtained the data corrected for pressure during the year 2012, one hour averaged, from the ROME station, since this station has a cutoff rigidity close to CaLMa.

2. In order to find measurements that are free of influences from particle events, such as FD and long-term solar cycle variations, a narrow window was define, for counts in the range of 153 and 154.5 events per minute. This interval has been selected to maximize the number of points available in our station during the same year.

3. From the previous sample, we choose the uncorrected data recorded in CaLMa at the same time as the corrected samples collected in ROME.

4. We proceed to fit the expression $N = N_0 * e^{\beta(P-P_0)}$, setting the parameter $P_0 = 935hPa$, and leaving the parameter N_0 and β free.

The results of the β parameter for the CaLMa station is $-0.0067 \pm 0.0002hPa^{-1}$ for a standarized pressure $P_0 = 935hPa$. The variation of the applied coefficient of correction with the pressure is plotted in figure 4-9. From these values get we that a variation of $10hPa$ of pressure leads to a correction of about 6% over the counts. This correction will be positive if the pressure is below $935hPa$ and negative if it above.

After applying this correction coefficient to the previous measurements results in a normal distribution of the data, that is now no longer affected by the pressure, as it is shown in figure 4-10, which is the sample plot as the one shown in figure 4-8 but now with corrected data for pressure.
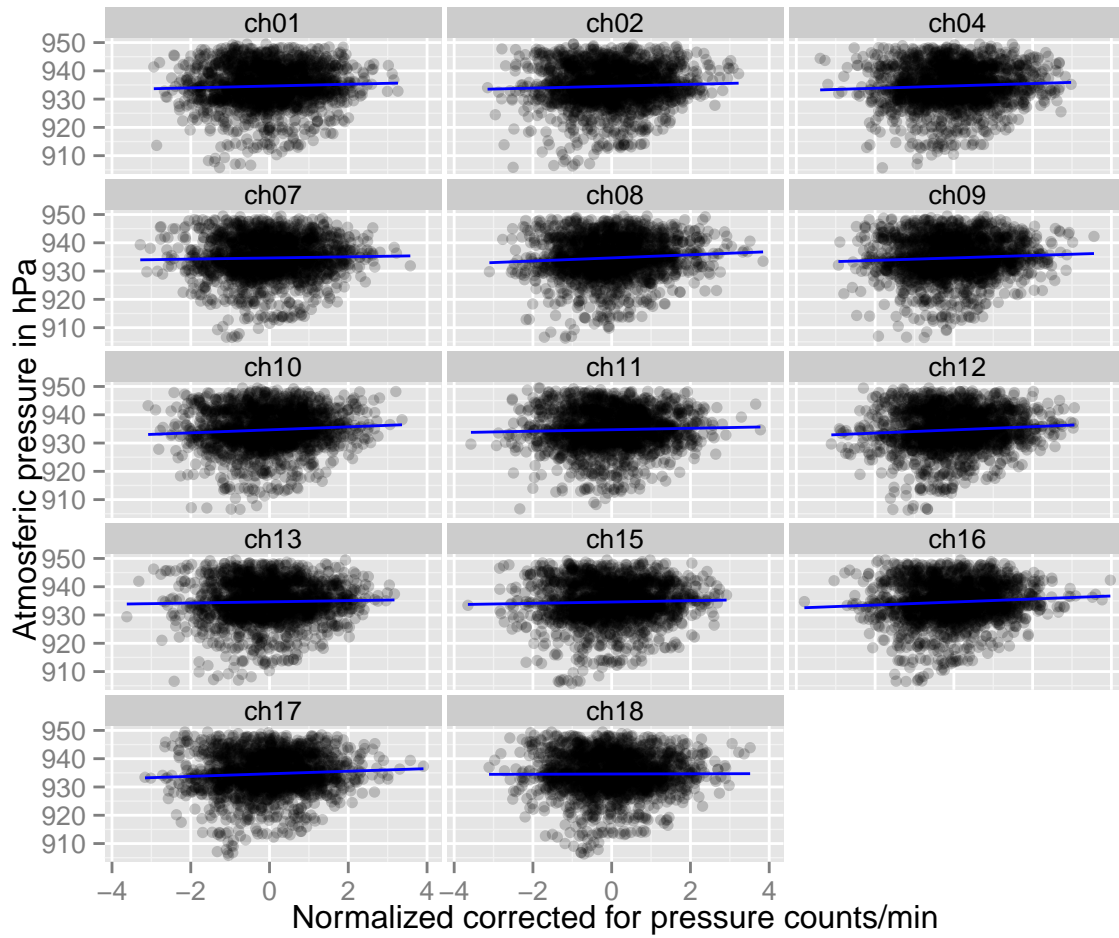
Figure 4-10: Atmosferic influence on the neutron corrected count.
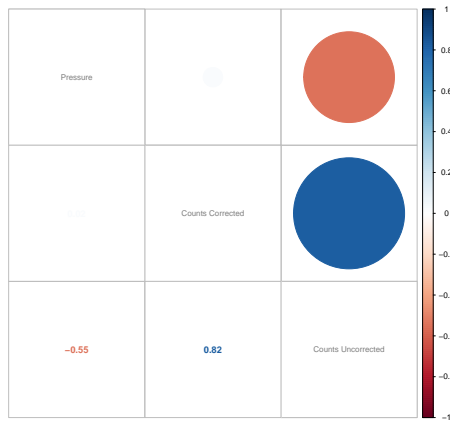
Figure 4-11: Counts and atmospheric pressure correlation matrix after pressure correction.
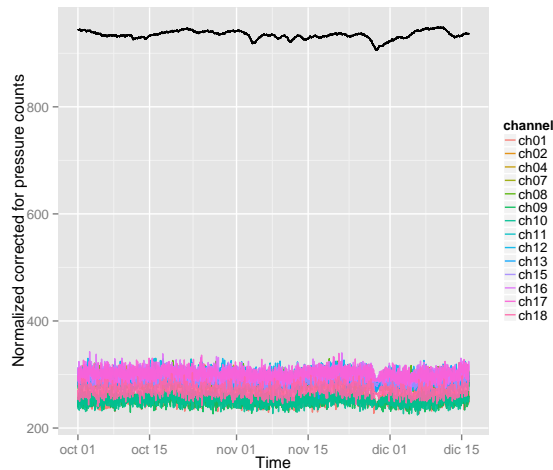
Figure 4-12: Normalized corrected for pressure counts vs. pressure

The new covariance matrix calculated for the new corrected data in figure 4-11 shows no correlation between corrected data and pressure, and figure 4-12 that plots the counts corrected for pressure (coloured lines) and the pressure itself (black line), shows the well known flat behavior of the neutron monitor output when there is no particle event in progress affecting the counting rate.

Although all the stations provide corrected for pressure data to the NMDB, the uncorrected data is published as well along with the barometric pressure registered. This way is it possible to test new barometric correction algorithms if needed.

4.2.4 The median editor

The goal of the editors in general is to provide a single value out of the measurements of all the counters in the station. With this in mind, the simplest editor is the one that

74

would add up the individual counts to obtain a final reading. But editors also tries to get rid off outlier values, such as the ones caused by spikes of transitory counter failure. They also leverage the central limit theorem to reduce the data dispersion by using bigger sample size each minute, so we can expect that a 18 counter tube neutron monitor would have less dispersion that an equivalent with only 3 counters.

One of the most popular editor is called the median editor. Although there are not formal publications about the original median editor, it is attributed to Victor Yanke and the IZMIRAN group. In the article *Median filtering algorithms for multichannel detectors* [11] there is a close description of this algorithm, but the final implementation used in the CaLMa station was based on an informal presentation by Victor Yanke himself during a NMDB meeting in Athens. The overall idea of this algorithm is to find out the median of the relative change of each counter tube with its base value. The resulting relative change is chosen to be the most likely representative change in the counts, and all the station is modulated using this change.

The base value of a counter tube is the average of all the values of this counter in a long time, once corrected for pressure and efficiency, and without outlier values. For the CaLMa station, the base line for all the counters are expressed in the following Python vector.

```
n0 = [255,   290,     0,   295,     0,     0,
      289,   291,   252,   254,   293,   299,
      298,   328,   299,   302,   302,   272]
```

In this vector, the first number 255 is for channel 1, and the last one 272 is for channel 18. The three channels with zero value are not used in CaLMa, since we only have 15 counters.

The following function in the Python programming language, is used to calculate the station value using as a function of `ch`, that is the vector with the current minute counts per detector tube, `n0` that is the vector with the base values, and `e0` that is a vector with the per detector efficiencies. In CaLMa this correction is not made at this points, so this vector is set to 1 and therefore has no effect in the total.

```python
def medianFilter(ch, n0, e0):

        # Ratio of countrate versus reference corrected for efficiency
        # filtering outliers
        r= [float(x)/float(y)/float(z) for x,y,z in zip (ch,e0,n0)
                if z>0 and (float(x)/float(z))< 10]

        s0 = sum(n0);
        tet=numpy.median(r)
        summa=s0*tet

        return summa
```

This algorithm implements a built-in outlier detector that will rule-out a channel with a change rate with respect to its baseline in excess of 100%.

4.3 Embedded data acquisition system for neutron monitors

The article with this title by Juan Jose Blanco, Raúl Gómez-Herrero, Christian T. Steigies, José Medina, Ignacio García Tejedor, Sebastián Sánchez Prieto and myself, was published by IOP Publishing for Sissa Medialab in the Journal of Instrumentation, on August 11, 2014.

In 2014, the Journal Citation Report assigned an impact index of 1.399. It was in the second quartile (Q2) in the Instruments and Instrumentation catetory, and according to Scimago, in this same year, the journal was also in the second quartile (Q2) for the same category.

The article includes a description of the data acquisition system in terms of hardware and software, but also compares the results obtained with this acquisition system with the ones from the old acquisition system that is already running in parallel. The result concludes that both systems retrieves the same measurements and therefore they are interchangeable.

TECHNICAL REPORT

Embedded data acquisition system for neutron monitors

Ó.G. Población,[a,1] **J.J. Blanco,**[b] **R. Gómez-Herrero,**[b] **C.T. Steigies,**[c] **J. Medina,**[b]
I.G. Tejedor[a] **and S. Sánchez**[a]

[a]*Computer Engineering Department, Universidad de Alcalá,*
 Madrid-Barcelona km 33.6, Alcalá de Henares, Madrid, Spain

[b]*Physics and Mathematics Department, Universidad de Alcalá,*
 Madrid-Barcelona km 33.6, Alcalá de Henares, Madrid, Spain

[c]*Institut für Experimentelle und Angewandte Physik, Christian-Albrechts-Universität zu Kiel,*
 Olshausenstr. 40, Kiel, Germany

 E-mail: oscar.gpoblacion@uah.es

ABSTRACT: This article presents the design and implementation of a new data acquisition system to be used as replacement for the old ones that have been in use with neutron monitors for the last decades and, which are eventually becoming obsolete. This new system is also intended to be used in new installations, enabling these scientific instruments to use today's communication networks to send data and receive commands from the operators.

 This system is currently running in two stations: KIEL2, in the Christian-Albrechts-Universität zu Kiel, Kiel, Germany, and CALMA, in the Castilla-La Mancha Neutron Monitor, Guadalajara, Spain.

---

[1]Corresponding author.

Contents

1 Introduction

1.1 Neutron monitors

A neutron monitor is a ground based instrument designed to measure cosmic rays penetrating the Earth's atmosphere with energies ranging from 0.5 to 20 GeV by means of detecting secondary neutrons produced by primary cosmic rays when interacting with the high atmosphere. The core of a neutron monitor is a tube filled with boron trifluoride BF_3, a gas with a large cross section for capturing thermal neutrons, and also features an anode placed along its axis. A high voltage is applied between this anode and the walls of the tube, thus creating a high voltage field. To be able to detect fast neutrons, a housing with a moderator material (polyethylene) surrounds the detector tube. Tubes are also surrounded by a lead producer, so that when a neutron reaches the producer, chances are that further low energy neutrons are generated. Combining this lead producer with the deflector material (also polyethylene) increases the probability of detection. Detection happens when a neutron enters the counter tube and interacts with a BF_3 molecule. In this moment, the following nuclear reaction may occur:

$$^{10}B + n \rightarrow\ ^{7}Li^* +\ ^{4}\alpha + 2310\text{keV}$$
$$^{10}B + n \rightarrow\ ^{7}Li +\ ^{4}\alpha + 2792\text{keV}$$
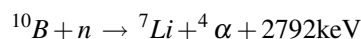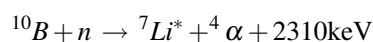
The kinetic energy of these resulting nuclei is transferred to the gas (ionizing the BF_3 molecules) before reaching the walls of the tubes [1], and the high voltage field created between the anode and the walls causes the resulting ionization electrons to move towards the anode thus generating an electrical current pulse. The maximum pulse amplitude is obtained when all kinetic energy of the nuclei resulting from the reaction is transferred to the gas.

If the generated pulse exceeds a given threshold, a digital pulse of about 300 mV [2] with a $22\mu s$ width is generated. This pulse reaches the data acquisition system through a coaxial cable where it is to be registered.

Typical count rates range from 4 counts/s per detector for stations located near the equator up to 15 counts/s per detector for polar stations. Given that stations seldom have more than 18 counters, and that a ground level enhancement might double the counting rate in polar stations, the acquisition system should be able to handle about 1800 counts per minute and per counter. Also, since the total count is affected by the air column over the monitor, it is necessary to provide a mechanism to obtain the current barometric pressure so it can be used by the corresponding correction algorithms.

1.2 Improvements

The new registration system has been designed taking into account several requirements. It will be able to handle the count signals of up to 18 counters, which is the typical number of channels for this type of stations. Acquisition will start at the beginning of the minute and will stop at the end, starting then a new acquisition cycle. The data from the last minute has to be buffered until it is transmitted to the handling system. It is very important to keep system's date and time synchronized with an authoritative reference. This way the readings of one station can be compared with the ones acquired in other monitors. The neutron monitor counts are strongly influenced by the atmospheric pressure [3], therefore the system must be able to record this pressure along with the counts, so the proper corrections can be made later. High voltage power supplies are also monitored to ensure that proper biasing voltage is being applied to the counter tubes. To overcome the problem of dealing with different power supply control techniques from different manufacturers, a new software layer has been developed to hide these details and provide an uniform application program interface for all of them. Also, to increase system's reliability, a low voltage power supply selection mechanism has been provided to allow the operator to switch between a main or a redundant unit.

Finally, the system will interface via the internet with the Neutron Monitor Database [5] (NMDB) and will upload the count measurements every minute, so that real time data is available to the end users. The NMDB is a global database where many international neutron monitor stations upload their data, making it available in real time to scientists and other interested parties. The NMDB project has been funded by the European Union's 7th Framework Program.

2 Electronic design of the new system

Figure 1 shows the three components that make up the data acquisition system. Each one is in a different printed circuit board: the counter interface and power redundancy control, the Linux embedded system and the FPGA-based counter board.
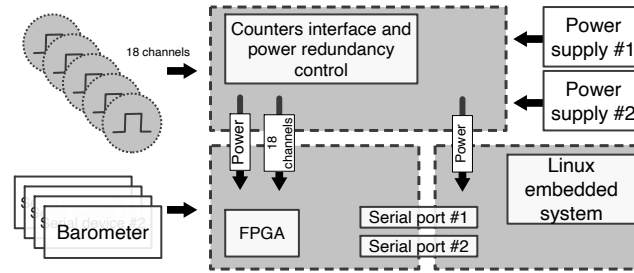
Figure 1. Block diagram of the system.

The first one provides a mechanical interface for the cabling and connectors of the counting tubes of each station. Some stations use BNC connectors like KIEL, others DB25 like KIEL2, other LEMO connectors like CALMA, and there might be other types in future stations. Whatever the type of the connector used, this board makes a mechanical conversion to a 40 pins IDC (*Insulation Displacement Connector*), which is the one used to interface with the FPGA-based board. This board also features a switch that enables the operator to select which power supply will be used to power up the system. Flipping this switch selects which of the two power supply input sets is output, to feed the rest of the components. Each set consists of three power rails of +12V, -12V and +5V respectively.

The second component is the FPGA board, which is the core of the data acquisition system. Its main purpose is counting the pulses from the detectors simultaneously and multiplexing the serial communications from other devices such as the barometer and the high voltage power supply. This component is described in detail in section 2.1, later in this document.

The third component is a Linux-based embedded system, which is mainly used for data handling. It is in charge of running all the algorithms for data processing, interfacing with the NMDB, keeping the date and time information synchronized, and downloading data from the barometer, the high voltage power supplies and the FPGA card and storing them in a SQLite database. This component will be further described in section 2.2.

2.1 FGPA-based counter board

The center of this subsystem is a Spartan 3E FPGA from Xilinx [4]. This is a powerful yet cheap and widely available part, with affordable developer tools in the market. It is packaged in TQFP-144 that can be soldered without using specialized tools and technologies. The FPGA loads its program from a serial EEPROM memory after a power-on reset. This memory can be programmed via JTAG ports, also present in the board.

The digital signals from the amplifiers reach a level shifter that adapts them to 3.3V LVTTL levels, suitable for interfacing with the general purpose input pins in the FPGA.

2.1.1 FPGA core definition

The intellectual property (IP) core synthesized and loaded in the FPGA has been designed to perform two basic tasks. The first is to implement the event counting procedure and the second is to control the serial port multiplexing. The FPGA acts like a slave peripheral, waiting for the com-
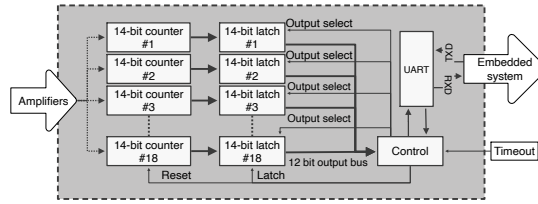
– 3 –

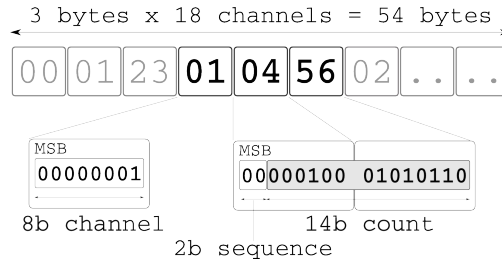**Figure 2**. Counter array fpga-core block diagram.

Figure 3. Sample protocol frame format.

mands that the Linux embedded system board will send over a serial line. There are four possible commands: SWITCH, READ_COUNTER, RESET_FPGA and FPGA_ACK.

As shown in figure 2, counting is performed by an array of 18 independent 14-bit digital counters triggered by the rising edge of the pulse coming from the amplifier/discriminator. The maximum count per channel is therefore $2^{14} = 16384$ cts. Considering that the maximum expected count rate is 1800 cts per minute and per channel, and that the integration time will be one minute, a maximum count of 16384 per channel is more than enough to accommodate any possible ground level event. If the counters reach this limit, they do not overflow but hold their maximum value without further increments. This allows the software to detect anomalies (possibly noise) in the counting. When the counting period is over, an array of 18 latches captures the counters' values and set them to zero to start counting again for the next minute. This capture process is driven by the embedded system, either by sending a special command over the serial port or asserting the timeout hardware signal. While the first method has the disadvantage of introducing software delays, it does not require a special line from the embedded system nor realtime capabilities to handle this signal. For this application the software method is preferred because the delays introduced are in the milliseconds order of magnitude, and therefore they are negligible.

Regardless the method used, counts are sent back to the embedded system over a serial line using a very simple protocol. Three bytes are sent for each counter; one indicates the channel number and the other two represent the actual count number, including a 2-bit sequence to help in the synchronization with the receiver. Figure 3 shows an example of the frame protocol.

2.1.2 Barometer interfacing

The barometer, as many other devices, has a serial communication line for sending pressure data to and receiving commands from the embedded system. The device acts as a slave device, so it never initiates communication. Instead, it waits to be addressed by the embedded system, which acts
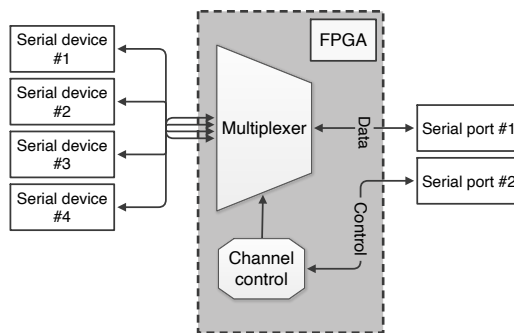
Figure 4. Serial port multiplexing.

like a master in this scenario. This is also the behaviour of any other devices that can be plugged to the system, such as high voltage power supplies, GPS and other time sources, analog to digital converters, etc. In a vast majority of embedded systems, serial line ports are very common but also limited in number. This is why a serial port multiplexer has been implemented in the FPGA. Figure 4 shows a block diagram of the IP core implementing this multiplexer.

The embedded system uses one of its serial lines to choose which serial device has to be selected for data transfer. This is done with a control command sent through the control serial line. This is the same mechanism used to control the general behavior of the event counters in the FPGA. This architecture has the advantage that once a channel has been selected, it behaves like a native serial device and there is no need for the special escape characters needed when both control and data are sent over the same communication line.

2.1.3 High voltage power supply interfacing

High voltage power supplies can be controlled either by means of an analog reference signal or by commands sent over a digital communications line. Monitoring can also be done by reading a feedback analog signal from the source or by reading back the result of the corresponding command from the digital communication line. This depends of course on the manufacturer and/or chosen model. Each neutron monitor where this data acquisition system is working has different types of sources: the ones used in KIEL/KIEL2 are analog while the ones used in CALMA are digital.

To interface digital sources there is no need for special hardware. They are attached to one of the inputs in the serial port multiplexer and the software in the embedded system takes care of them. For the analog ones, a special add-on board has been designed to convert from analog to digital and vice versa. This board is connected to the embedded system through one of its serial peripheral interfaces (SPI) and a dedicated piece of software commands the read and write operations. Figure 5 shows a block diagram of this board.

The high voltage power supplies in KIEL/KIEL2 provide a reference V_{out} DC signal with a voltage in the 0V to 10V range, which is linearly proportional to the high voltage output they are providing at any given time. This signal is converted with an analog to digital converter and the resulting data is transmitted via SPI to the embedded system, where it is recorded. Conversely, the embedded system can send a voltage reference value through the SPI channel which is in turn
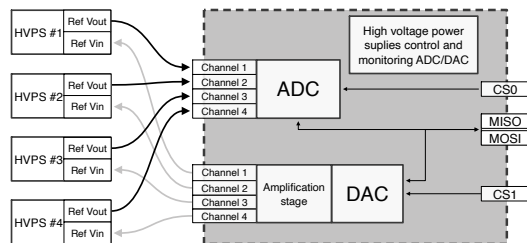
Figure 5. High voltage power supplies ADC-DAC control board.

converted by a digital to analog converter to set a reference V_{in} input signal, also between 0V and 10V, which is used by the high voltage power supplies to adjust their voltage output proportionally.

2.2 The Linux embedded system

To fulfill the requirements of data processing and handling, a Linux embedded system has been used. This type of system is optimal for this purpose because of its low cost while providing high reliability and flexibility. It doesn't have any moving parts, can operate in a wide range of temperatures and has very low power consumption. When browsing the market for a candidate processor board, the hardware features required were: ethernet interface, SPI channel support, serial port, external flash storage card support and a good Linux support. Attending to these constraints and some other external factors like market availability, we have chosen the NGW100 mkII from Atmel.

2.2.1 Realtime synchronization

One of the most important pieces of software running on the embedded system is the *Network Time Protocol NTP* daemon. This software is able to perform clock synchronization over a variable-latency network such as the internet. Thus, small adjustments can be made to the local clock to keep it up to date. Accuracy using the internet typically ranges between 5ms and 100ms [10], enough for the real time constraint of the Neutron Monitor Data Base (NMDB) [5], which is 1 minute.

Typical values for CALMA are 4.58 ms of offset difference with the time master source, pulling every 1024 seconds. Although having a battery-backed real time clock is a desirable feature, it is often dropped to keep the price low. This is the case of the NGW100. Thus, when booting the system the clock is not set and the offset with the master clock reference is too large to be compensated by NTP. To overcome this problem, a startup script is executed to setup the local clock with the master clock. From this point on NTP takes over.

2.3 Data processing and storage

Figure 6 shows the overall data processing and storage architecture implemented in CALMA. There are three main elements in this architecture: the embedded data acquisition system, the laboratory server and the public server. The purpose of each of these elements is to capture the data, to store the data locally in its original format and to publish data in the NMDB respectively.

The embedded data acquisition system runs a multithreaded C program that controls the acquisition procedure. When debugging or installing a new system it can be launched in test mode. This mode runs the software interactively, and thus the operator can issue any of the available
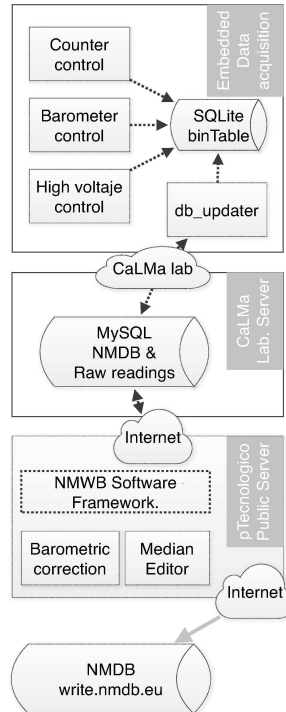
Figure 6. General server layout for CALMA.

commands and receive the answer as it is available. This makes it possible to check if the FPGA board is online, check the counter value for each channel, read barometer and high voltage sources information and do some other housekeeping tasks.

When the software runs in loop mode, two execution threads are launched. The first thread handles the counting process of the FPGA board and the second gathers data from the auxiliary devices: the barometer and the high voltage power supplies in this case. The counting thread synchronizes with the current time of day and requests the operating system to be woken up right in the first second of the next minute. When that happens, it sends a READ_COUNTER command to the FPGA board to retrieve the counter values and to start a new counting period. The counter values are then properly parsed and stored in a SQLite database. The corresponding table scheme includes the total count value of each of the potential eighteen channels, the voltage readout from a maximum of three high voltage power supplies and the atmospheric pressure reading. Once all this is done, the thread sleeps again until the start of the next minute.

Figure 7 shows an example of the readings for each detector over a month, along with the atmospheric pressure recorded in the CALMA station. Figure 8 shows a sketch of the physical layout of the different counter tubes for this station.

If any of the commands sent to the PFGA board fails, there is a watchdog mechanism in order to attempt a system recovery. The first time a command fails, the software tries to soft-reset the FPGA board up to three times. This soft-reset is a command that resets the internal IP core to a known state. If communication is reestablished at this point, the failure event is logged and the system operation is resumed. Otherwise, a hard-reset is attempted. This is a physical reset on the
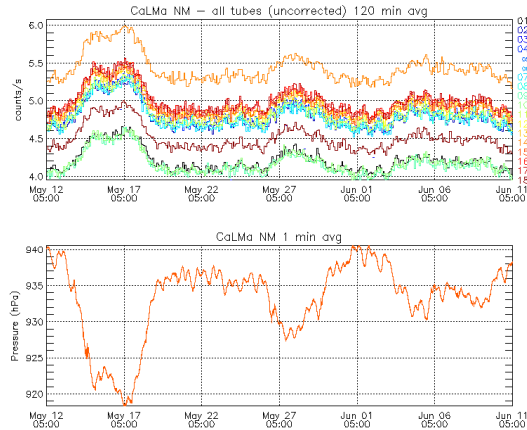
Figure 7. Raw readings and atmosferic pressure taken from the data acquisition system.
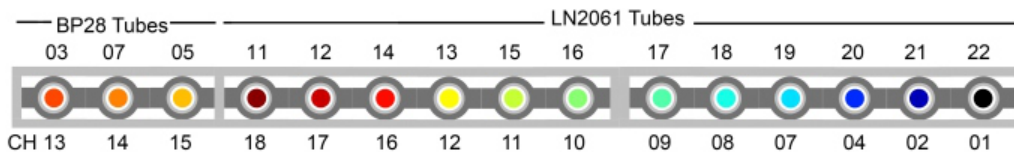
Figure 8. CALMA counter tubes setup.

FPGA board that forces the core to be reloaded, hopefully restoring normal operation.

Every minute a cron job called `db-updater` is activated in the embedded system, which connects via ethernet with an external MySQL database installed in the Linux laboratory server and retrieves the date of the last time the data was updated. The system then transfers all data starting at that date from the local SQLite database to the MySQL server.

Finally, a public server whose IP address has been authorized to access the NMDB database, contacts the MySQL server using a dedicated virtual private network. In this computer, a program written in Python [8] calculates a global value for the station, which is the result of the application the median editor algorithm described in [11]. This algorithm calculates the median of the rate between the detectors actual count and the base count. The base count is the average event count per detector over a long period of time in which there were no strong count fluctuations such as a Ground Level Enhancement (GLE) or a Forbush Decrease (FD). The rate is then used to correct the base count of all counters, and the sum of all these corrected values is the global station value. Once data have been corrected for pressure, the NMDB database is contacted and the new data are sent. This real-time one-minute resolution makes the NMDB a perfect data provider for radiation monitoring and alert systems like the one implemented by the Physics Department, section of Nuclear and Particle Physics, in the University of Athens [6]. Also, this server hosts the station's web page [9] and provides some data backup facilities.

3   Results

The data acquisition system described in this article has been installed successfully in two European stations: the first in the Christian-Albrechts-Universität zu Kiel, Germany (KIEL2), and the second
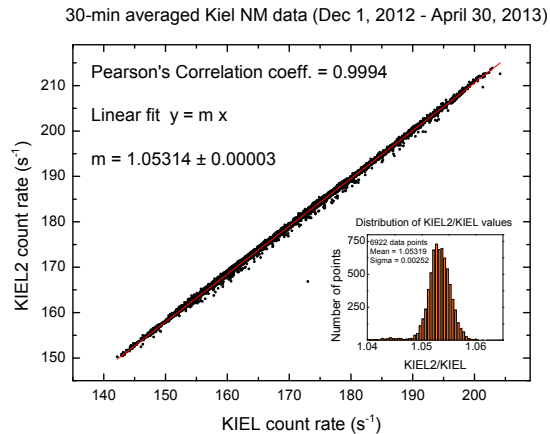
Figure 9. 30-min averaged KIEL vs KIEL2 correlation.

in the Castilla-La Mancha Neutron Monitor (CALMA) in Guadalajara, Spain. The results of these two installations will be described in the next sections.

3.1 Kiel's neutron monitor acquisition system

Kiel's neutron monitor is running both the original acquisition system and the new one described in this paper for the duration of the transition from one to the other. Digital signals coming from the counters are split to feed both systems, each one processing the data according to its own independent algorithm, and then both sets are published to NMDB as KIEL and KIEL2, corresponding to the old and the new system respectively. Unlike KIEL2, KIEL is not able to publish data in real time because the computer in charge of the data processing algorithms runs the MS-DOS operating system and does not have network hardware. Furthermore, samples are taken based on the system's clock which has a strong time drift that has to be manually corrected and that affects per-minute data.

Figure 9 shows the correlation between the 30-min averaged KIEL2 and KIEL raw counting rates registered from December 1, 2012 through April 30, 2013. This averaging interval is sufficiently long to smooth-out the effect of clock-synchronization fluctuations between KIEL and KIEL2. Both datasets show a clear linear correlation, with a linear-fit slope of 1.0531 and a correlation coefficient of 99.94%. The bottom-right insert shows the histogram of the KIEL2 to KIEL ratio for the same period, with a mean value of 1.0531. Although we have a clue about why this slope is slightly different than one, further research on the old registration system history is needed before drawing a conclusion.

Figure 10 shows a comparison of KIEL and KIEL2 30-averaged counting rates measured during the period December 1, 2012 to April 30, 2013. KIEL measurements have been multiplied by the factor 1.0531 described above (see figure 9). The top panel shows raw counting rates, while the rates shown in the bottom panel have been corrected from the effect of atmospheric pressure [3]. This period includes both, quiet periods and Forbush decreases, the most prominent one during the second half of March, 2013 (clearly seen in bottom panel).
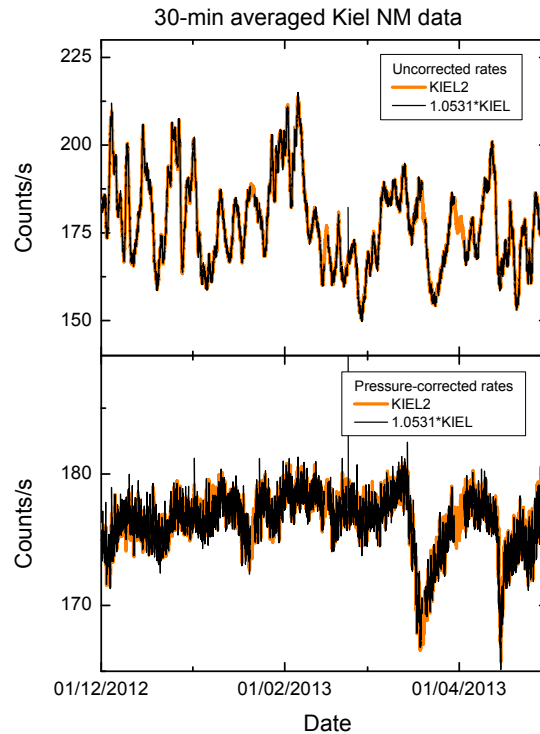
Figure 10. 30-min averaged KIEL vs KIEL2 overplot.

3.2 CALMA neutron monitor acquisition system

Castilla-La Mancha Neutron Monitor (CALMA) [7] has been running the data acquisition system presented in this paper since July 2012. The neutron monitor setup is shown in figure 8, and the raw readings as they are captured by the system are in figure 7.

The strong fluctuations present in all the counter tubes are caused by the influence of the air column above the neutron monitor and must be therefore corrected. The data acquisition system is able to read the pressure from an external Meteolabor BM35 barometer connected to a serial port as described in 2.1.2 and this information will be used for this purpose in the post-processing stage (see 2.3). One of the first signs of proper operation is indeed this strong anti-correlation shown in figure 7 between atmospheric pressure and uncorrected count rate. Once the raw readings have been corrected for pressure, a median filter is applied to obtain a single value for all the counters. Figure 11 and figure 12 show respectively a quiet time period and an active interval with a prominent Forbush decrease, related to solar activity in the preeceding days, recorded by the data acquisition systems in KIEL2, KIEL and CALMA (from top to bottom).

Some differences are observed during this quiet period between KIEL, KIEL2 system and CALMA (figure 11). These differences can be attributed to the different rigidity cutoff of the two stations and the stronger statistical fluctuations of CALMA data due to the lower base count rates. Nevertheless, a clear correlation appears during the FD because it is a global effect, which means that a FD is observed by neutron monitors around Earth and the observed differences are caused mainly by the rigidity cutoffs in each station (figure 12).
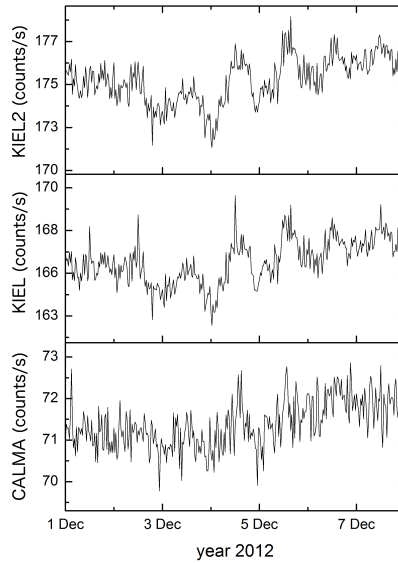
Figure 11. Quiet time seen by KIEL2, KIEL and CALMA.
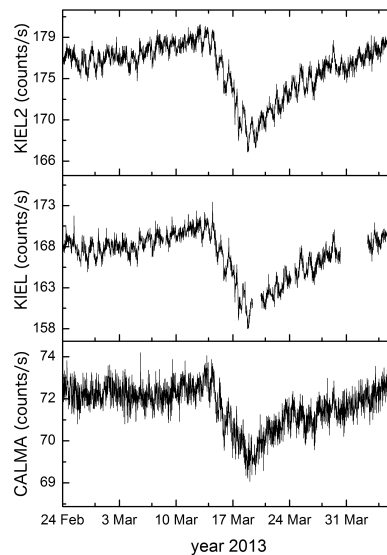
Figure 12. Active time seen by KIEL2, KIEL and CALMA.

4 Conclusions and future work

The data acquisition system described in this paper has been designed not only to fulfill the experiment's requirements, but also to keep its production costs low by using widely available components that don't require special soldering tools. The resulting printed circuit board is a four layer eurocard (DIN 41612), and the approximate cost breakdown[1] for the hardware is as follows: printed circuit board; 18 €, FPGA: 30 €, embedded system: 100 €, other electronic components: 50 €.

---

[1]Regular customer prices by mid 2014, with no bulk rates or any other special pricing applied.

The board manufacturing files and embedded software used are both freely available upon request.

In this paper we have proven that this new acquisition system is a cost-effective replacement for neutron monitor stations, some of them operating with old electronics for which replacement parts are not available.

Parallel tests conducted in KIEL and KIEL2 stations show that both systems provide almost identical results. By adding a simple correction for efficiency factor described previously, the existing historical data will be comparable to the data from the new system. This is important as it allows the study of the long-term variations of solar activity.

The results of the new CALMA station, where this acquisition system has been in uninterrupted operation since December 2011 show an adequate behaviour, as was expected.

Further work continues to improve this acquisition system with new functionalities, such a counter diagnostics by pulse height analysis and a web interface for data inspection and instrument configuration. Also, new installations in some other European and American stations are being considered in the near future.

Acknowledgments

References

[1] W. Abson et al., *Boron trifluoride proportional counters*, *IEEE Proc.*. **B 105** (1958) 357.

[2] Chalk River, Ontario, Canada, *BP28 Chalk River neutron counter operating data*.

[3] J.M. Clem and L.I. Dorman, *Neutron monitor response functions*, *Space Sci. Rev.* **93** (2000) 335.

[4] Xilinx Inc., *Xilinx spartan 3e*, online (2013).

[5] H. Mavromichalaki et al., *Applications and usage of the real-time Neutron Monitor Database*, *Adv. Space Res.* **47** (2011) 2210.

[6] H. Mavromichalaki et al., *GLEs as a warning tool for radiation effects on electronics and systems: a new alert system based on real-time neutron monitors*, *IEEE Tr. Nucl. Sci.* **54** (2007) 1082.

[7] J. Medina et al., *Castilla-La Mancha neutron monitor*, *Nucl. Instrum. Meth.* **A 727** (2013) 97.

[8] C.T. Steigies, *A collection of Python scripts to work with the Neutron Monitor Database (NMDB)*, (2013).

[9] The CaLMa Neutron Monitor Team, *CaLMa web page*, (2014).

[10] The NTP team, *NTP.org web page*, (2013).

[11] V. Yanke. *Primary processing of multichannel cosmic ray detectors*, in the proceedings of the 32nd *International Cosmic Ray Conference (ICRC2011)*, August 11–18, Beijing, China (2011).

Chapter 5

Conclusions

Years after its initial inception the Neutron Monitor Database is still in operation, collecting data from 68 stations, CaLMa and another 27 stations uploading high resolution real time data.

The NMDB is providing the scientific community with valuable information about cosmic rays, such as density, anisotropy, pitch angle, solar and galactic spectra and radiation doses. Also it allows several Ground Level Enhancement Alert Systems to provide an early warning about the arrival of high energy particle events. This data is also used in radiation dosimetry due to cosmic rays, and this has been applied to the measurement of the radiation exposure of aircrew, specially of airplanes that flight over the polar regions.

Since the data in the NMDB is stored and indexed in a relational database enables the researchers to explore the entire data set efficiently to find patterns and time series that can be easily correlated with other sources.

Although several stations have ceased their operations, their data is still a valuable source of historical information, and the NMDB can be use to store this information as well. Also, day after day, operational stations are upgrading their data acquisition systems to join NMDB and provide real-time data to the community.

The CaLMa station is been operational since October 2010, providing real-time data to the NMDB since the very beginning. The station has undergone several changes and upgrades. Starting with only three NM64 counter tubes, it was upgraded with twelve LND2061 tubes in July 2011. For all these counters, an initial data analysis was performed to confirm the were in optimal operational conditions. This included a plateau test to determine the biasing high voltage level, a response spectrum to identify at least the strongest energy peak, the determination of the base line of each counter, and the determination of the barometric atmospheric coefficient. Another minor upgrade was to include a front panel polyethylene cover, but it was enough to cause a visible step in the data when plotting the values prior to this change. To solve this, a correction for efficiency coefficient was applied to the published data. CaLMa has been cited in several publications and is still in operation at the time this document is written. The ongoing research activities include data quality and maintenance, data analysis based on machine learning techniques and the OrCA experiment that will take a mini neutron monitor to the Spanish station

in Antarctica.

As a result of our work in the Neutron Monitor Database FP7 project, a new data acquisition system has been designed, built and put in operation in two different stations in Kiel, Germany and in Guadalajara, Spain. This acquisition system is been a proof of concept about the use of FPGA technologies for data acquisition in Neutron Monitors, and although it is out of the scope of this work, it will allow in future projects to introduce new measurements such as inter-pulse distance, pulse height estimation, inter-channel correlations, etc. Different IP cores have been designed and tested, using two different main approaches: synthesize vectors of digital counters and synthesize a logic state change detector that will turn channel pulses into time-stamped events. Although the first approach is easier to implement, less error prone and fulfils the main requisite of the acquisition, the second is really promising as it will allow a much deeper data analysis. The first approach is known is our group as Core1, and this has been the one chosen for CaLMa and KIEL2 data acquisition systems. Both systems have been running simultaneously for a long time, and also in the case of KIEL2, in parallel with the old data acquisition system. The comparison of the data provided by all these system has helped to validate that all of them provide the same output.

From the architectural point of view, the FPGA has been used to isolate the acquisition hardware from the processing hardware. Independently of the technique used to record the data from the counter tubes, the output of the FPGA system will be provided through a asynchronous serial communication channel. Despite the limitations of this kind of communication channel, it has been chosen because it is ubiquitous, or at least very easy to include, in almost all computational hardware available. This is important to overcome the problem of obsolescence of this part of the hardware, that on the other hand plays a very important role in the acquisition system, since it is in charge of processing the data from the FPGA, combine other data sources such as barometric pressure, provide long term storage and communicate with the Internet. In this work we have chosen a Linux embedded system from Atmel known as the NGW100. This system has proved to be very stable and reliable. At the time this document was written, the uptime of the NGW100 system running in the CaLMa station was 642 days, while the uptime of the server in the laboratory was only 32 days. Unfortunately this component has reached the end of its life and it is no longer recommended for new designs. Because of this, the new acquisition systems that have been developed in our group have used the Beagle Bone Black Linux embedded system.

During the operations of the CaLMa station, special care has been taken about the quality of the data that is uploaded to the NMDB. There two most common issues with the data quality are the continuity of the measurements and the spikes in the data. Since the network connectivity is not always as good as desired, and even though the data acquisition system will upload missing data delayed up to three days, from time to time it is necessary to manually fill gaps in the data. The spikes on the other hand are single values that are tenths or hundredths times away of the standard deviation of the station, and are therefore considered as noise. The median editor does a good work identifying and voiding spikes when they happen in a few

detectors, but not when they affect almost all of them. In these cases there are some other automatic detection tools, but we prefer to correct them manually after human supervision. To this end we have developed a software tool to help the station operator to identify and remove spikes in the data. This work was published by IOP Publishing Ltd [10], in 2015.
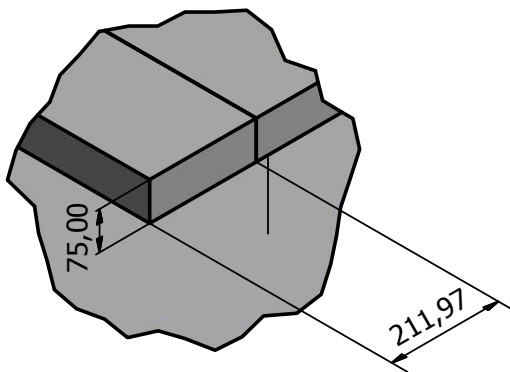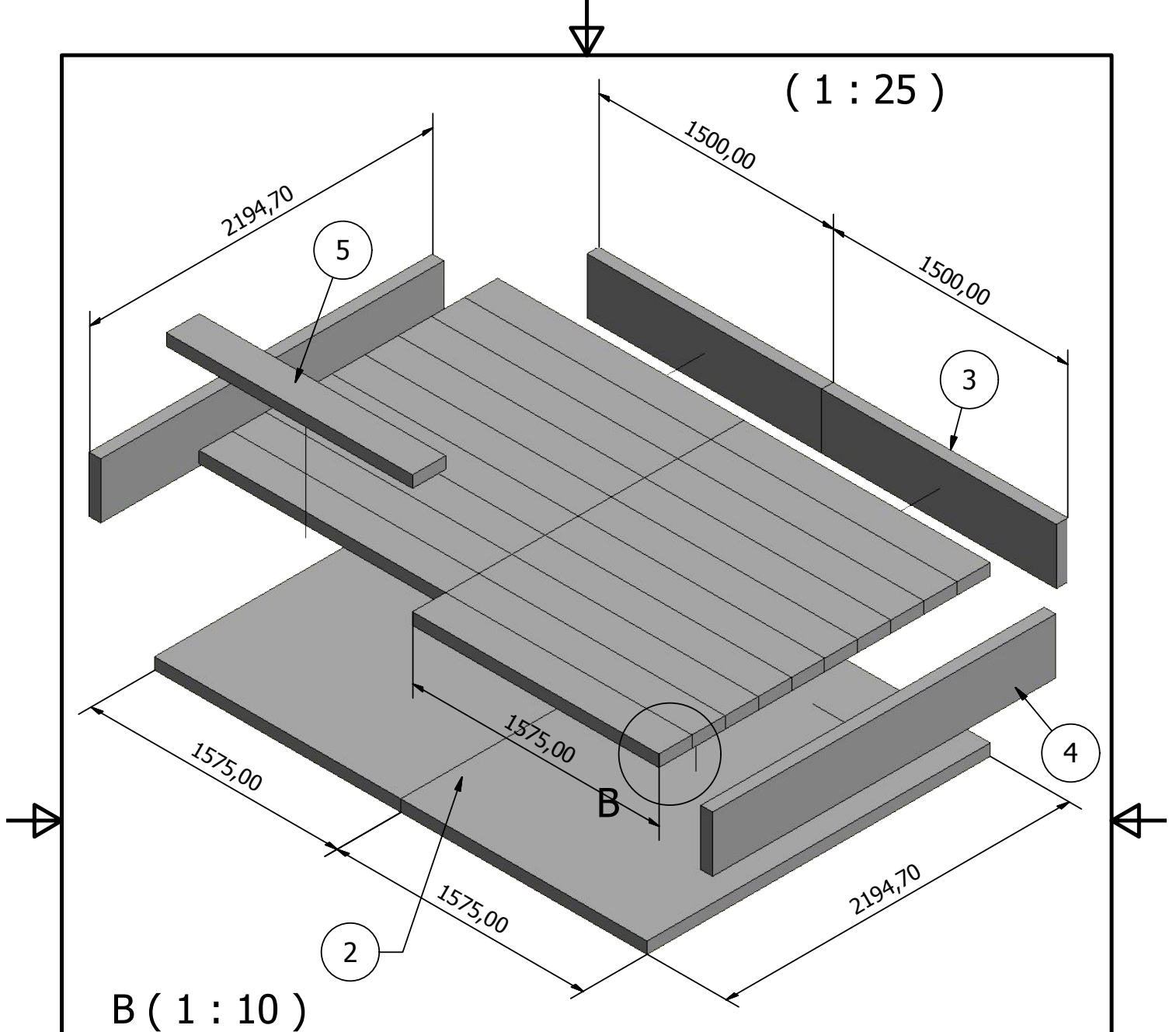
The future works derived from the CaLMa station and its data acquisition system are focused in two lines: the construction of a small neutron/muon in the Spanish station in Antarctica and the applications of new data analysis techniques to the data that will be soon available from the new Core2. We hope that this will provide the scientific community with new and interesting insights about the galactic cosmic rays and the interaction of the Sun with the Earth.

Appendices

Appendix A

CaLMa

A.1 The CaLMa neutron monitor breakdown

(1 : 25)

2194,70

1500,00

1500,00

5

3

1575,00

1575,00

1575,00

B

2194,70

4

2

B (1 : 10)

75,00

211,97

Part list			
#Elem	Quant.	Description	Mass/Unit
2	2	Bottom slabs	246,8 kg
3	2	Rear slabs	38,1 kg
4	2	L/R slabs	55,8 kg
5	20	Top slabs	23,8 kg

Diseño de	Revisado por	Aprobado por	Fecha		Fecha	
Óscar García					20/07/2015	

51,10mm

80,00mm

R178,00mm

R127,00mm

123,00mm

123,00mm

Diseño de	Revisado por	Aprobado por	Fecha		Fecha	
Óscar García					20/07/2015	

CaLMa	CaLMa	
	Lead rings assembly	Edición / Hoja 3 / 5

D

2044,00mm

5

2

3

3

1

6
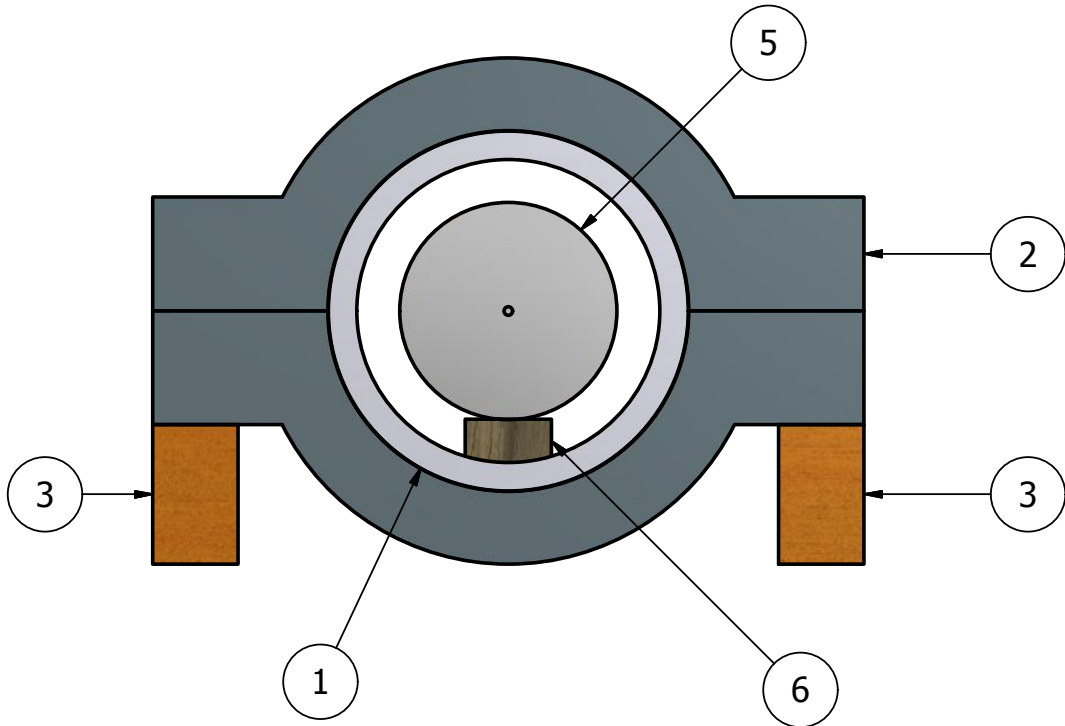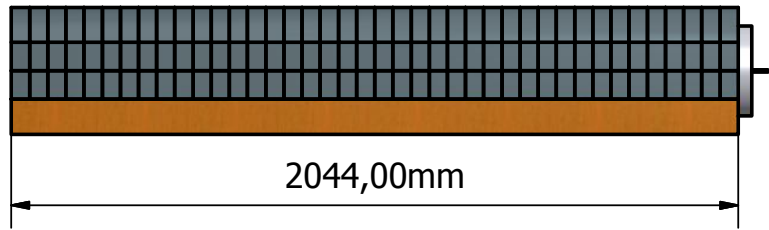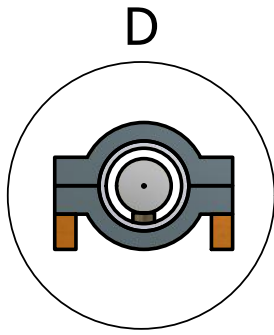
Part List			
Part.#	Quant.	Part.	Mass
1	1	Moderator	29,028 kg
2	80	Lead Half-Ring	21,408 kg
3	2	Wood stripe	6,610 kg
5	1	LND2061	8,040 kg
6	2	Wood chuck	0,122 kg

E (1 : 10)
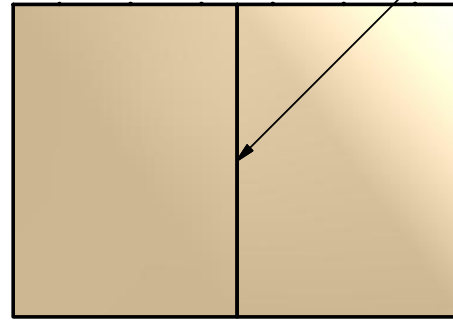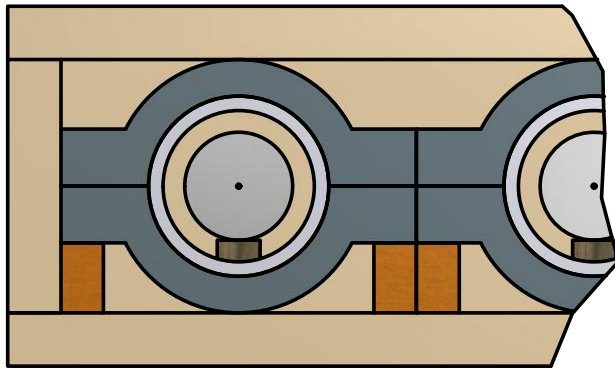
Dectector unit detail

E
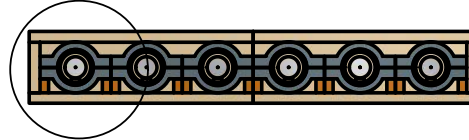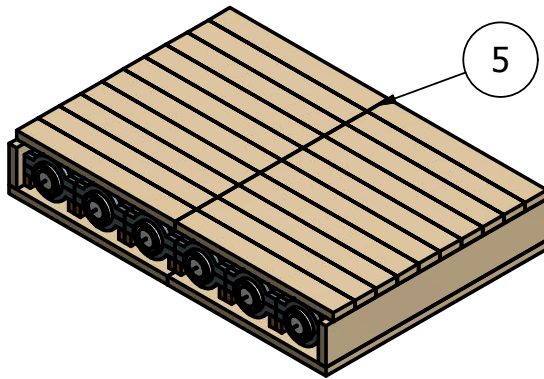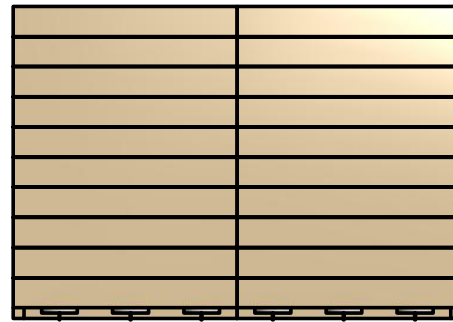
Total mass: 11737,24 kg
Botton surface: 6913305,00 mm^2
Structural overload: 1698 kg/m^2

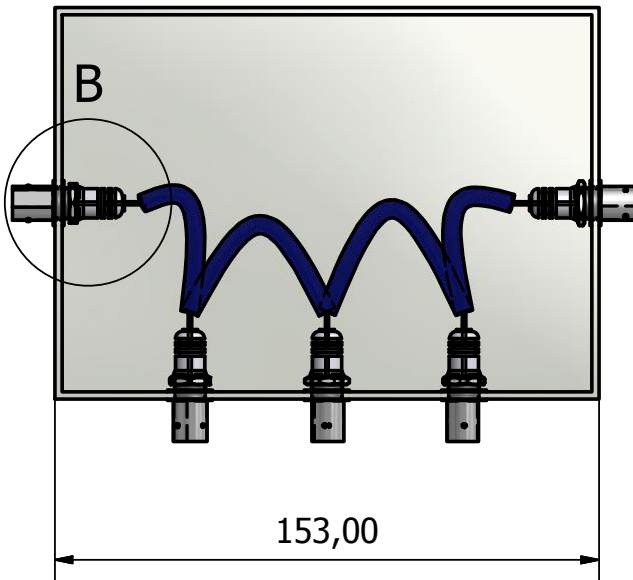| Part List			
Part.#	Quant.	Part	Mass
1	6	Detector unit	1763,177 kg
2	2	Bottom slabs	246,805 kg
3	2	Rear slabs	38,128 kg
4	2	L/R slabs	55,786 kg
5	20	Top slabs	23,837 kg

A.2 The high voltage splitter box

31,50

110,00

B

B (1 : 1)

153,00
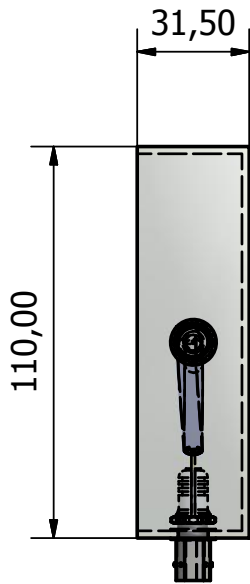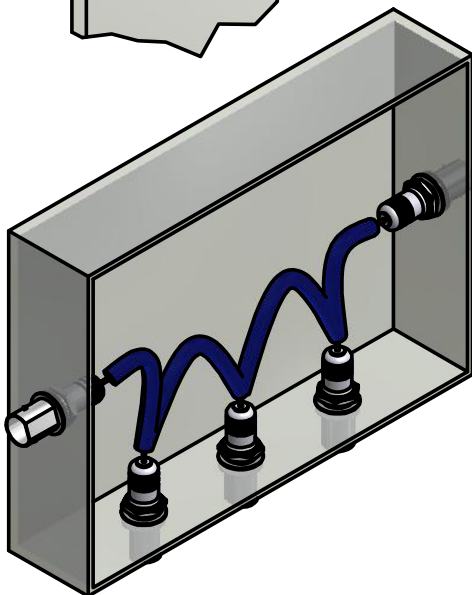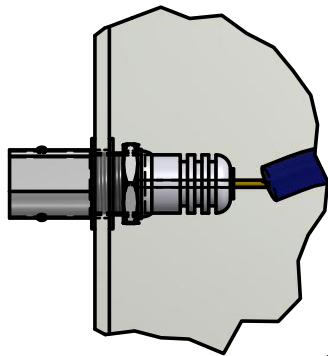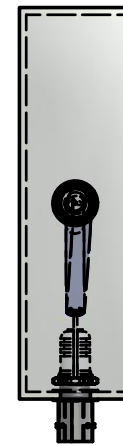
LISTA DE PIEZAS

ELEMENTO	CTDAD	Nº DE PIEZA
1	1	HV-Splitter Box
2	5	Conector BNC-HT-2
3	5	arandela
4	5	Pieza1
5	1	HV-Splitter Box.Arnés1
6	5	10.Piezas 02.14 Tuerca M10
7	1	HV-Splitter Box.Arnés5

Diseño de	Revisado por	Aprobado por	Fecha	Fecha	
Óscar García				06/06/2015	

High Voltage Splitter Box

CaLMa

HV-Splitter Box

Edición

Hoja

1 / 2

15,75

31,50

31,50

15,75

38,00

76,50

115,00

153,00

110,00

55,00

E

E (2 : 1)

Ø9,60

THIS PAGE INTENTIONALLY LEFT BLANK

Bibliography

[1] & Zwicky F. Baade W. Cosmic rays from super-novae. *Proceedings of the National Academy of Sciences of the United States of America*, 20(5):259–263, 1934.

[2] Horace W. Babcock. Magnetic variable stars as sources of cosmic rays. *Phys. Rev.*, 74:489–489, Aug 1948.

[3] J. J. Blanco, E. Catalán, M. A. Hidalgo, J. Medina, O. García, and J. Rodríguez-Pacheco. Observable effects of interplanetary coronal mass ejections on ground level neutron monitor count rates. *Solar Physics*, 284(1):167–178, May 2013.

[4] H Carmichael, M Bercovitch, M A. Shea, M Magidin, and R W. Peterson. Attenuation of neutron monitor radiation in the atmosphere. 46, 02 1968.

[5] Chalk River, Ontario, Canada. *BP28 Chalk River Neutron Counter Operating Data*.

[6] JohnM. Clem and LevI. Dorman. Neutron monitor response functions. *Space Science Reviews*, 93(1-2):335–359, 2000.

[7] Wikimedia Commons. File:detector regions.gif — wikimedia commons, the free media repository, 2018. [Online; accessed 3-June-2018].

[8] Wikipedia contributors. Cosmic ray — wikipedia, the free encyclopedia, 2016. [Online; accessed 20-May-2016].

[9] S. E. Forbush. On world-wide changes in cosmic-ray intensity. *Phys. Rev.*, 54:975–988, Dec 1938.

[10] O García-Población, H Ivanov, I García-Tejedor, J J Blanco, J Medina, R Gómez-Herrero, E Catalán, and D Radchenko. The neutron monitor control panel. *Journal of Physics: Conference Series*, 632(1):012055, 2015.

[11] A. Hovhannisyan and A. Chilingarian. Median filtering algorithms for multi-channel detectors. *Advances in Space Research*, 47(9):1544 – 1557, 2011.

[12] Glenn F Knoll. *Radiation detection and measurement; 4th ed.* Wiley, New York, NY, 2010.

[13] T. Kuwabara, J. W. Bieber, J. Clem, P. Evenson, and R. Pyle. Development of a ground level enhancement alarm system based upon neutron monitors. *Space Weather*, 4(10):n/a–n/a, 2006. S10001.

[14] USA LND Inc. Oceanside, New York. 2016 cylindrical bf3 neutron detector specifications, online 2014.

[15] J. Medina, J. J. Blanco, O. García, R. Gómez-Herrero, E. J. Catalán, I. García, M. A. Hidalgo, D. Meziat, M. Prieto, J. Rodríguez-Pacheco, and S. Sánchez. Castilla-La Mancha neutron monitor. *Nuclear Instruments and Methods in Physics Research A*, 727:97–103, November 2013.

[16] Ó G Población, J J Blanco, R Gómez-Herrero, C T Steigies, J Medina, I G Tejedor, and S Sánchez. Embedded data acquisition system for neutron monitors. *Journal of Instrumentation*, 9(08):T08002, 2014.

[17] S. V. Poluianov, I. G. Usoskin, A. L. Mishev, M. A. Shea, and D. F. Smart. Gle and sub-gle redefinition in the light of high-altitude polar neutron monitors. *Solar Physics*, 292(11):176, Nov 2017.

[18] J. A. Simpson. The Cosmic Ray Nucleonic Component: The Invention and Scientific Uses of the Neutron Monitor - (Keynote Lecture). *ssr*, 93:11–32, July 2000.

[19] G. Souvatzoglou, A. Papaioannou, H. Mavromichalaki, J. Dimitroulakos, and C. Sarlanis. Optimizing the real-time ground level enhancement alert system based on neutron monitor measurements: Introducing gle alert plus. *Space Weather*, 12(11):633–649, 2014.

[20] Rühm W., Ackermann U., Pioch C., and Mares V. Spectral neutron flux oscillations of cosmic radiation on the earth's surface. *Journal of Geophysical Research: Space Physics*, 117(A8).